UNIVERSITY OF READING

Department of Meteorology

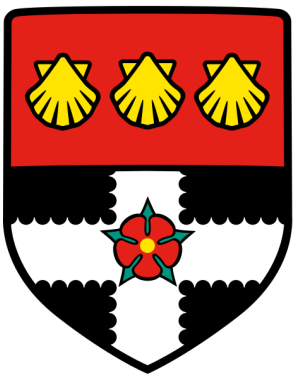

Understanding Tropical Cyclone Precipitation in the Northern Philippines

Bernard Alan B. Racoma

A thesis submitted for the degree of Doctor of Philosophy

January 2024

Declaration

I confirm that the content herein is my own work and the use of any other material from other sources has been properly and fully acknowledged.

Bernard Alan R. Racoma

Consent and Acceptance

We hereby consent and accept that the following papers, which have been reformatted for use here along with typographical and formatting adjustments, are submitted as parts of the manuscript in partial fulfillment of the requirements of the PhD (by Distance) in Atmosphere, Oceans, and Climate at the Department of Meteorology, University of Reading, United Kingdom, for which we serve as PhD supervisor or co-supervisor/ and co-author can be part of Bernard Alan Racoma's thesis for the degree.

1. **Racoma, B. A. B.**, Klingaman, N. P., Holloway, C. E., Schiemann, R. K. H., and Bagtasa, G. (2022). Tropical cyclone characteristics associated with extreme precipitation in the northern Philippines. International Journal of Climatology, 42(6), 3290– 3307. https://doi.org/10.1002/joc.7416
2. **Racoma, B. A. B.**, Holloway, C. E., Schiemann, R. K. H., Feng, X. and Bagtasa, G. (2022). The Effect of the Cordillera Mountain Range on Tropical Cyclone Rainfall in the Northern Philippines. Manuscript submitted for publication.

We also hereby consent and accept that, due to the nature of the Dual PhD Program between UP and UoR, essentially the same manuscript, which have been reformatted for use here along with minor typographical and formatting adjustments to adhere to the formatting standards of each university, will be submitted by Bernard Alan Racoma in fulfilment of the requirements for the PhD (by Research) in Meteorology at the University of the Philippines, for which we serve as PhD supervisor/adviser or co-supervisor/co-adviser.

Christopher Holloway, PhD Associate Professor UoR Supervisor (UoR)	Gerry Bagtasa, PhD Professor UP IESM Supervisor (UPD)	Reinhard Schiemann, PhD Associate Professor NCAS, UoR Co-supervisor	Xiangbo Feng, PhD Postdoctoral Research Assistant NCAS, UoR Co-supervisor

Dedication

"Beyond the clouds, the sun never stops shining."

I dedicate this thesis to my younger self.

Embrace who you are. Be kind to yourself.

Acknowledgements

I would like to thank all my supervisors, Chris Holloway, Gerry Bagtasa, Reinhard Schiemann, and Xiangbo Feng. Thank you for always being supportive and understanding, and for always believing in me. I would also like to thank my Monitoring Committee, Miguel Teixera and Nicolas Bellouin. I am also grateful for Nick Klingaman's guidance during my first years at Reading. I am also grateful for Ralf Toumi: the questions and revisions raised during my viva have lead to me having a deeper appreciation of our field.

Many thanks goes to Jane Delfino for being my PhD buddy these past four years. We did it, finally.

I thank my two institutes, the Department of Meteorology of University of Reading, and the Institute of Environmental Science and Meteorology of University of the Philippines. I thank all my mentors, colleagues, teachers, professors, and administrative staff from both institutes.

I am also grateful to the Commission of Higher Education and the British Council for the Joint Development of Niche Programmes through Philippine-UK Linkages Transnational Education Programme for providing financial support for my PhD studies.

I would like to thank my psychiatrist for helping me discover my disability, and for helping me find out what works, and what doesn't as I finished up my studies.

To my family, thank you for the unending support and the unconditional love. I couldn't have done this without all of you and I wouldn't be here right now if it weren't for you. Mahal na mahal ko kayo.

To my partner, Denden, thank you, for the love and support. Thank you for going through this journey with me. I look forward to a brighter future together.

Maraming salamat po.

Abstract

In this thesis, I investigate different factors that affect Tropical Cyclone (TC) precipitation and characteristics in Luzon, the northern regions of the Philippines. This thesis is is divided into two parts: an observational study to establish relationships between TC characteristics and rainfall in Luzon, and modeling experiments to understand and explain the processes that link TC rainfall with the topography of Luzon.

In the first part of this thesis, I investigate the relationship between TC extreme precipitation, TC characteristics, and the orography of the Philippines. I first introduced the Weighted Mean Precipitation Exceedance (WPE), a measure of extreme precipitation. WPE is adapted from different studies that calculate extreme precipitation based on extreme thresholds for specific regions, as well as the spatial coverage of precipitation in the said region. As the WPE calculates both intensity and extent in a single value, we are easily able to compare extreme precipitation for different TCs.

For all TCs that cross Luzon between 1978-2015, we find that when comparing between intensity or movement speed categories, stronger or slower TCs that make landfall significantly yield higher WPE. The proportion of landfalling strong TCs, or Typhoons, is lower during June to September (29.58%) compared to the proportion of Typhoons making landfall in October to December (60.71%). However, the proportion of TCs that exceed the median WPE is higher during June to September (71.43%) compared to those making landfall during October to December (61.76%). This shows that the relationship between TC intensity and WPE is more pronounced during the months June to September — the Southwest Monsoon season in the Philippines. These results suggest that it is important to consider the pre-landfall cyclone movement speed, intensity, and season to anticipate extreme precipitation of incoming TCs.

To explain the underlying processes that link TC winds, precipitation, and orography, for the second part of this thesis I conduct Numerical Weather Prediction experiments for eight different TCs for different heights of the Cordillera Mountain Range (CMR): Control, Flat, Reduced (0.5x height), and Enhanced (2x height). From the results, we find that precipitation along the mountain range increases for increasing CMR height on

average. Comparing precipitation rates for the Flat and Reduced terrain profiles with the Control terrain shows an average increase of 5 mm/hr rain rates, with precipitation rates similarly increasing by 5 mm/hr between the Control and Enhanced terrain.

There are no significant changes for TC movement speeds and TC position for different terrain profiles. Regarding TC intensity, TCs weaken as early as 21 hours prior to landfall for higher CMR elevation when comparing the Enhanced and Control experiments, while the TC strength is similar between the Flat/Reduced and Control experiments. It is possible that TC intensity is less sensitive to mountain ranges at or below the height of the actual CMR. We also find that mechanical uplift caused by stronger winds blowing up steeper slopes results in higher amounts of precipitation along the CMR.

The results of this two-part study highlight the complexity of the relationships between TC characteristics, orography, environmental wind, moisture, and TC rainfall. Nevertheless, this study shows that features such as more intense TCs, the June to September monsoon season, and steeper mountain range slopes, are fundamentally linked to higher amounts of TC precipitation in the Philippines. The findings of this study can be used to fill gaps in current forecasting limitations and may help improve our response to potential hazards associated with TCs.

Table of Contents

List of Acronyms

Acronym	Definition
ACE	Accumulated Cyclone Energy
APHRODITE	Asian Precipitation - Highly-Resolved Observational Data Integration Towards Evaluation
AMO	Atlantic Multidecadal Oscillation
CMR	Cordillera Mountain Range
DPE	Direct Positional Error
ENSO	El Niño Southern Oscillation
GPM	Global Precipitation Measurement Mission
IBTrACS	International Best Track Archive for Climate Stewardship
IMERG	Integrated Multi-satellitE Retrievals for GPM
JJAS	June, July, August, September
MJO	Madden-Julian Oscillation
MSLP	Mean Sea Level Pressure
Non-TY	Non-Typhoon
NTC	Northern tracking TC
NWP	Numerical Weather Prediction
OND	October, November, December
PDO	Pacific Decadal Oscillation
SST	Sea Surface Temperature
STC	Southern tracking TC
TC	Tropical Cyclone
TCWV	Total Column Water Vapour
TY	Typhoon
TRMM	Tropical Rainfall Measuring Mission 3B42
WNP	Western North Pacific
WPE	Weighted Mean Precipitation Exceedance
WRF model	Weather Research and Forecast model

List of Figures

List of Tables

Chapter 1

Introduction

1.1 Motivation

This study was motivated by the need to augment our understanding of Tropical Cyclones (TC) that affect Luzon, the northern region of the Philippines. It is important to understand the interaction between TCs and the complex orography of Luzon to fill gaps in current forecasting limitations and to improve our response to rainfall associated with the orography of the country. While it is known that TCs change upon landfall or upon interaction with large land features, these interactions are yet to be investigated and quantified for the Philippines. The ability to estimate precipitation in advance based on TC characteristics and TC sensitivity to topography can help our forecasters estimate the properties and impacts possible incoming TCs.

1.2 Objectives and Science Questions

The objectives of this study are two-fold: to quantify the relationships between TC characteristics and TC extreme precipitation using historical observations, and to evaluate the effects of orography on TCs using a Numerical Weather Prediction (NWP) model.

Specifically, this PhD project aims to answer the following questions:

1. What characteristics of landfalling TCs are associated with extreme precipitation in Luzon, Philippines?
    - What is the relationship between TC intensity and extreme precipitation?
    - What is the relationship between TC movement speed and extreme precipitation?
    - Does TC-associated extreme precipitation differ between two Philippine monsoon seasons, the Southwest Monsoon (June to September) and the Northeast Monsoon (October to December)?

2. What is the effect of the orography of Luzon on the characteristics and precipitation of TCs?

    - Specifically, how does the height and slope of the Cordillera Mountain Range (CMR) affect the track, flow, intensity, and precipitation distribution of TCs that make landfall in Luzon, Philippines?

The first part of this thesis takes a novel approach in evaluating extreme precipitation where the probability of TC-associated extreme precipitation is estimated based on its characteristics. For the second part of this thesis, NWP model experiments are conducted for different orographic profiles to investigate and explain how the CMR affects TC intensity, movement, and precipitation.

1.3 Thesis Outline

This thesis is divided into six chapters. Following this introductory chapter, Chapter 2 covers a brief background of TCs, TCs in the Philippines, and then finally, the study area, Luzon. Chapter 3 discusses the data and methodology used in this study. This is followed by the results in Chapters 4 and 5 where we respectively evaluate historical TCs, and conduct NWP experiments for selected TC cases and orographic profiles. It is worth mentioning that Chapter 4 has already been published in Racoma et al. (2021) while Chapter 5 was published in Racoma et al. (2023). Finally, we end this thesis with Chapter 6 where we discuss our conclusions and our further recommendations for future studies that aim to understand TCs affecting the Philippines.

Chapter 2

Scientific Background

In this Chapter, we provide scientific background about Tropical Cyclones (TCs), tropical precipitation, land and atmosphere interactions, and then finally, impacts of TCs on the Philippines.

2.1 Tropical Cyclones

In this subsection, we define TCs in terms of their characteristics, formation, structure, movement and strength. Towards the end of this subsection we examine TC seasonality, variability, and then discuss recent studies that focus on TCs and climate change.

2.1.1 Definition, Characteristics, and Structure

According to the World Meteorological Organization (WMO), TCs are powerful and destructive storms originating in the tropics, and are characterized by a low-pressure center, organised convection, and a closed atmospheric circulation which spirals towards the center (World Meteorological Organization, 2020). TCs can affect many different countries (Figure 2.1), and depending on where they form and what regions they affect, TCs are either called Typhoons in the Western Pacific, Hurricanes in the Atlantic and Eastern and Central Pacific, or Cyclones in the Northern Indian Ocean. Different regions (which are divided by basins) have their own TC monitoring agencies (Figure 2.2).

TCs are considered the most destructive natural hazards, responsible for nearly half of all disaster losses worldwide (Kunze, 2021). Due to their organisation, energy, wind strength, and the associated precipitation, TCs can be devastating in nature, especially if they make landfall in populated areas. According to the Sixth Assessment Report of the Intergovernmental Panel on Climate Change (IPCC AR6), extreme storms such as

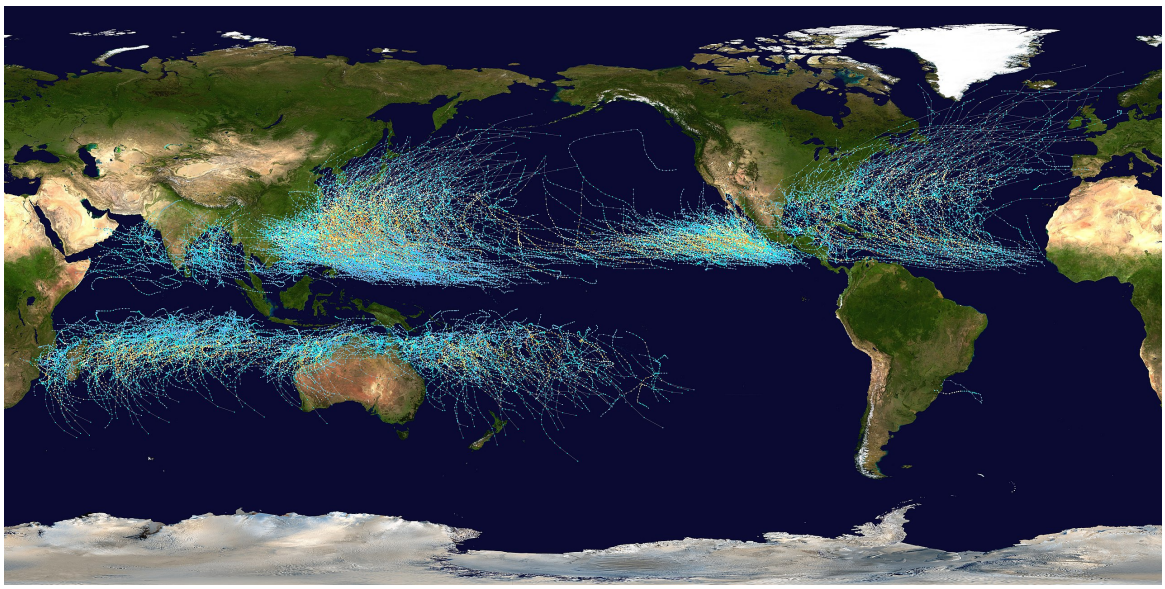

Figure 2.1: Global historical TC tracks between 1985 and 2005 as collated by the National Hurricane Center, Central Pacific Hurricane Center, and the Joint Typhoon Warning Center. The colour gradient represents the Saffir-Simpson Hurricane Scale, with warmer colours representing more intense TCs. Reproduced from Wikimedia Commons (2022)

TCs have substantial societal impacts especially along coastal communities due to the compounding effects of different hazards associated with TCs (Seneviratne et al., 2021). Bakkensen and Mendelsohn (2019) reveal that throughout the globe, TCs cause an average of 8,000 deaths and about $26 billion in damages every year. As such, understanding TC characteristics, rainfall, and associated hazards is of utmost importance.

A well-developed TC has a distinct, organised structure that includes several key components (Figure 2.3). Towards the center of the TC is the eye: a calm and clear region of low pressure where air subsides. Surrounding the eye is the eyewall, a ring of intense convection where the most intense winds and maximum upflow occurs (Emanuel, 2003). The eyewall's vertical structure extends high into the upper troposphere where maximum velocities occur (Jorgensen et al., 1985). Radiating outwards from the eye and eyewall are spiraling, concentric rainbands of towering convective cumulonimbus clouds often bringing high amounts of precipitation (Emanuel, 2003).

2.1.2 Cyclogenesis

TCs form over warm tropical oceans intensifying while usually moving westward (Tory and Frank, 2010; Emanuel, 2003). Gray (1998) lists six factors necessary for cyclogenesis to occur:

1. Sea Surface Temperatures greater than $26°C$
2. sufficient relative humidity in the mid-troposphere
3. a non-zero Coriolis parameter
4. weak tropospheric vertical wind shear
5. high values of low-level relative vorticity

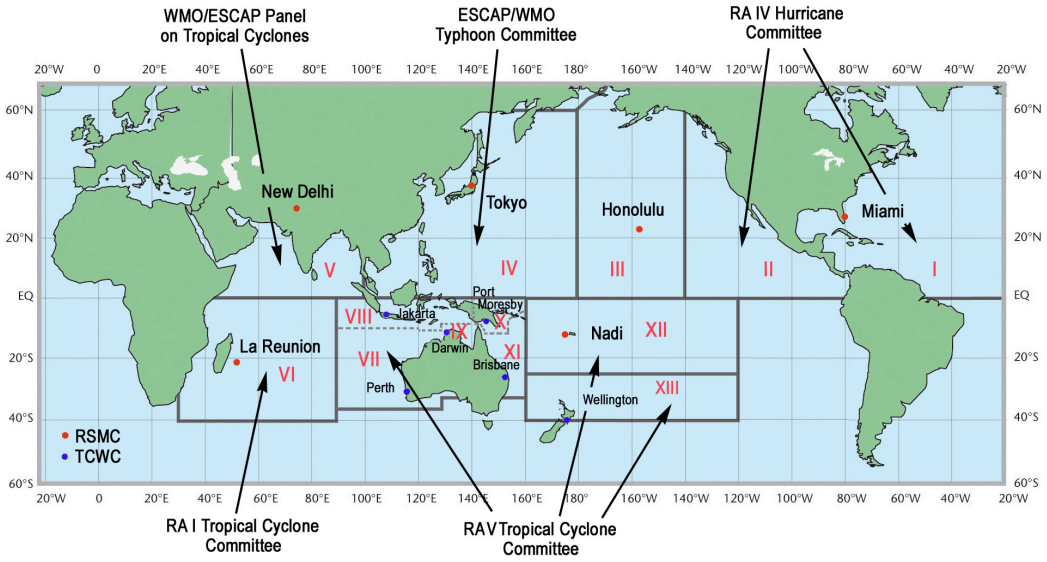

Figure 2.2: TC basins of the world. Reproduced from the National Oceanic and Atmospheric Administration (2021)

6. surface-based layer of conditional instability

During TC cyclogenesis, warm oceans lead to increased evaporation. Moist air rises, and upon reaching the Lifting Condensation Level the atmosphere becomes saturated and the conditional instability in the surface kick-starts the TC formation. The Coriolis force promotes the circulation of winds and vortexes, and with little to no vertical wind shear to inhibit organisation, a TC forms and then continues to intensify. The aforementioned factors will be further discussed in the following subsections.

2.1.2.1 Oceanic and Atmospheric Conditions for Cyclogenesis

The formation of TCs begins over warm ocean waters of Sea Surface Temperatures (SSTs) generally exceeding $26°C$. This provides the necessary heat that promotes evaporation which provides the atmosphere with moisture. Lifted moist air cools, condenses, and forms clouds and precipitation. This causes the release of latent heat which fosters further atmospheric instability that promotes TC formation (Palmén, 1948).

However, while the $26°C$ temperature threshold is useful in rapidly assessing possible sites of cyclogenesis, recent research by suggests that it is also important to consider other coupling index thresholds in addition to the traditional temperature threshold. McTaggart-Cowan et al. (2015) emphasises the importance of the gradient between upper and lower level equivalent potential temperature as complementary to the SST threshold. The difference in temperature between the ocean and the atmosphere initiates evaporation, while the difference in equivalent potential temperatures between lower and upper levels, promotes further instability.

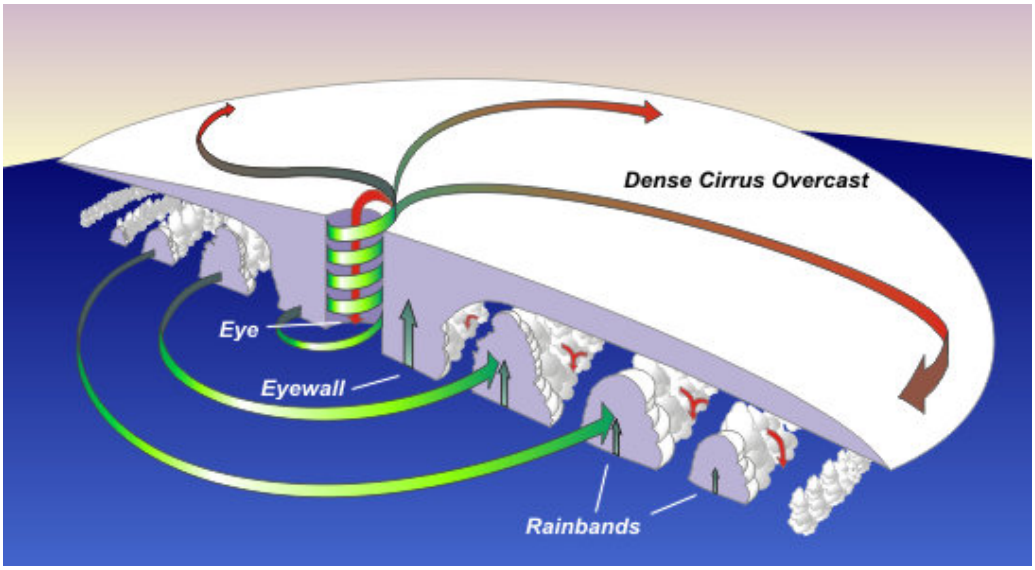

Figure 2.3: Cross section of a typical TC in the Northern Hemisphere. The green arrows show the clockwise movement of the cyclone winds from the surface, with stronger updrafts in the eywall of the TC. As the winds rise from the surface, they start to move outwards (outflow) in an anticlockwise direction near the tropopause. Reproduced from the National Oceanic and Atmospheric Administration (2023)

2.1.2.2 The Role of the Coriolis Effect and Low Vertical Wind Shear

The Coriolis Effect is essential in starting the cyclonic rotation of weather systems such as TCs. Objects that move over a rotating surface, such as the Earth, experience an apparent change in motion or deflection relative to the coordinate system of the fixed surface (Wylie, 1953). In the context of meteorology, as winds move along the surface of the Earth, they are deflected towards the right in the northern hemisphere, and deflected towards the left in the southern hemisphere (Figure 2.4). The horizontal deflection due to the Coriolis Effect is weakest along the equator and strongest in the poles (Persson, 1998). A strong deflection or rotation is necessary for TC formation and intensification, thus, TCs typically do not occur near the equator due to the low Coriolis force in the region.

While the deflection of horizontal winds is important in TC formation and intensification, the change of wind and direction with altitude — the vertical wind shear — results in the opposite effect. High wind shear disrupts the vertical structure of developing cyclones, impeding their organisation and intensification (Gray, 1968).

2.1.2.3 Trigger Mechanisms and Pre-existing Disturbances

TCs often form due to pre-existing disturbances in the atmosphere that provide low-level convergence and uplift necessary for genesis and development. These disturbances include, but are not limited to, tropical waves, frontal boundaries, or low-pressure systems.

The review article by Tang et al. (2020) differentiates how environmental, internal, and radiative processes trigger the formation of TCs. For example, the El Niño Southern Oscillation (ENSO) modulates TC cyclo-

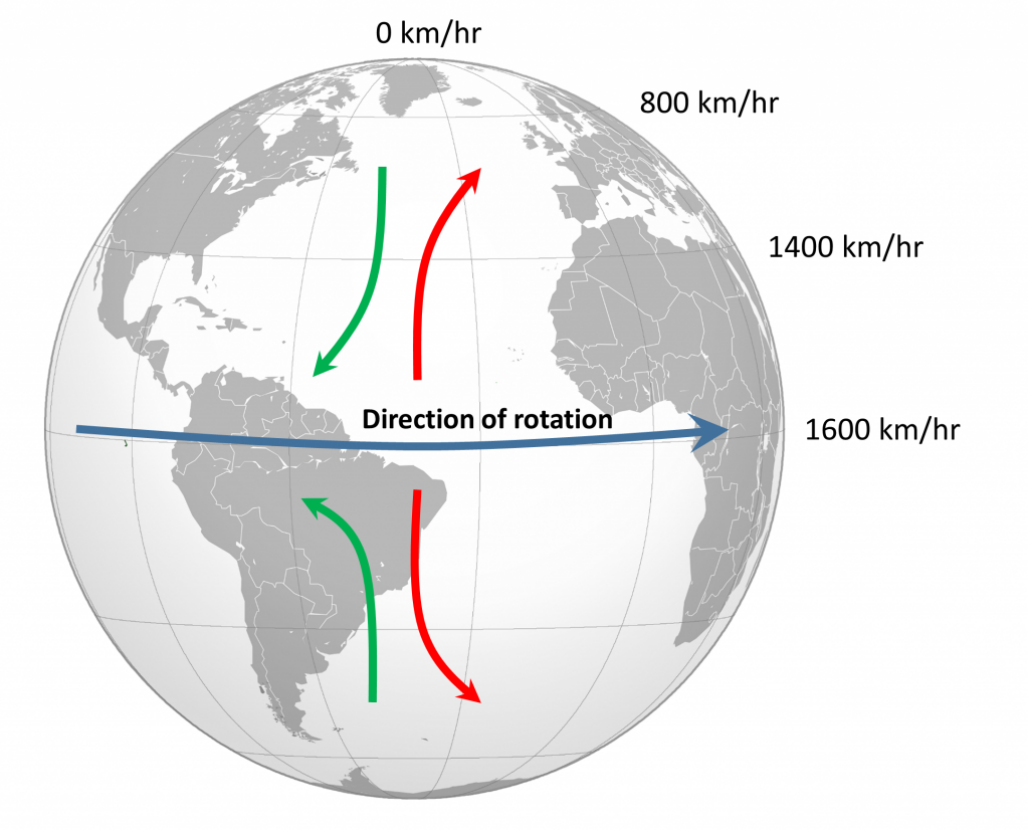

Figure 2.4: Diagram showing the deflection of winds due to the Coriolis Effect. In the Northern Hemisphere, winds are deflected to the right, while winds are deflected to the left in the Southern Hemisphere. This leads to equatorward winds deflecting to the west (green arrows), and the poleward winds deflecting to the east (red arrows). Reproduced from the Webb (2020)

genesis by affecting vertical wind shear and atmospheric and oceanic temperatures, resulting in temperatures conducive for TC formation (Lin et al., 2020), and regions of disturbances with high vorticity and instability, both of which are important in cyclogenesis, are introduced during the active phase of the Madden-Julian Oscillation (MJO) (Sobel and Maloney, 2000; Liebmann et al., 1994).

Besides the ENSO and the MJO, other environmental factors such as equatorial Rossby waves, and mixed Rossby-gravity waves can cooperatively act to modulate vertical wind, shear, mid-level moisture, while intensifying local circulation through upward motion, deep convection, and low-level circulation Tang et al. (2020). Synoptic-scale systems such as the monsoon trough and the Intertropical Convergenze Zone or ITCZ (Chia and Ropelewski, 2002; Xiang et al., 2013) can also serve as cyclogenesis sites due to the large values of low-level relative vorticity in nearby regions.

2.1.2.4 Stages of Development and the Role of Surrounding Environment

The development of a TC can be summarised in the following stages: initial disturbance, formation of depression, organisation of tropical storm, and then finally, the cyclone stage. The processes that govern TC formation also lay the groundwork for its subsequent intensification. Besides serving as sites for cyclogenesis, warm ocean waters provide the primary source of a TC's energy through heat, moisture, and convective

processes within the storm (Gray, 1998; Emanuel, 1986; Craig and Gray, 1996). TCs continue to intensify in environments with low vertical wind shear and high amounts of mid-level moisture (Tang et al., 2020).

Conversely, TCs may weaken or dissipate due to a number of different factors that include but are not limited to the following: a sharp decrease in sea surface temperatures, TCs moving towards areas of large environmental vertical wind shear, entrainment of dry air towards a TC's eyewall, and landfall of a TC (Fei et al., 2020) where evaporation and convective activity is inhibited (Tuleya and Kurihara, 1978).

2.1.3 TC Track

While the development of a TC involves various atmospheric and oceanic conditions conducive to its genesis and intensification, the track of the cyclone – the path it follows – is influenced by a different set of dynamics. For further understanding of the fundamentals of TC motion, the paper by Ito et al. (2020) discuss recent progress in understanding TC motion. In this section, I will adapt parts of the discussion from the aforementioned paper, and briefly mention atmospheric steering currents, the Coriolis Effect and β Effect, and influences of geographical features such as topography, the interaction between the atmosphere and ocean, and finally, the variability and predictability of TC motion.

2.1.3.1 Atmospheric Steering Currents

A TC's path is largely dictated by synoptic-scale atmospheric steering currents. A TC tends to follow the large-scale flow in which it is embedded (Simpson, 1946; Wu and Chen, 2016). The Western Pacific Subtropical High, in particular, besides playing a major role in the global circulation of atmospheres and oceans, is also considered an important component of TC movement in the Western Pacific. The existence of a semi-permanent anticyclonic high-pressure area inhibits poleward movement of TCs in the western Pacific especially if the subtropical high extends westward (Zhou et al., 2009). Conversely, as the subtropical high retracts to the east, TCs can start to move poleward. However, "conventional" atmospheric steering currents may not take into account short-time fluctuations that cause deviations from steering currents (Wu and Chen, 2016; Ito et al., 2020), and hence may be more representative of average movement.

2.1.3.2 Impact of the Coriolis Effect and the β Effect

The Coriolis Effect, besides influencing TC formation (as mentioned in Subsection 2.1.2.2), is also an important factor in TC movement. As a TC moves away from the equator and is steered by surrounding flow, the Coriolis effect causes the deflection or curve of the storm's path (Chan, 2005a). In addition to steering currents and the Coriolis Effect, Holland (1983) highlights the subsynoptic-scale assymetric circulations called β Effect" or "β-gyres".

As a TC moves away from the equator, the combination of rotating TC winds and stronger Coriolis Effect

leads to vorticity asymmetries towards the left and right regions relative to the TC movement (Figure 2.5). If there are no environmental winds, for a poleward moving TC, the β-effect results in a net westward deflection (Figure 2.6). In addition, the β Effect is stronger in more intense storms, hence leading to larger magnitudes of deflection (Arlene Laing, 2011)

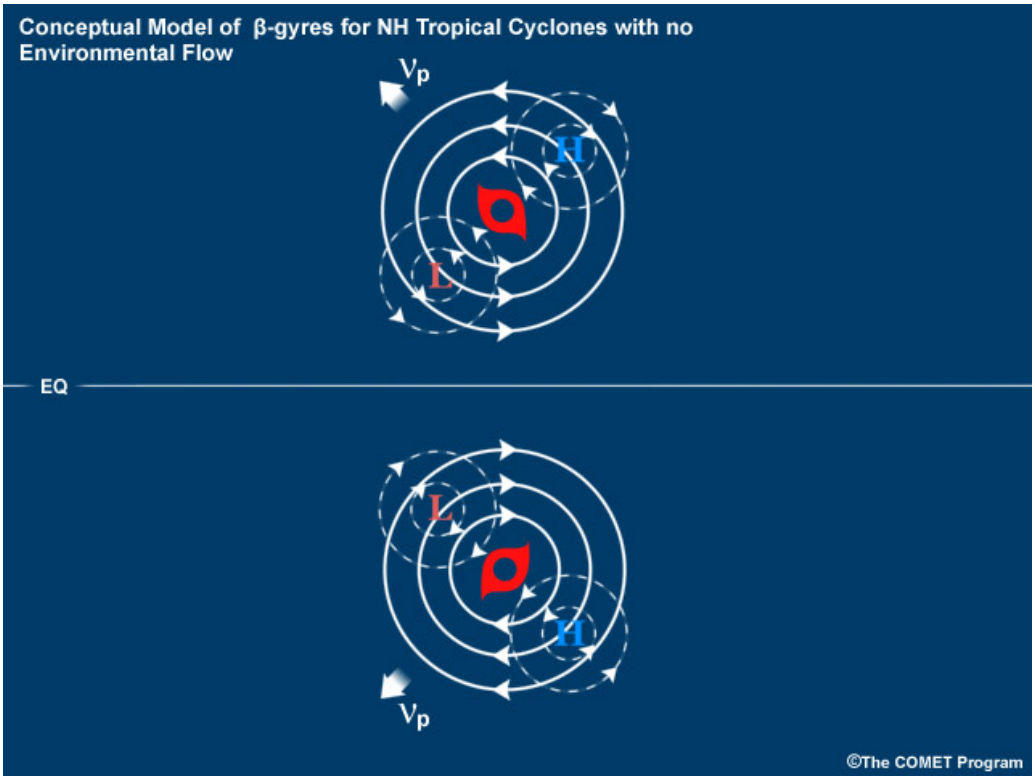

Figure 2.5: A conceptual model showing the β-gyres TCs in the Northern Hemisphere (top) and Southern Hemisphere (bottom). The source of this material is the COMET® Website, adapted from Arlene Laing (2011)

2.1.3.3 Impact of Topography

Significant track deflections can occur as a TC approaches and crosses land (Tang and Chan, 2014). The interactions between terrain and basic flow is non-linear (Ito et al., 2020), especially as surface vorticity is increased due to orographic blocking, and new regions of Potential Vorticity and asymmetries are introduced as TCs cross mountains (Lin et al., 1999). In an updated study Lin et al. (2016) propose that upstream track deflection may be explained by the following mechanisms: advection by orographically blocked basic flow, channeling effects, asymmetric latent heating, asymmetric mid-level steering flow, terrain-induced gyres, and approach and landing location. The interactions between TCs and land is further discussed in Subsection 2.3.

2.1.3.4 Impact of the Ocean

In addition to serving as an important factor in TC genesis and intensification, SST forcings can also affect TC tracks (Ito et al., 2020). In a recent paper, Delfino et al. (2023) reported that from model simulations using a pseudo global warming approach, increases in atmospheric and oceanic temperatures may lead to more

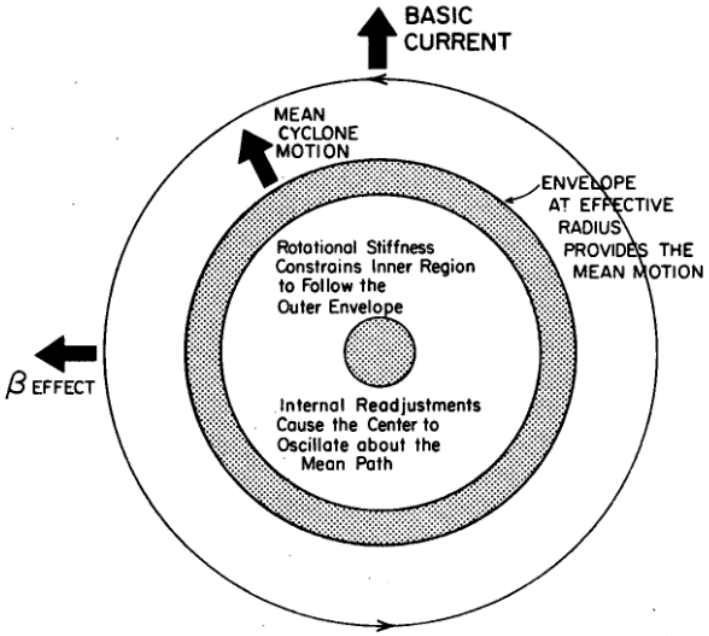

Figure 2.6: A simple schematic diagram showing the theoretical deflection of TC tracks due to the β Effect. Reproduced from the Holland (1983)

northward tracks or stronger deflections in simulated storms. Based on a series of case studies, Ren et al. (2014) reports that while the relationship between SSTs and TC tracks tend to be complex, some simulations show that TCs tend to recurve over warm pools. However, similar to the β Effect (Subsection 2.1.3.2), the time-scales involved in considering the effects of atmosphere-ocean coupling on TC tracks tend to be shorter. Nevertheless, SST patterns have large influences on steering flows in longer time scales (Ito et al., 2020).

2.1.3.5 Variability and Predictability of Cyclone Tracks

While there are general patterns in TC tracks, they are difficult to predict especially since the tracks are highly variable across different TC basins (Figures 2.1 and 2.2). In addition, the movement of TCs are highly sensitive to environmental factors such as vertical wind shear, moisture, the Coriolis Effect, and atmospheric steering currents, which themselves, are highly variable depending on the season. The review article by Roy and Kovordányi (2012) lists different techniques and advances to predict TC tracks. These include (but are not limited to), statistical modelling techniques based on previous cyclones, modelling based on physical forces affecting TCs, and pattern detection by human experts or forecasters.

More recently there have been attempts to integrate machine learning techniques into TC forecast and track modelling based on previous statistical models (Chen et al., 2020). However, while machine learning techniques offer rapid predictions, understanding the variability and predictability of TC tracks requires comprehensive knowledge of key physical processes that have been discussed in previous subsections.

2.1.4 TC Intensity and Activity

In this section, we now discuss the aspect of TC intensity. We first define TC intensity in terms of measurement of wind speed, and then continue to discuss factors affecting TC intensity, such as Ocean Heat Content, wind shear, and land interactions.

2.1.4.1 Definition and Measuring TC Intensity

Winds associated with TCs vary as a function of distance from the TC's centre (Figure 2.7). Towards the centre of the TC is the eye (Figure 2.3) where winds are relatively calm. As we move away from the TC's centre, tangential winds immediately reach their maximum values towards the eyewall. Moving further away from the eyewall, tangential winds start to decrease.

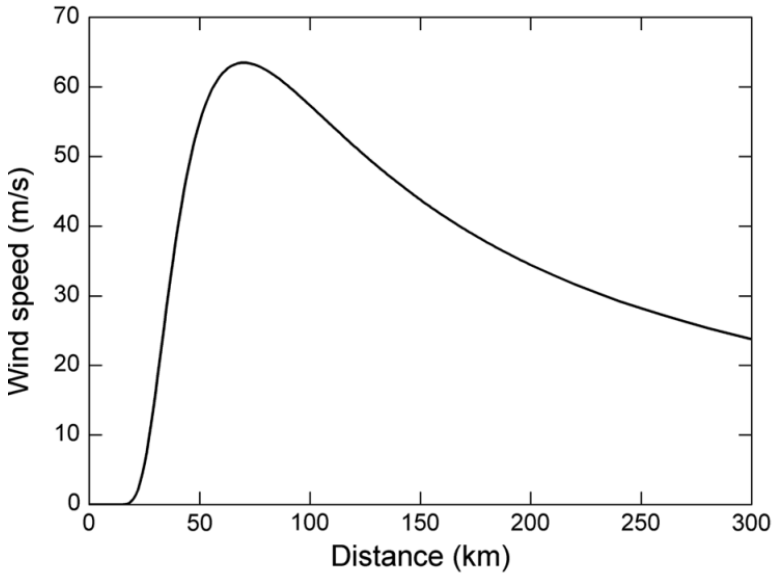

Figure 2.7: Surface TC winds as a function of distance from the centre. Reproduced from the Chen and Yu (2016)

As winds vary across the TC, TC intensity is typically measured either as the TC's central pressure at the sea surface (which is lowest towards the centre), or the maximum sustained wind speed 10 metres above the surface, which is recorded by taking the average wind speeds in a 1 or 10 minute period. While central pressure and maximum sustained wind speeds are estimated separately, studies by Chavas et al. (2017) test the theoretical prediction of TC wind speed based solely on the central pressure. However, they have reported that to measure the central pressure deficit (or the difference between the minimum central pressure near the surface, and the environmental pressure towards the edge of the storm), it is important to consider numerous factors such as maximum wind speed, storm size, and background rotation rate.

The seasonal activity of a TC basin can be represented by the Accumulated Cyclone Energy (ACE) index. ACE is a function of the TC intensity, and is calculated from the sum of the 6-hourly square of the maximum sustained wind speeds while a TC is of strength Tropical Storm or greater (Waple et al., 2001)

Different agencies around the world maintain records of the different tracks and intensities of TCs in their

respective basins (Figure 2.2, with different agencies having different calculations of maximum sustained wind speeds. As such, efforts such as the International Best Track Archive for Climate Stewardship, or IBTrACS aims to establish an archive of all recorded TC data around the world. The IBTrACS dataset is further discussed in Section 3.1.1.

2.1.4.2 Ocean Heat Content

As mentioned in Section 2.1.2, one of the primary factors necessary for TC formation is sufficiently warm SSTs. In addition to causing TCs to form, sufficient ocean heat content, particularly in the upper layers of the ocean is also necessary for TC intensification. As previously mentioned, warm ocean waters provide the necessary evaporation for TC genesis, development, and intensification.

Warmer and deeper waters tend to promote further TC intensification. However, the movement of TCs along the ocean also has an effect on ocean heat transport due to mixing and upwelling. According to Jansen and Ferrari (2009), heavy winds by TCs generate strong upper ocean mixing. TC activity along the tropics is shown to significantly increase the poleward transport of ocean heat content (Scoccimarro et al., 2011).

2.1.4.3 ENSO and TC Activity

In addition, it was mentioned in Subsection 2.1.2.3 that ENSO modulates TC genesis and intensification by affecting ocean temperatures and atmospheric humidity. During the inactive phase of ENSO, the ocean is typically much warmer towards the western region of the WNP (Figure 2.8a. However, during the warm phase of ENSO, warmer SSTs extend further towards the east (Figure 2.8b). According to Camargo and Sobel (2005), the ACE index is correlated strongly with ENSO indices up to six months later. In the Philippines, in particular, moisture flux is increased during ENSO events (Lyon and Camargo, 2009), while (Corporal-Lodangco et al., 2016) reported higher ACE during ENSO events due to increased TC days (longer TC lifespan) and higher TC intensities.

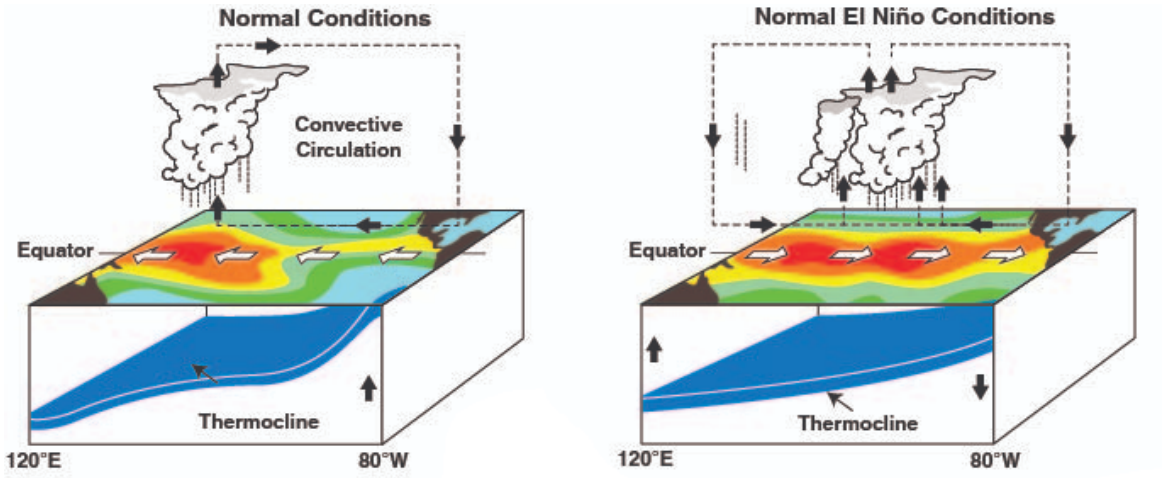

Figure 2.8: Sea surface temperatures along different longitudes for the (a) inactive ENSO phase, and (b) warm ENSO phase. Warmer oceans are shown in redder colours. Reproduced from the Royal Meteorological Society (2020)

Additionally, there has been observed spatial clustering of cyclogenesis locations and TC paths for different ENSO 'flavors' (Patricola et al., 2018), particularly the Cold Tongue and Warm Pool El Niño, where higher SSTs are observed towards the eastern and central regions of the Pacific Ocean, respectively. Figure 2.9 shows that in general, TC cyclogenesis and activity is enhanced towards the the Western Pacific for both Cold Tongue and Warm Pool El Niño (Figures 2.9a-c), whereas TC activity is suppressed during La Niña (Figure 2.9d).

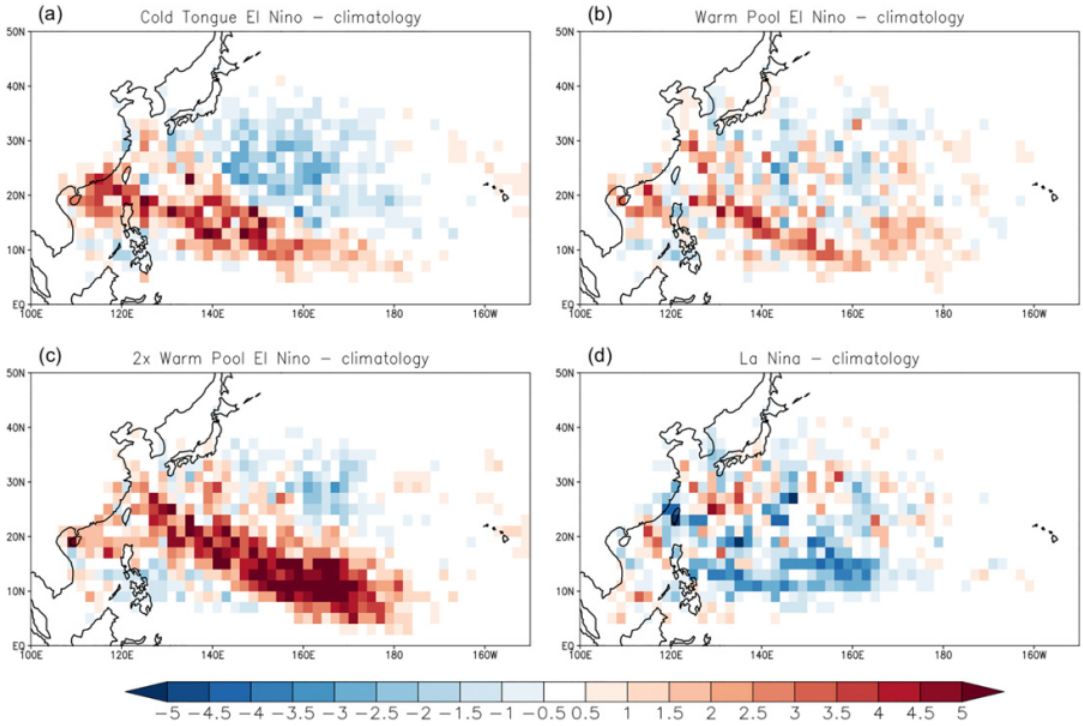

Figure 2.9: TC Track density for (a) Cold Tongue El Niño, (b) Warm Pool El Niño, (c) doubled Warm Pool El Niño, and (d) La Niña simulations minus the climatology simulation. Adapted from Patricola et al. (2018).

2.1.4.4 Atmospheric Conditions and Wind Shear

Besides the sea-air interface affecting TC intensification, the atmospheric environment also significantly influences TC intensity. High humidity levels in the mid-troposphere (Gray, 1998) are favourable for TC development due to lower amounts of evaporative cooling: high evaporative cooling can result in stronger downdrafts and suppressed eyewall convection, and thus, weaker TCs (Li et al., 2015).

In addition to humidity levels, strong vertical wind shear — or the change in wind speed or direction along different vertical levels of the atmosphere — are considered to be "hostile" to TC development and intensification. The presence of strong vertical wind shear impedes further organisation of a TC and weakens TCs until they dissipate.

In contrast, Smith and Montgomery (2015) reports that some real-world TC cases in fact intensify despite strong vertical wind shear. While large values of vertical wind shear suppressed TC genesis and intensification, moderate or weak vertical shear may introduce pathways where dry air may be entrained within the TC, effectively causing either suppression, or weakening (Nolan and McGauley, 2012). The intrusion of dry air within

the TC suppresses moist convection, effectivly inhibiting TC development and intensification (Ge et al., 2013).

2.1.4.5 TC and Land Interactions

As a TC continues to develop and intensify, it may eventually interact with land, halting further TC development, and drastically affecting intensity. When a TC makes landfall, it loses its primary energy source, which is the warm ocean waters as mentioned in Subsection 2.1.4.2. Additionally, factors such as the topography of the landfall area, the TC's size, and the TC's movement speed along land, and amount of TC precipitation can influence the rate of its weakening over land (Touma et al., 2019). Atmosphere and land interactions will be further discussed in Section 2.3

2.1.5 TC Seasonality

The seasonality of TCs varies considerably across the different TC basins due to the variations in regional climatic conditions. In the North Atlantic basin (I in Figure 2.2) the peak of the Hurricane season is from August to October, when SSTs are the warmest in the region (Truchelut et al., 2022). Conversely, the WNP basin (II, III, and IV in Figure 2.2) experiences a longer cyclone season due to the broader regions of favorable SSTs and monsoonal interactions (Zhan et al., 2012; Corporal-Lodangco and Leslie, 2016; Feng et al., 2021).

As mentioned in Subsections 2.1.2 and 2.1.4.2, SSTs are a critical factor in determining TC seasonality as warmer waters provide the necessary conditions for cyclogenesis and intensification. Thus, TC activity is highest during periods of warm SSTs. The seasonal variation of SSTs due to the variation of solar forcing throughout the year (Pezzulli et al., 2005) may in turn affect ENSO activity (discussed in Subsection 2.1.4.3).

2.1.6 Inter-annual Variability and Large Scale Oceanic Patterns

The inter-annual variability of TCs is significantly influenced by large-scale oceanic and atmospheric phenomena. In addition to ENSO (which was previously discussed in 2.1.4.3), longer-term climate variability patterns such as the Atlantic Multi-decadal Oscillation (AMO), Pacific Decadal Oscillation (PDO) and short-term patterns such as the Madden-Julian Oscillation (MJO) either enhance or suppress TC genesis and intensification due to shifts in atmospheric circulation patterns and SST anomalies (Chia and Ropelewski, 2002; Chan, 2005b).

2.1.7 TCs and and Climate Change

There has been extensive scientific research on the relationship between TC activity and climate change. While it is challenging to attribute individual storms or seasons solely to climate change (Kossin et al., 2013), there is a growing consensus that certain changes in TC behaviour are consistent with the broader context of a warming world . The Intergovernmental Panel on Climate Change (IPCC) states in its Sixth Assessment Report

that climate extremes may increase in the future due to human-induced greenhouse gas emissions (Seneviratne et al., 2021). Studies have suggested that while there is a possible decrease in overall frequency of TCs in some basins, there may be an overall increase in frequency of more intense storms (Knutson et al., 2010, 2020). Additionally selected re-forecasted TCs exhibited stronger intensities in model simulations for warmer climates (Delfino et al., 2023) . This is consistent with the expectation that warmer atmospheric and sea surface temperatures may provide more energy for intense storms (Emanuel, 2005).

Besides affecting cyclogenesis and intensification, climate change may also influence TC movement and geographical distribution, hence, regions of impact. According to Feng et al. (2021), the average location of TCs in the western North Pacific (WNP) basin has shifted further north between 1979 and 2018. In addition, there has been a 70% increase in TC activity in the "less active" season (i.e. the months from December to February) of the WNP, leading to 480% more landfalls in the southern regions of the Philippines (Basconcillo and Moon, 2021). Thus, the combination of a rising global population along with stronger TCs affecting regions not usually affected by TCs is of great concern, especially in the context of disaster preparedness and mitigation in a changing climate (Mendelsohn et al., 2012).

However, there still remains significant uncertainty in projections of how TCs will respond to climate change. This is due to the complexity of systems involved and limitations of current climate models. Nevertheless, recent significant improvements in global climate models, as well as in data collection and management, have led to reduced uncertainty in future TC projections (Knutson et al., 2010; Walsh et al., 2016). While data collection in terms of quality and quantity, remains a challenge, historical data suggest detectable TC track changes in some regions related to climate change according to (Knutson et al., 2019). As such, climate change continues to pose rising global TC risk, particularly with respect to sea level rise (high confidence), precipitation rates (medium to high confidence), intensity (medium to high confidence), TC frequency (low confidence), and translation speed (low confidence) (Knutson et al., 2020). In the context of a warming climate, the combination of these factors may lead to higher probabilities of extreme precipitation in future TCs.

2.2 Tropical Precipitation

The Tropics are the region surrounding the equator, spanning approximately 23.5°CN and 23.5°CS. Temperature variation is minimal across the region as the Tropics receive maximum amounts of solar energy yearlong. Thus, SSTs, humidity, and rainfall are highest in the Tropics due to the amount of solar energy involved. This can be seen from satellite observations, with Figure 2.10 showing higher average precipitation recorded within the vicinity of the Tropics as recorded from satellite data.

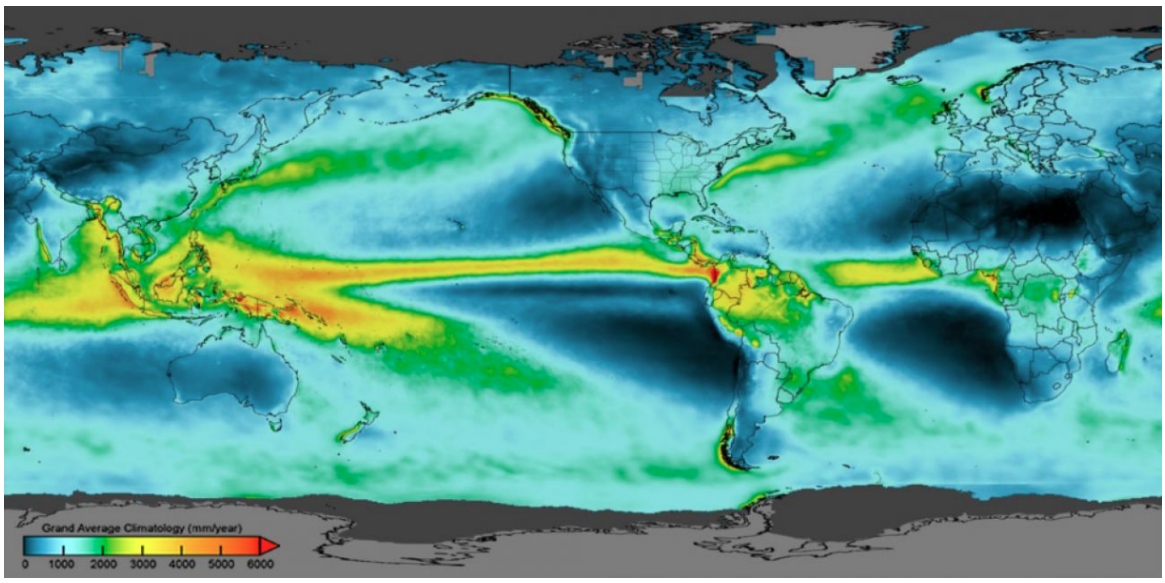

Figure 2.10: World map showing the grand average precipitation climatology between June 2000 to May 2019. Reproduced from the GSFC (2018), available online at `https://gpm.nasa.gov/data/imerg/precipitation-climatology`

2.2.1 Tropics and SST

Tropical SSTs are consistently warm, creating an environment conducive to convective activity and TC formation and intensification. The warm Tropical waters drive the global thermohaline circulation (Wunsch, 2002) that distribute energy around the world. In addition, Tropical SSTs interact closely with atmospheric phenomena such as the ENSO and the MJO. The warm phase of ENSO is characterised by anomalously high SSTs (Royal Meteorological Society, 2020), while the convective activity of MJO is highly sensitive to SST values (Stan, 2018).

2.2.2 Monsoons and Tropical Rainfall

Monsoons are seasonal wind patterns that cause distinct wet and dry seasons in the Tropics. These are characterised by seasonal reversal of winds between the Boreal summer and winter. The East Asian Winter Monsoon typically brings in surges of cooler, drier air (Chan and Li, 2004), and hence, lower amounts of rainfall, while on the other hand, the East Asian Summer Monsoon brings abundant rainfall in the western Pacific and South China Sea (Yihui and Chan, 2005). The seasonal march of rainfall due to the monsoon has significant impacts in the agricultural output of the countries such as the Philippines (Akasaka et al., 2007; Cruz et al., 2013).

2.2.3 TCs and Precipitation

Large amounts of precipitation is one of the most significant impacts of a TC. TC precipitation is dominated by two primary precipitation processes: convective (characterised by strong updrafts) and stratiform (characterised by weak vertical motion) (Rogers et al., 2005). As mentioned in Section 2.1.1, TC precipitation

mostly occurs along the rainbands: regions of intense convective activity and towering cumulonimbus clouds. TC rainfall is typically limited to 1,000 km radius from the TC center (Kubota and Wang, 2009; Bagtasa, 2017), and mean precipitation decreases with increasing distance from the TC center (Rogers et al., 2005).

Higher TC-related rainfall is generally associated with slower TC speeds due to the longer duration of a TC's influence over a region (Emanuel, 2017; Lai et al., 2020). TC-precipitation studies focused on Taiwan revealed that TCs with slower translation speeds tend to produce more rainfall (Hsu et al., 2013). At the same rainfall intensity, slower-moving TCs will remain longer in a region and thus are associated with larger precipitation totals. Cheung et al. (2008) also noted that besides translation speeds, variations in TC track affect the spatial distribution of rainfall. They have proposed that TC rainfall prediction should be based on climatologically-based statistical models of TC rainfall as well as the persistence of an ongoing TC's 3-hour accumulated precipitation to augment model forecasts. Kossin (2018) suggests that the global slowing of TCs due to atmospheric warming caused by anthropogenic climate change may increase TC-related rainfall in the future as TC-related rainfall depends on both rain rate and translation speed. While the validity of the relationship between climate change and TC movement speed in Kossin (2018) is arguable due to the inhomogeneity of the best track data used (Lanzante, 2019; Moon et al., 2019; Yamaguchi et al., 2020).

Conversely, Tu et al. (2022) reports that TC rainfall accumulation significantly increases with translation speed. The increase in rainfall rate and accumulation with respect to TC translation speed is due to two main factors: the relative speed-induced net inflow and vertical wind shear, both of which can enhance convection and rain-rate (Tu et al., 2022). However, the study by Tu et al. (2022) includes data for all TCs in all basins for the whole lifetime of each TC, i.e., from formation, landfall, and then dissipation. As these were generalised observations, the effects, impacts, and relationships of TC movement speed and precipitation in specific regions in the world were not differentiated in their study.

2.3 Land and Atmosphere Interactions

The interactions between land and atmosphere are fundamental in understanding regional climate, TC precipitation, as well as TC characteristics and development (i.e. intensification, track, etc). In this section, we discuss a brief overview of the interaction between mountainous terrain and atmospheric flow, as well as orographic precipitation.

2.3.1 Orographic Lifting and Precipitation

Mountains act as physical barriers to atmospheric flow. In the simplest model of orographic lifting, winds impinge on mountain slopes, causing air to mechanically rise. Roe (2005) describes additional mechanisms of orographic lifting (Figure 2.11), the most straightforward of which is stable uplsope ascent due to partial blocking (Figure 2.11a). For weaker flow and more stable atmospheres, air may be unable to ascend, and flow

may be partially blocked and in lower levels (Figure 2.11b).

The presence of features such as valleys, and narrow mountains lee-side convergence may result in strong down-valley flow (Figure 2.11c) and lee-side convergence (Figure 2.11d), respectively. Additionally, the presence of mountains can trigger unstable convection by lifting air above the level of free convection, either through solar-heating (Figure 2.11e) or mechanical lifting (Figure 2.11f). Finally, mountain ranges may also amplify precipitation over hills through the seeder-feeder mechanism (Figure 2.11g), where there is a large scale precipitating cloud (the ”seeder”), introducing additional moisture in the clouds below (the ”feeder”), leading to stronger rainfall due to coalescence or riming.

While the previous paragraphs briefly outline the different mechanisms, further details of each mechanism are further discussed in Roe (2005).

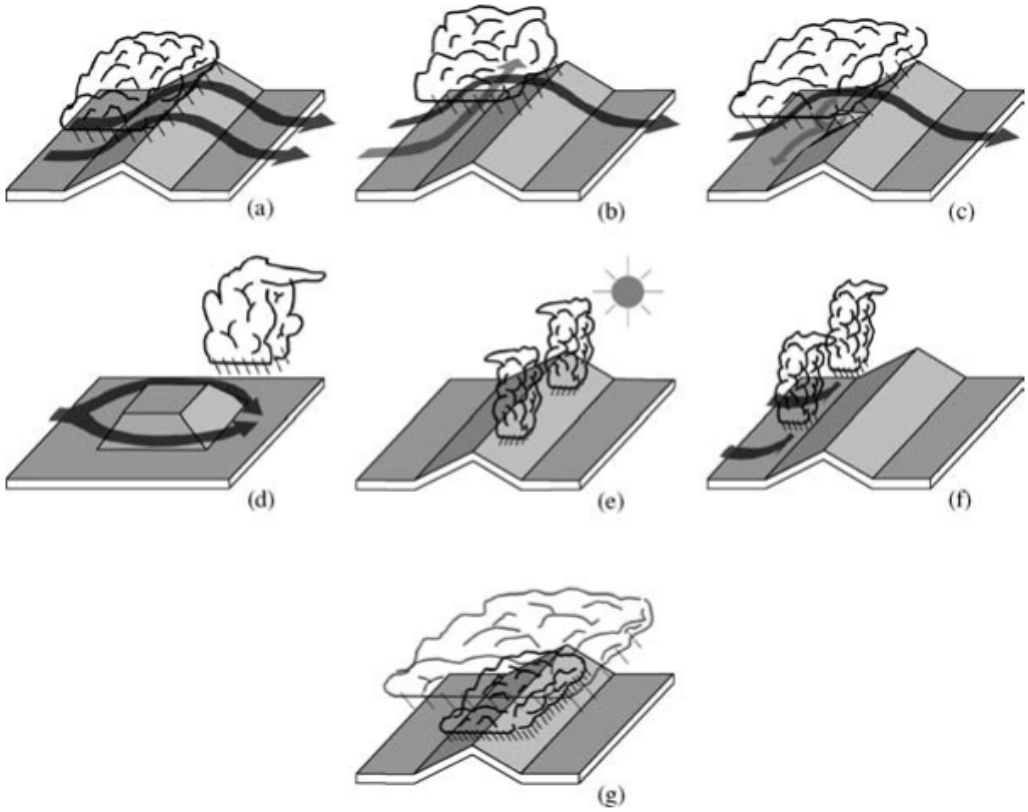

Figure 2.11: Schematic illustrations of different mechanisms of orographic precipitation. Reproduced from Roe (2005)

In addition to serving as physical barriers blocking atmospheric flow, topography has been shown to have a large influence on local rainfall, a phenomenon known as orographic precipitation (Smith, 1979; Roe, 2005). Forced mechanical lifting of moist air along slopes leads to condensation and then precipitation along the windward flanks of the mountain (Roe, 2005).

2.3.2 Impact of Mountains on TC Trajectory and Structure

Mountainous terrain can significantly alter TC trajectories (Tang and Chan, 2014). Through idealised models and simulations of real and bogus vortices, it was found that mountain influence on TC track is not

limited to direct land-TC interaction upon landfall. Track-deflecting vortices are induced at the approach, during landfall, and even upon the exit of TCs after landfall (Lin et al., 2002, 2016; Huang et al., 2016, 2020).

Lin et al. (2005) defines the vortex Froude number V_{max}/Nh given the maximum tangential wind speed of a TC (V_{max}), the Brunt–Väisälä frequency (N), and the mountain height (h). Lower values of the vortex Froude number implies either weaker winds or taller mountains, or in other words, stronger orographic blocking, while higher values imply weaker orographic blocking. Figure 2.12 shows different responses of westward moving cyclones to different strengths of orographic blocking. Weaker orographic blocking results in a slight northward deflection but continuous movement (Figure 2.12a). A stronger deflection and a generation of a secondary vortex is observed for moderate blocking (Figure 2.12b). Finally, strong orographic blocking leads to a similar response to the moderate blocking case (i.e. generation of additional cyclones), with the track deflecting southwards, leading to a discontinous cyclone movement (Figure 2.12c).

Based on an observational study by Man-chi and Chun-Wing (2015), there is a slight bias for TCs to deflect leftwards (relative to movement direction) upon leaving Luzon, Philippines. Additionally, they observed that track deflection is dependent on landfall approach angle: a TC that was deflected to the right upon Luzon landfall was more likely to deflect towards the left after leaving Luzon (Figure 2.13a), while a TC that was deflected to the left upon landfall was more likely to deflect to the right upon exit (Figure 2.13b).

In addition to track deflection, the rugged terrain of mountains can disrupt the internal structure and basic flow of a TC due to the advection of dry air near the mountain tops (Bender et al., 1987a; Tang and Chan, 2014). In fact, larger mountain ranges (such as the Central American mountains) can inhibit TC activity and climatology, as these mountain ranges may interrupt moisture transport from the oceans towards land (Fu et al., 2021).

2.3.3 Mountains and TC Rainfall

The effects of Mountains on TC rainfall is an emerging field of intensive research. Diagnostic models for orographic precipitation have been proposed by previous studies. Sinclair (1994) has devised a simple model estimating orographic precipitation by determining topographically induced vertical motion, where condensation was assumed to arise due to saturated ascent. A study by Rostom and Lin (2021) has devised a modified Orographic Rain Index (ROI) as a predictor for heavy orographic TC precipitation in the Appalachian Mountains. In predicting local orographic precipitation, ROI considers the following factors: incoming horizontal wind speed, steepness of the mountain, relative humidity, TC movement speed, and TC horizontal scale (Rostom and Lin, 2021).

While topography may suppress precipitation due to numerous factors such as forced descent, flow blocking, vertical mixing, and depletion of atmospheric moisture, precipitation may be enhanced due to convection caused by terrain-induced ascent overcoming local convective inhibition (Kirshbaum et al., 2018). Using idealised simulations, Lin et al. (2016) report that landfall location and approach angle over mountain ranges affect

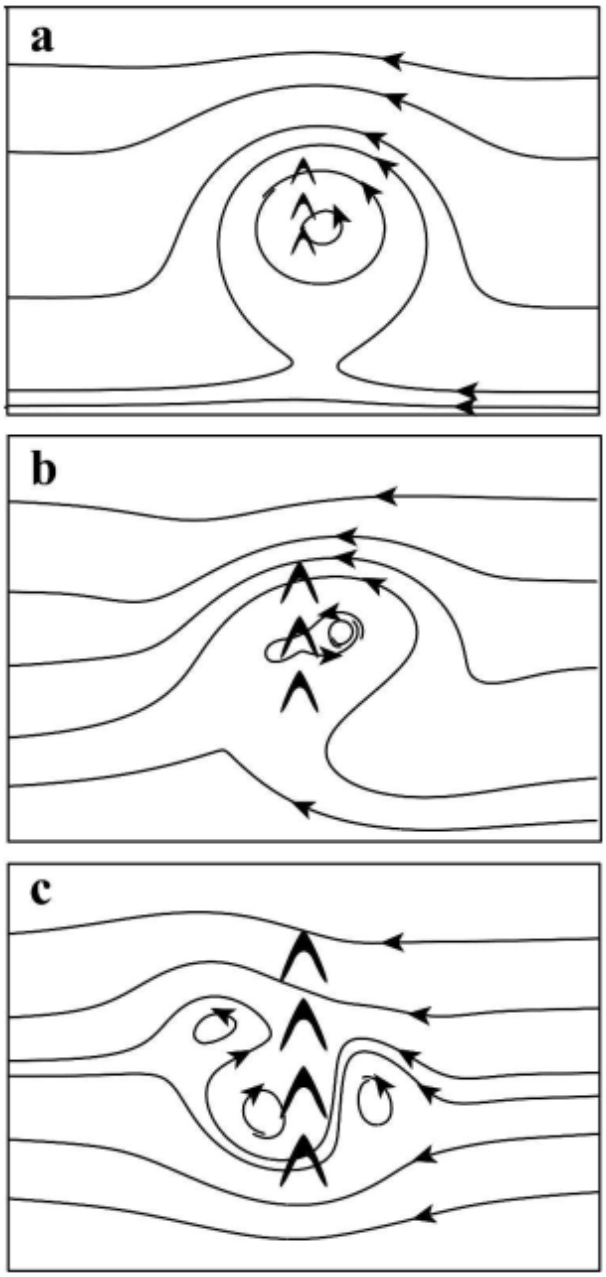

Figure 2.12: Conceptual model of the deflection of a westward moving cyclone for (a) weak blocking, (b) moderate blocking, and (c) strong blocking. Reproduced from Lin et al. (2005)

TC movement. This has profound effects on the spatial distribution of precipitation (Lin et al., 2016). Similarly, Liu et al. (2016) reported that TCs making landfall towards the north of the Appalachian Mountains tend to deflect due to strong vorticity advection around the northern region of the mountain range, while TCs making landfall towards the south experience weaker orographic blocking.

Precipitation simulations by Huang et al. (2020) reveal that for westbound TCs, rainfall along an idealised mountain rainfall during TC passage is highly sensitive to steering wind speed. As TCs cross the centre of a mountain range, stronger steering winds cause peak rainfall only along the southwestern slopes (i.e. windward) of the mountain (Huang et al., 2020). This implies that stronger oncoming winds tend to cross over the northeastern windward side of the mountain, causing higher amounts of rainfall as the winds flow back to the

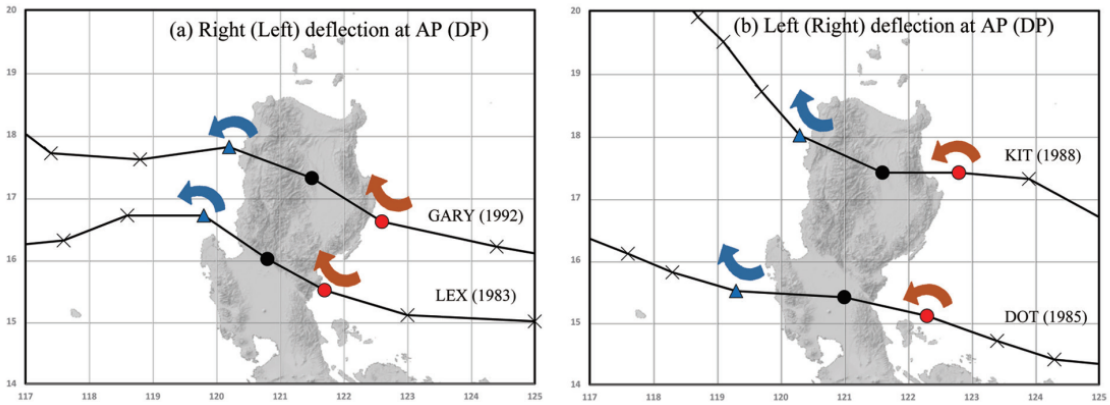

Figure 2.13: Observed (a) rightward deflection of TCs during landfall approach (AP) with leftward deflection upon exit (DP), and (b) leftward deflection during AP with rightward deflection upon DP. Reproduced from Man-chi and Chun-Wing (2015)

southwestern windward region.

However, case studies reveal that it is also important to consider local atmospheric environments in studying mountain-TC-rainfall interactions. For example Tang and Chan (2014) discusses that the difference in atmospheric environments between Taiwan and the Philippines result in different mechanisms for orographic TC precipitation. Besides having moister environments, the mountains of Luzon in the Philippines are much lower than the Central Mountain Range of Taiwan. This leads to a comparatively weaker TC track deflection when a TC passes over Luzon.

2.4 TCs and the Philippines

In this section, we briefly discuss TCs in the context of our study area, the Philippines. We first discuss the location of the Philippines with respect to the regional TC basins, the economic impacts of TCs on the country, anticipating extreme rainfall due to TCs, and orographic precipitation of TCs in the country. In the last subsection, we introduce our study area, the northern regions of the Philippines.

2.4.1 Impacts of TCs on the Philippines

The Philippines is in the southwestern portion of the WNP basin (Figure 2.2), the most active TC basin in the world (Sobel et al., 2021). As such, the country experiences many TCs every year. According to Cinco et al. (2016), an average of 9 TCs per year made landfall in the Philippines between 1951 and 2013.

Besides the wind hazards that these TCs pose, they also bring substantial rainfall to the country. Around 40% of the total yearly rainfall of Luzon, the northern region of the Philippines, is caused by TCs (Bagtasa, 2017). Rain from TCs is a very important resource to support Philippine agriculture, with 42.5% of the country's total land area dedicated to permanent crops and pastures (World Bank, 2022). However, while TCs bring much needed rain, extremely intense rainfall from TCs causes hazards such as floods, landslides, and debris

flows.

Landfalling TCs have significant impacts on the economy of the country. Cinco et al. (2016) previously reported that between 1971 and 2013, TCs cost the Philippines 440.5 billion Philippine Pesos (approximately 7.6 billion US Dollars in 2022) in total damages. One example of devastating TCs is Tropical Storm Ketsana in 2009, where gauge-recorded precipitation reached as much as 413 mm in nine hours, triggering exceptional floods causing 2 billion Philippine Pesos worth of property and infrastructure damage (Abon et al., 2011). The torrential rains of Super Typhoon Bopha of 2012 similarly caused widespread flooding and debris flows in the New Bataan municipality of Mindanao, immediately burying and killing 566 people (Rodolfo et al., 2016). In December 2017 two consecutive TCs, Tropical Storms Kai-Tak and Tembin, caused an unprecedented amount of rain in Visayas and Mindanao, the central and southern regions of the Philippines. According to Lagmay and Racoma (2019), Kai-Tak brought a total of 571.5 mm in three days; during the following week, Tembin brought 297 mm in a similar timespan. These two consecutive TCs caused flash floods and landslides with 91 confirmed deaths and 199 people missing in the Visayas and Mindanao (Lagmay and Racoma, 2019).

2.4.2 TC Precipitation in the Philippines

As such, anticipating and understanding extreme precipitation that TCs bring is of great importance and interest. To our best knowledge, no previous study has analyzed the statistical relationships between TC intensity or movement speed and precipitation in Luzon. Previous studies of Philippine TCs focused on long-term trends of TC activity (Cinco et al., 2016; David et al., 2013), impacts of the El Niño Southern Oscillation on inter-annual variability in TC activity (Corporal-Lodangco et al., 2016), precipitation enhancement due to TCs interacting with the monsoon (Bagtasa, 2019; Cayanan et al., 2011), the contribution of TC precipitation to total precipitation (Bagtasa, 2017), and case studies on the effect of topography on TC rainfall (Lagmay et al., 2015; Minamide and Yoshimura, 2014; Racoma et al., 2016).

Methods for predicting extreme rainfall and hydrological hazards associated with landfalling TCs still need improvement. Cheung et al. (2018) discusses Super Typhoons Nepartak and Meranti affecting China in 2016. These TCs had similar characteristics yet caused very different impacts. While both TCs had similar strengths and landfall locations, Nepartak only caused localised thunderstorms while Meranti caused widespread rainfall along the Taihu Lake Basin (Cheung et al., 2018). While some progress is being made in understanding the internal rainfall dynamics of TCs in forecasts through NWP models (Cheung et al., 2018), estimating incoming TC precipitation using NWP models remains computationally expensive. NWP models also exhibit biases and errors in predicting TC-related rainfall, resulting from limited horizontal resolution and errors in sub-gridscale physical parameterizations. For example, the Met Office NWP model shows significant dry biases in predicting TC-related precipitation over Luzon and Visayas (Peatman et al., 2019).

2.4.3 Orographic Precipitation in the Context of TCs and the Philippines

While orographic precipitation is a well-studied phenomenon, there is limited literature focusing on the orographic effect during TCs in the Philippines. In Racoma et al. (2016), we previously found that the distribution of TC rainfall in the Philippines is sensitive to the track of a TC. Different TC tracks may introduce varying windward sides which can result in different regions where precipitation is orographically enhanced (Racoma et al., 2016). While in Chapter 4 and Racoma et al. (2021), we investigated the overall statistical relationships between TC rainfall and TC characteristics (cyclogenesis, track, intensity), and other environmental factors such as environmental moisture and seasonality, it remains unclear what processes determine the TC precipitation patterns over land.

Previous studies of orographic precipitation of TCs in Asia focused on the effects of Taiwan's Central Mountain Range on TCs. One study suggests that in the case of Typhoon Morakot (2009), rainfall in the southwestern region of the Central Mountain Range was orographically enhanced and was proportional to the oncoming wind speed multiplied by the background precipitation (Yu and Cheng, 2013). Idealised studies revealed that higher wind speeds from TCs tend to produce higher amounts of rainfall towards the southern region of the Central Mountain Range in Taiwan (Huang et al., 2020).

A study by Tang and Chan (2014) used the WRF model to simulate the effects of the Central Mountain Range of Taiwan and the mountain ranges of Luzon, Philippines on incoming TCs. According to the aforementioned study, in Taiwan, TC tracks are deflected toward the North prior to landfall due to the asymmetric diabatic heating caused by the topography of the Central Mountain Range. However, Tang and Chan (2014) argued that not all mechanisms that occur in the Central Mountain Range are present in the Philippine mountain ranges due to the lower mountain height and moister air over the mountains on Luzon Island. The difference in environments and mechanisms the Philippines shows the need to further investigate the orographic precipitation of TCs in the Philippines.

2.4.4 Study Area

In this thesis, we focus on a region encompassing the northern and central parts of Luzon (hereafter referred to as Luzon). Figure 2.14 shows the topographic map of Luzon generated using elevation data from the NASADEM Merged DEM Global 1 arc second (or approximately 30 meters) dataset (NASA JPL, 2020). Luzon is located in the northern Philippines and is bordered by the CMR to the northwest (Figure 2.14a), the Zambales Mountain Range towards the southwest (Figure 2.14b), the Sierra Madre Mountain Range spanning north to south in the east (Figures 2.14c and 2.14d), and the volcanic region of Batangas towards the south. Due to its large land area and location, 20.2% of all TCs that form in the WNP basin cross the general region of Luzon (Cinco et al., 2016; David et al., 2013).

While the CMR induces monsoon blocking effects affecting precipitation over Luzon (Olaguera et al.,

2022), TCs contribute as much as 54% of precipitation along the western coast of Luzon (Bagtasa, 2017). Additionally, Luzon is where two major river basins of the Philippines are located, specifically within the boundaries of CMR. These river basins are the Cagayan River basin to the east and the Pampanga River basin to the south of the CMR. Due to TCs making landfall in the region, both river basins have experienced major flooding in recent years (Macalalad et al., 2021; Shrestha et al., 2014), and understanding how the CMR affects TC precipitation in Luzon, especially for stronger storms, will be helpful in regional flood forecasting efforts.

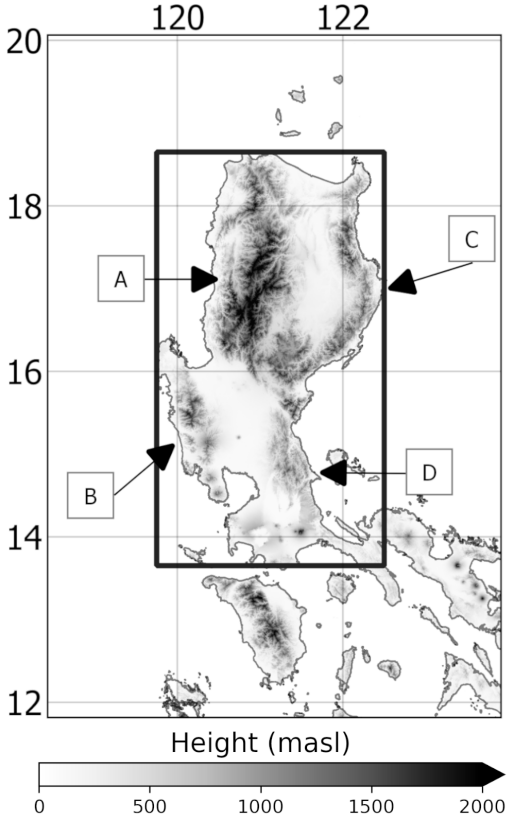

Figure 2.14: Topographic map of the Northern and Central Regions of Luzon with the black arrows indicating the general regions of (a) the Cordillera Central Mountain Range, (b) Zambales Mountain Range, and the (c) northern and (d) southern portion of the Sierra Madre Mountain Range. Darker shades show higher elevations (metres above sea level, masl). The study region is enclosed in the box. Elevation is taken from the NASADEM Merged DEM Global 1 arc second dataset (NASA JPL, 2020).

Chapter 3

Data and Methodology

3.1 Data

3.1.1 TC Best-Track Data

In evaluating historical TC characteristics, we use data from International Best Track Archive for Climate Stewardship (IBTrACS). IBTrACS collects historical tropical cyclone best-track data from all available agencies in a publicly available centralised repository (Knapp et al., 2010). The position, intensity, and minimum central pressure of TCs, as reported by different agencies, are combined using a series of algorithms described in (Knapp et al., 2010). While the database includes 6-hourly TC tracks ranging from as early as the 1800s, TC wind and intensity data are only available from 1978 onwards, with 3-hourly records available only in more recent years (Knapp et al., 2018; Racoma et al., 2021). As the Philippines is part of the WNP (as mentioned in Chapter 2.4, we use the Western Pacific subset of IBTrACS, taking the maximum sustained TC wind (averaged over 1 minute) data from the Joint Typhoon Warning Center (JTWC) data column. IBTrACS is available online via https://www.ncei.noaa.gov/products/international-best-track-archive?name=ib-v4-access.

3.1.2 Gridded Precipitation Data

Three different gridded precipitation datasets will be used in this study. Due to different resolutions and coverages, APHRODITE and TRMM will be used in the historical extreme precipitation analysis conducted in Chapter4, while IMERG will only be used for model evaluation in Chapter 5. A brief description for each dataset is outlined below.

3.1.2.1 APHRODITE

To evaluate TC-related precipitation in Chapter 4, we use data from Asian Precipitation – Highly-Resolved Observational Data Integration Towards Evaluation (APHRODITE) Monsoon Asia versions V1101 and V1101EX. APHRODITE offers daily gridded precipitation at a spatial resolution of 0.25° latitude/longitude between 1951 and 2007 for V1101, with V1101EX extending this to 2015 (Yatagai et al., 2012). The APHRODITE gridded data are derived by interpolating daily precipitation from a dense network of observation stations across Asia using an interpolation method that considers a region's climatology and topography to fill gaps between stations (Yatagai et al., 2012). APHRODITE is available via: http://aphrodite.st.hirosaki-u.ac.jp/.

3.1.2.2 TRMM

We also use precipitation data from Tropical Rainfall Measuring Mission 3B42, version 7, or hereafter referred to as TRMM, to validate results in Chapter 4. TRMM produces precipitation products by combining precipitation estimates from multiple satellites while verifying with in-situ measurements (Huffman et al., 2007). TRMM provides precipitation estimates every 3 hours at a spatial degree of 0.25° latitude/longitude resolution. While TRMM performs well in estimating daily precipitation in eastern Luzon, measurements below the threshold of 100mm are overestimated (Jamandre and Narisma, 2013). Hence, TRMM is only used for the purposes of validating APHRODITE with a higher temporal resolution dataset. TRMM data is available via: https://disc.gsfc.nasa.gov/datasets/TRMM_3B42_7/summary and published by Precipitation Processing System (PPS) At NASA GSFC (2018).

3.1.2.3 IMERG

To evaluate the model outputs in Chapter 5, we use rainfall estimates from the Integrated Multi-satellitE Retrievals for Global Precipitation Measurement (IMERG). IMERG builds upon TRMM, and offers high spatial ($10km \times 10km$) and temporal resolution (up to half-hourly) precipitation products derived from a multi-satellite platform (Hou et al., 2014; NASA Goddard Earth Sciences Data And Information Services Center, 2019). While IMERG does measure regional precipitation patterns well, it has large uncertainty in measuring precipitation over mountainous terrain due to numerous factors such as limitations in satellite-derived precipitation algorithms (Hsu et al., 2021; Pradhan et al., 2022). For this thesis, we will visually compare 24 hour precipitation accumulations of IMERG with 24 hour precipitation accumulations derived from the model output. IMERG is available online via https://doi.org/10.5067/GPM/IMERGDL/DAY/06 and published by NASA Goddard Earth Sciences Data And Information Services Center (2019).

3.2 Methodology

3.2.1 TC Selection Process and Rainfall Metrics for Chapter 4

3.2.1.1 TC Selection

From the IBTrACS, we select TCs between June and December to coincide with the peak TC occurrence months in the Philippines falling on two monsoon seasons. According to Cruz et al. (2013) the Southwest Monsoon (local name *Habagat*) typically lasts from June to September. On the other hand, the Northeast Monsoon (local name *Amihan*) lasts from October to March. We define landfall in this study as the TC point coming from the East and nearest to the coasts of Luzon. Figure 3.1 shows that the average monthly number of TCs making landfall in Luzon increases in June, decreases by August and September, increases again by October, and then finally tapers off by December. From this we then classify TCs into two seasons: June to September (JJAS) and October to December (OND). As there are few TCs making landfall between January and March, these were not included in this study.

We then select all TCs from the WNP that cross the study region (enclosed in box in Figure 2.14) with a generally westward direction (or a bearing between 180° to 360° angle from North) upon making first landfall on the eastern coast of Luzon north of 13.5°N. This also eliminates TCs that move eastward or stay across the region for longer periods due to the Fujiwhara effect where two cyclones interact and move around each other (Fujiwhara, 1923). Similarly, eastward-moving TCs originating in the South China Sea were also not included in the dataset. All of these were to create a homogeneous TC dataset with similar paths upon landfall in Luzon: originating from the WNP, crossing Luzon from an East to West direction, and then exiting through the South China Sea. The similar westward moving TC tracks reduces the possible uncertainties that discontinuous or dissimilar tracks may introduce in the dataset. As TC intensity data is only available starting 1978 and the APHRODITE record ends in 2015 we limit our TC selection between 1978 and 2015. A total of 127 TCs were included, with Figure 3.2 showing the TC track points one day (24 hours) before making landfall in red, one day after making landfall (including the earliest instance of landfall) in blue, as well as all the other TC points in grey.

3.2.1.2 Deriving Sub-daily TC-Related Precipitation Data from APHRODITE

According to Kubota and Wang (2009), on average, a TC's precipitation is mainly limited to a 1000 km radius from the TC center. Bagtasa (2017) also used a similar measure of radius of TC-induced rainfall at 10° latitude/longitude (∼1110 km). For the TCs selected in this study, the median distance between the nearest coast of Luzon and the TC points 24 hours before landfall is 205.73 km, while the median distance for TC points 24 hours after landfall is 46.32 km (Figure 3.2. This means for most TCs in this study, Luzon is well within the 1000 km range of a TC's radius of precipitation.

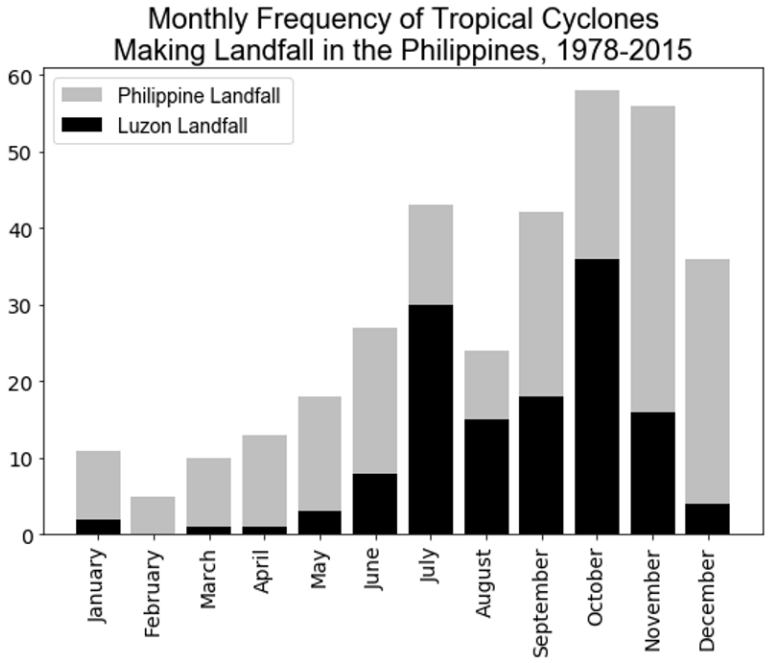

Figure 3.1: Total monthly number of TC landfalls in Luzon (black) and in the Philippines (black and grey combined) between 1978 – 2015. These are calculated from IBTrACS. Only westward travelling TCs are included.

Using APHRODITE, we calculate precipitation in Luzon (between 13.00 - 18.65°N and 119.75 - 122.50°E) for each TC by collecting the 48 hours of TC points centered on the first landfall (red and blue points in Figure 3.2) to account for TC-associated rain from rainbands before and after landfall. The date of each 3-hourly TC point was then matched with their corresponding daily APHRODITE precipitation. To account for a TC spanning different dates during the 48 hours (and hence different daily APHRODITE precipitation fields), daily APHRODITE precipitation for each grid point was converted to 3-hour values by assuming uniformly distributed precipitation within the day (hereafter referred to as $APHRO_{uniform}$). Afterward, the total precipitation over Luzon for the 48 hours centered on TC landfall is accumulated from the 3-hour values.

As $APHRO_{uniform}$ is derived from a daily precipitation dataset, it is possible there is a reduction of the signal of extreme precipitation by assuming a uniformly distributed precipitation throughout the 48-hour period. Due to this limitation, the higher temporal resolution 3-hourly precipitation records of TRMM 3B42, version 7, hereafter $TRMM_{3hr}$, was also included in this study. However, as $TRMM_{3hr}$ is only available between 1998-2019, this considerably reduces the number of TCs that we can analyse from 127 to 75.

To consider the uncertainty in TC-related precipitation due to difference in temporal resolutions, we evaluated three precipitation datasets: $APHRO_{uniform}$, $TRMM_{uniform}$ (derived from the daily TRMM 3B42, version 7), and $TRMM_{3hr}$. $TRMM_{uniform}$ was calculated similarly to $APHRO_{uniform}$ by uniformly distributing the 48-hour accumulated precipitation over Luzon in 3-hourly segments. For $APHRO_{uniform}$, $TRMM_{3hr}$, and $TRMM_{uniform}$, precipitation was calculated by accumulating precipitation for the 48-hour period centered on TC landfall for each TC in 1998-2015 (totaling to 51 TCs). Afterward, the mean precipitation across the grid was taken to compare the datasets.

We see from Figure 3.3 that while $TRMM_{uniform}$ yields higher precipitation than $APHRO_{uniform}$, the

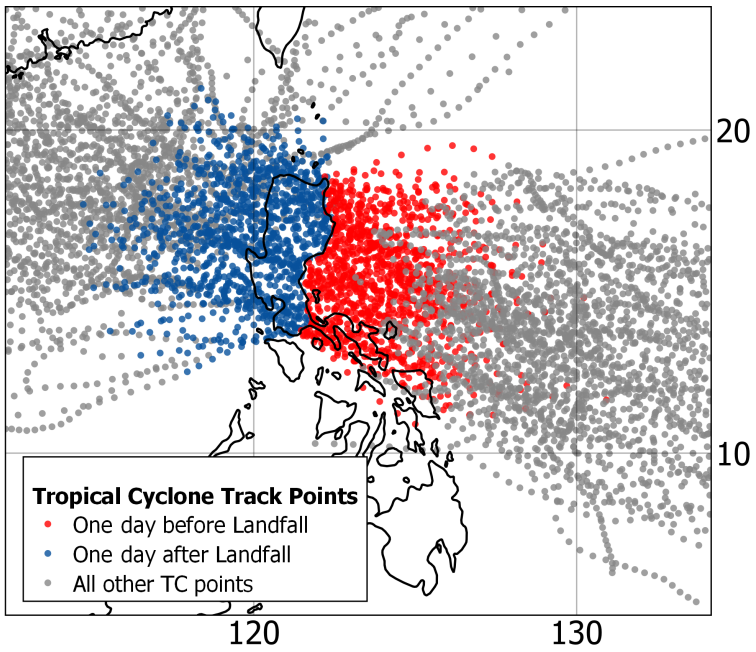

Figure 3.2: Three-hourly track points of TCs included in this study, with the points one day before landfall in red, one day after landfall (starting at time of landfall) in blue, and all other points in grey. Data are from IBTrACS.

two datasets are positively correlated ($r = 0.73$, $P < 0.001$) with a slope of 1.52. Consistent with the results of Jamandre and Narisma (2013), TRMM, in general, tends to yield higher estimates compared to APHRODITE. As such, as long as the difference in magnitude is considered, this shows that both daily datasets behave similarly in terms of measuring precipitation for TC events.

We then compared 48-hour precipitation derived from the same data source recorded at different time intervals: $TRMM_{3hr}$ with $TRMM_{uniform}$. It can be seen from Figure 3.4 that $TRMM_{3hr}$ and $TRMM_{uniform}$ show a statistically significant positive correlation ($r = 0.99$, $P < .001$) with a slope of 1.08. $TRMM_{uniform}$ is also biased towards the lower range, with the lower precipitation estimates of $TRMM_{uniform}$ much nearer to the values of $TRMM_{3hr}$. As the values of $TRMM_{3hr}$ on average are only 5% higher than $TRMM_{uniform}$, we believe that assuming a uniformly distributed precipitation throughout the day for a daily dataset does not significantly reduce the signal for the occurrence of extreme precipitation.

The previous analysis shows that while some signals for extreme precipitation are indeed reduced in a uniformly distributed daily dataset thus, increasing uncertainty, it is still acceptable for use in our study. Similarly, besides significantly reducing the number of TCs included, using $TRMM_{3hr}$ in our analysis did not affect our observations and conclusions. While we continued to use APHRODITE to ensure that we are able to analyse a higher number of TCs, for the purposes of completeness and comparison we also proceeded with calculations of extreme precipitation using $TRMM_{3hr}$.

Bowman and Fowler (2015) reports a detectable diurnal variation of TC precipitation. Thus, we initially considered diurnal adjustments to the 3-hour APHRODITE precipitation. However, previous studies on the diurnal precipitation of TCs mostly focused on TCs over the ocean (Leppert and Cecil, 2016; Rios Gaona and Villarini, 2018; Wu et al., 2015). While Nesbitt and Zipser (2003) reported a marked afternoon rainfall

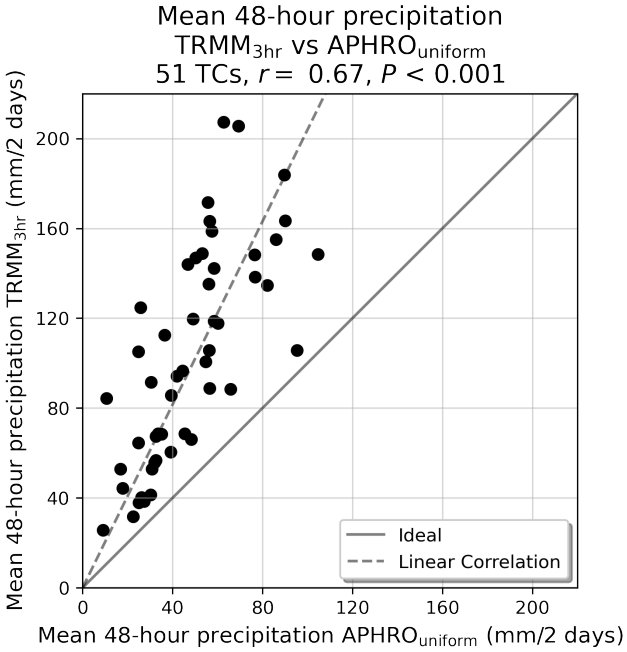

Figure 3.3: Comparison between mean 48-hour accumulated precipitation over Luzon derived from $TRMM_{uniform}$ and $APHRO_{uniform}$. The solid line shows an ideal 1:1 correspondence, while the dashed line shows the correlation.

maximum for TCs over land, according to idealized studies by O'Neill et al. (2017), the weakening of TCs upon making landfall further complicates establishing this diurnal cycle. We tested a simple diurnal scheme, with a sinusoidally varying adjustment up to 30% of the daily mean, but this did not affect our conclusions. Based on that result, and the uncertainty in observation-based estimates of TC diurnal rainfall variability, we continued to assume uniformly distributed precipitation throughout the day.

3.2.1.3 The Weighted Precipitation Exceedance

While taking the mean TC-associated precipitation across grid points in Luzon is useful to measure rainfall volume, this does not necessarily represent extreme precipitation. Given the same area coverage, mean precipitation is sensitive to the spatial distribution of precipitation, particularly when high and focused precipitation is observed in a small region while little precipitation is recorded elsewhere. Rather than directly taking the mean precipitation, we calculate precipitation for each TC event against an extreme precipitation threshold. To establish this threshold, we adapt extreme precipitation as defined by Diffenbaugh et al. (2005), Guo et al. (2017), and Kim et al. (2019) by calculating a 2-day 95^{th} percentile precipitation map using all 2-day windows with recorded rainfall ($precipitation > 0$) from June to December in 1978-2015. Any 2-day accumulated precipitation that exceeds this local 95^{th} percentile threshold is considered *extreme precipitation*.

From the extreme precipitation threshold, we then evaluated the Weighted Precipitation Exceedance, or WPE, for each of the TCs affecting Luzon. WPE is defined as the area mean of precipitation over Luzon that exceeds the local 95^{th} percentile threshold (total precipitation minus 95^{th} percentile threshold). Grid cells where precipitation does not exceed the 95^{th} percentile (negative differences) are set to zero for the WPE

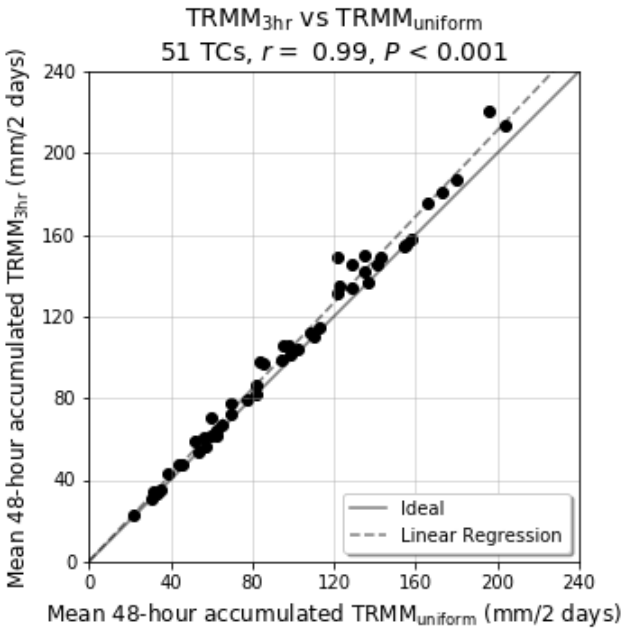

Figure 3.4: Similar to Figure 3.3 but for $TRMM_{3hr}$ and $TRMM_{uniform}$

calculation. This gives us a single value that reflects both the magnitude and spatial extent of the TC-associated precipitation that exceeds the 95^{th} percentile. Due to the nature of the WPE calculation, any TC with positive WPE exceeds the 95^{th} percentile threshold in at least some locations and, as such, is considered to produce extreme precipitation.

Figure 3.5 shows Typhoon Xangsane as an example to illustrate how WPE is calculated. Typhoon Xangsane was a particularly intense (1-minute maximum sustained wind speed of 89 knots) TC that brought strong winds along with high amounts of rain in the Philippines, leaving 26 dead and 17 Million USD (in 2001 currency) worth of property and crop damage in its wake (Emerald Group Publishing Limited, 2001). Figure 3.5a shows the accumulated 2-day precipitation during Typhoon Xangsane's landfall in Luzon (from 2000-10-27 06z to 2000-10-29 06z) while Figure 3.5b shows the 95^{th} percentile precipitation threshold for all 2-day windows with precipitation in the months of July to December for the years 1978-2015. The WPE of this TC is calculated by subtracting the precipitation threshold (Figure 3.5b) from the Typhoon's 2-day precipitation (Figure 3.5a), and the exceedance is shown in blue in Figure 3.5c. The area-weighted mean of all exceedances (including zeroes) is taken, and the calculated WPE for this TC is at 61.00 mm/2 days.

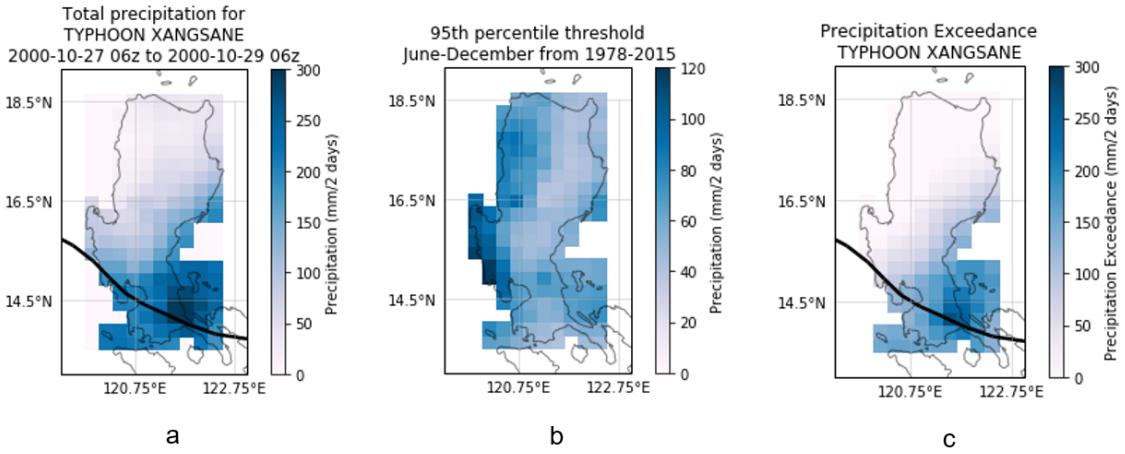

Figure 3.5: Using APHRODITE, from the (a) accumulated precipitation for 48 hours centered on landfall for Typhoon Xangsane we subtract the (b) 95^{th} percentile threshold to get the (c) precipitation exceedance with gridpoints where the precipitation does not exceed the threshold are set to zero. WPE is then calculated by taking the area. mean of the exceedance. Note that the precipitation scales for all three panels are different. The track for this TC is shown in solid black lines, and the WPE for this TC is 61.00 mm/2 days.

3.2.2 The Weather Research and Forecasting (WRF) Model and Experimental Setup for Chapter 5

3.2.2.1 The WRF Model

We used the WRF model version 3 (Skamarock et al., 2008) to investigate the effects of the CMR located in Luzon, Philippines on the precipitation and characteristics of high WPE TCs. A summary of the options used are listed in Table 3.1. Choices of physical parametrization schemes and model configuration were adapted from Delfino et al. (2022), which conducted sensitivity tests for TC simulations in WRF. Additionally, we adapted the Planetary Boundary Layer scheme based on the study of Cruz and Narisma (2016) due to its performance in simulating heavy precipitation over Luzon. The European Centre for Medium-Range Weather Forecasts Reanalysis fifth generation (ERA5) (Hersbach et al., 2020) data are used as the initial and boundary conditions for the WRF model. We defined two nested domains with horizontal grid spacings of 15 km and 5 km (Figure 3.6). The outer domain was configured to resolve the genesis and development of a TC over the Pacific Ocean, while the inner domain was configured to simulate precipitation over the Philippines. For the model runs, the "adaptive time-step" option of WRF was enabled, and the model output was set at 3-hourly intervals. To allow for model spin up within the domain, simulations were initialised at 96 hours before TC landfall and ended at 24 hours after landfall.

Number of Domains	Two
Horizontal Grid Spacing	15 km (outer), 5 km (inner)
Cumulus Parametrization	Kain-Fritsch Scheme
Microphysics	WRF Single-Moment 6-class microphysics scheme
Planetary Boundary Layer	ACM2 scheme
Longwave Radiation	Rapid Radiative Transfer model scheme
Shortwave Radiation	Dudhia scheme
Surface Physics	Unified Noah land-surface model
Model time-step	Adaptive time-step
Initial and Boundary Conditions	ERA5

Table 3.1: Summary of selected WRF configuration schemes.

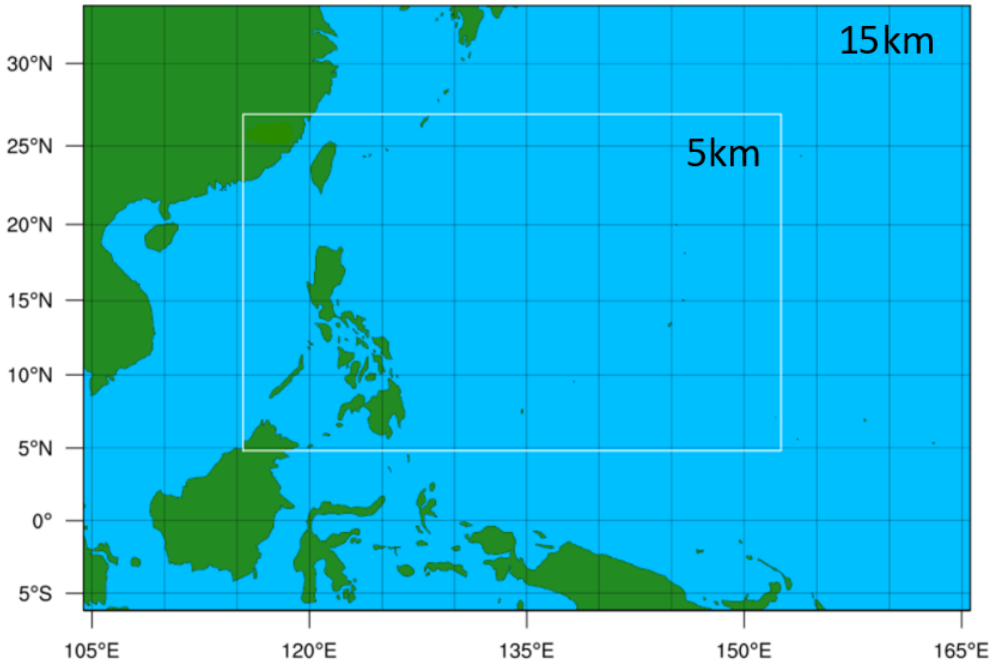

Figure 3.6: The two-way nested model domains, with the outer domain at 15 km resolution, and the inner domain at 5 km.

3.2.2.2 Isolating and Modifying the CMR

We then modified the orography of the CMR (the main mountain range within the red region enclosed in Figure 3.7) in the sensitivity experiments of WRF simulations. The general boundaries and location of CMR were identified by first manually enclosing the mountain range in rectangles and then isolating regions greater than 400 metres above sea level (masl). Besides the original orography (Control, Figure 3.7a), the elevation of the CMR was set to zero in the Flat experiment (Figure 3.7b) either reduced by a factor of two in the Reduced experiment (Figure 3.7c), and enhanced by a factor of two in the Enhanced experiment (Figure 3.7d). The edges of the modified orography were also smoothed along the perimeter so as not to introduce large deviations between the modified CMR and its neighbouring regions. This was done by extending the identified CMR boundaries 4 pixels (or 20 km) outward, and then applying a smoothing factor of 1.5 for Enhanced, and 0.75 for Reduced and Flat. While any smoothing factor can be applied, the selected factors were sufficient for the

purposes of this study.

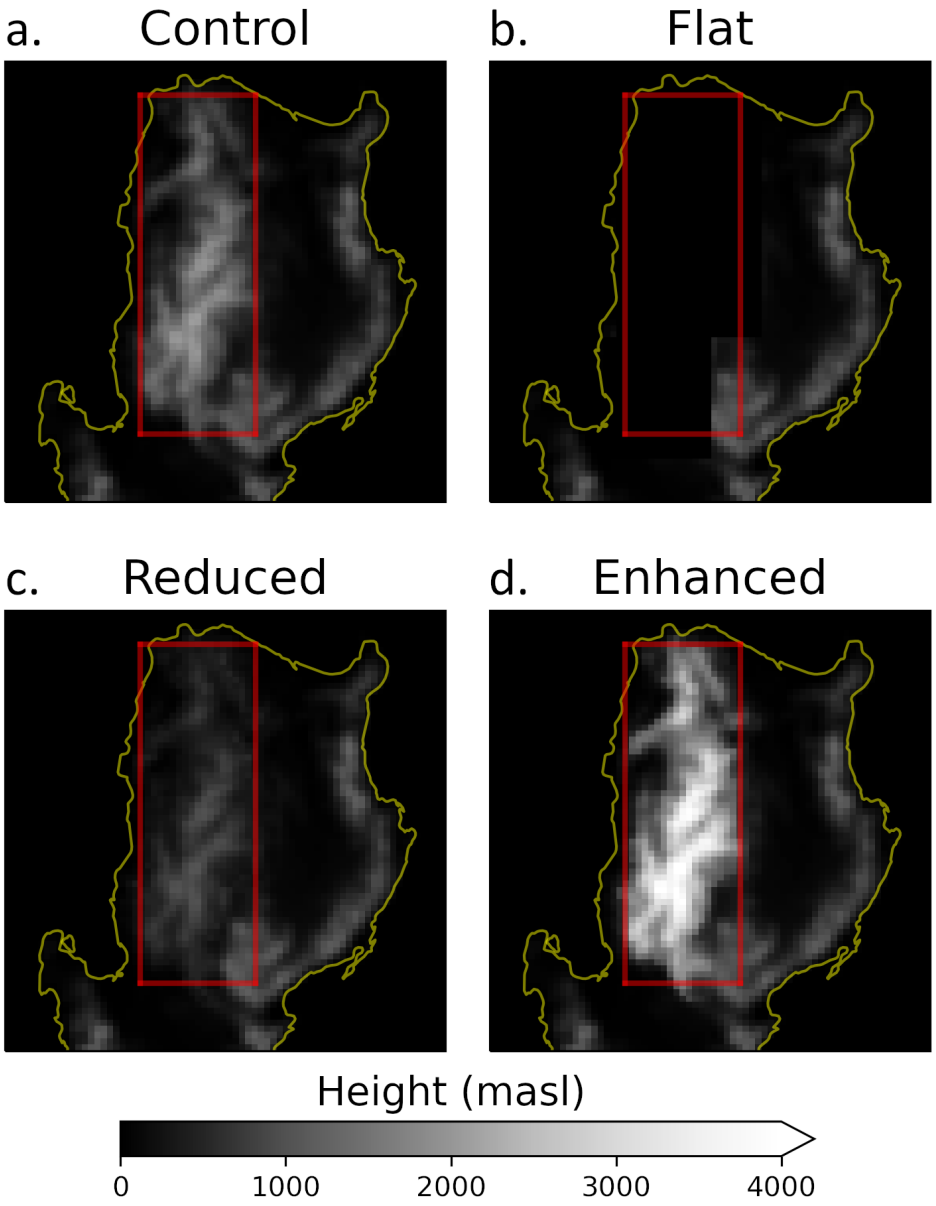

Figure 3.7: The orographic height (masl) for (a) Control, (b) Flat, and (c) Reduced, and (d) Enhanced orography experiments. CMR is enclosed in the red box.

Chapter 4

Tropical Cyclone Characteristics Associated with Extreme Precipitation in the Northern Philippines

In this Chapter, we discuss our findings in answering the first objective of this thesis, which is to determine which TC characteristics are associated with extreme precipitation in Luzon. This part of the thesis was motivated by the need to quantify the relationships between TC characteristics, such as intensity, movement speed, and season, and how we can anticipate incoming TC precipitation based on these characteristics. We do this by comparing the characteristics of 127 TCs that made landfall in Luzon with their associated extreme precipitation. The complete methodology for evaluating extreme precipitation through the Weighted Mean Precipitation Exceedance (WPE) was previously discussed in Section 3.2.1.3.

We first establish the seasonal variability of TC precipitation, tracks, intensity, and cyclogenesis in Section 4.1. In Section 4.2, we compare TC characteristics with mean precipitation and WPE. We also group TCs into categories based on intensity, season, and movement speed to allow us to compare inter-storm WPE between conveniently identifiable categories in a more probabilistic manner (Section 4.2.2). From a generated comprehensive database of WPE associated with different TC categories, we then establish a decision table in which we can rapidly estimate an incoming TC's possible precipitation over Luzon based on TC pre-landfall characteristics (Section 4.3). As precipitation data used in this part of the study was derived from APHRODITE, a daily dataset, we validated these results with TRMM, a higher temporal resolution precipitation dataset (Section 4.4). This chapter highlights the importance of considering a combination of pre-landfall TC characteristics to anticipate extreme precipitation in Luzon. Along with the methodology outlined in Section 3.2.1, results in this

section are published in Racoma et al. (2021).

4.1 Tropical Cyclone Characteristics and Precipitation Between the Philippine Seasons

4.1.1 TC Precipitation and Tracks

Figure 4.1 shows the seasonal mean 2-day precipitation and the mean precipitation during the 2 days centered on the time of Luzon landfall, as well as the TC tracks for JJAS and OND. According to Akasaka et al. (2007), the western region of the Philippines has a distinct rainy season starting in the middle of May, peaking in August, and withdrawing towards early November. This can be seen in the higher precipitation regions towards the west in JJAS (Figure 4.1a). Westward moving TCs that make landfall in Luzon during JJAS (Figure 4.1c) tend to cause more precipitation towards western Luzon, particularly the western flanks of Cordillera Central with higher amounts along the Zambales Mountain Range in the southwest (Figure 4.1b). This spatial distribution of landfalling TC-related precipitation is similar to the seasonal mean during JJAS, albeit with much higher magnitudes. It is also consistent with the spatial distribution of TC-contributed rainfall in Bagtasa (2017), where TCs contribute as much as 50% of precipitation in western Luzon. The interaction between the monsoonal flow and TCs also results in enhanced convergence and ascent, leading to increased precipitation in western Luzon (Cayanan et al., 2011).

In contrast, mean 2-day precipitation in OND is generally lower than in JJAS, except for higher amounts of rain towards the eastern portion of the southern Sierra Madre Mountain Range (Figure 4.1d). Akasaka et al. (2007) notes that eastern Luzon experiences maximum rainfall in autumn and winter (starting from October) marked by the abrupt change from westerly to easterly winds around the Philippines. This eastward shift along with generally lower amounts of precipitation can also be attributed to the change from southwesterly moist flow from the Indian Ocean in summer to northeasterly cooler and drier air from the subtropical Pacific during winter (Yihui and Chan, 2005). Landfalling OND TCs tend to bring precipitation to otherwise climatologically drier regions of Luzon. These TCs also cause higher precipitation in a much wider area further to the north compared to the seasonal mean precipitation during OND. This increase in precipitation is more evident, especially towards the eastern flanks of the CMR and the northern portion of the Sierra Madre Mountain Range (Figure 4.1e). Compared to of JJAS TCs which tend to make landfall and track towards the northern region of Luzon (Figure 4.1c), OND TCs tend to make landfall near the central portion of Luzon and then continue to move westward (Figure 4.1f).

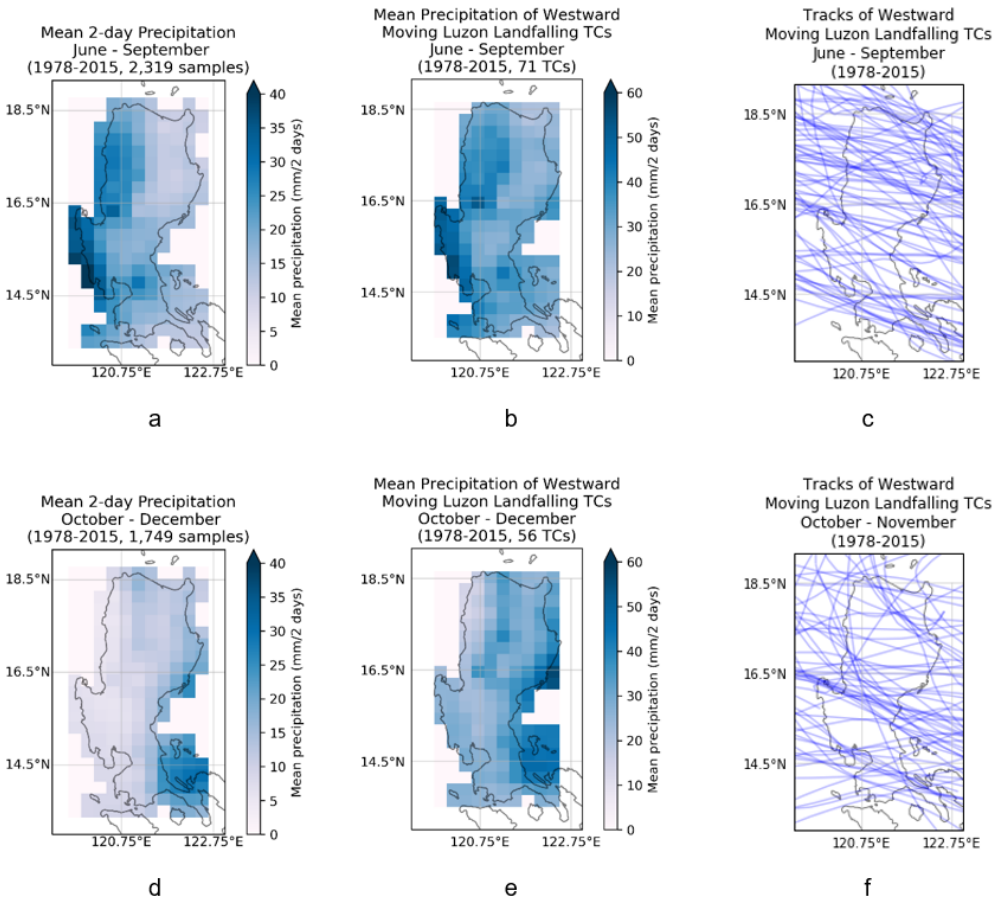

Figure 4.1: The first row shows JJAS (a) seasonal mean 2-day precipitation, (b) 2-day mean precipitation for westward moving Luzon landfalling TC, and (c) TC tracks. The second row shows OND (d) seasonal mean 2-day precipitation, (e) 2-day mean precipitation for westward moving Luzon landfalling TC, and (f) TC tracks. Precipitation is calculated from APHRODITE with scales ranging from 0 to 40 mm/2 days for the seasonal means and from 0 to 60 mm/2 days for the landfalling TC precipitation means. TC tracks in blue lines are from IBTrACS.

4.1.2 TC Intensity and Cyclogenesis Locations

Before evaluating extreme precipitation for each TC, we first look at the characteristics of TCs between JJAS and OND one day before landfall (or pre-landfall). We compared the pre-landfall movement speed between JJAS and OND TCs (Figure 4.2a) as well as the pre-landfall intensity between the two seasons (Figure 4.2b) using a Kruskal-Wallis test (Kruskal and Wallis, 1952) at a significance level of $\alpha = 0.05$. There is no significant difference in the pre-landfall movement speed of TCs between JJAS and OND ($P = .62$), while OND typically has TCs with higher pre-landfall intensities ($P < 0.001$). The difference in TC intensities between the seasons is likely explained by the cyclogenesis locations of TCs, which may lead to more time for TC intensification. From all TCs in the region in JJAS (Figure 4.3a) and OND (Figure 4.3b), with a median cyclogenesis longitude of 135.45°E, TCs that make landfall in Luzon during JJAS (Figure 4.3c) tend to form nearer the coasts of the Philippines compared to those of in OND that form at a further median cyclogenesis longitude of 142.33°E, towards the central portion of the WNP basin (Figure 4.3d). This is consistent with Corporal-Lodangco and Leslie (2016), in which TC formation clusters further to the southeast during winter due to the monsoon trough shifting further to the east and the western Pacific subtropical high extending further

west towards the South China Sea (Chia and Ropelewski, 2002; Xiang et al., 2013). In addition, we found that TCs that have longer durations between cyclogenesis and landfall have higher intensities (Figure 4.4). Comparing the median time between cyclogenesis to landfall of TCs in JJAS and OND, the median time of OND TCs is significantly higher at 142.5 hours compared to JJAS TCs with a median time of 117 hours ($P = .0059$). As such, TCs that make landfall in Luzon in OND may be stronger because they stay over the ocean longer, which allows for further TC intensification.

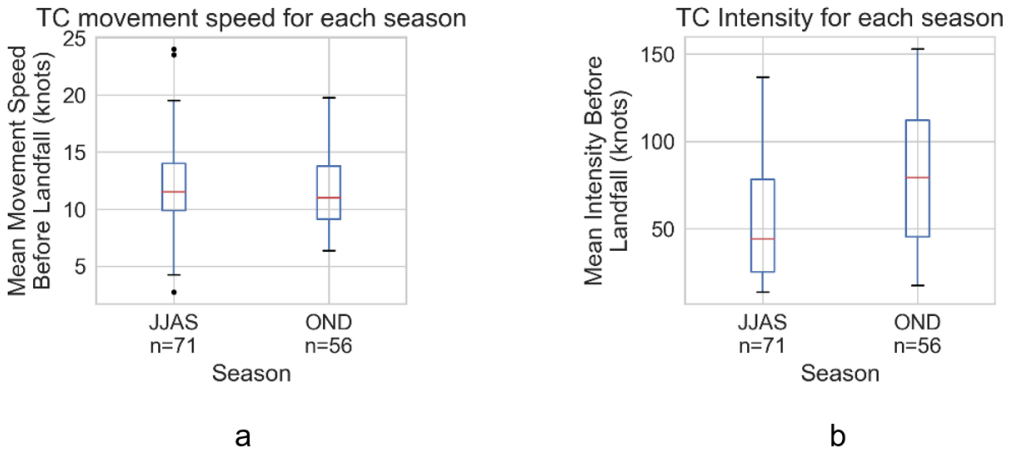

Figure 4.2: (a) 1-day Mean TC movement speed before landfall for JJAS and OND, (b) 1-day Mean TC intensity before landfall for JJAS and OND. These boxplots show the median (red line) and the interquartile range (IQR) at 25^{th} percentile ($Q1$) and 75^{th} percentile ($Q3$) (upper and lower boundaries of the box). The whiskers show the spread of the data, with lower whiskers showing the minimum, and upper whiskers showing the maximum calculated as $1.5 \times IQR + Q3$. Any values beyond the upper whisker are plotted as outliers (black dots).

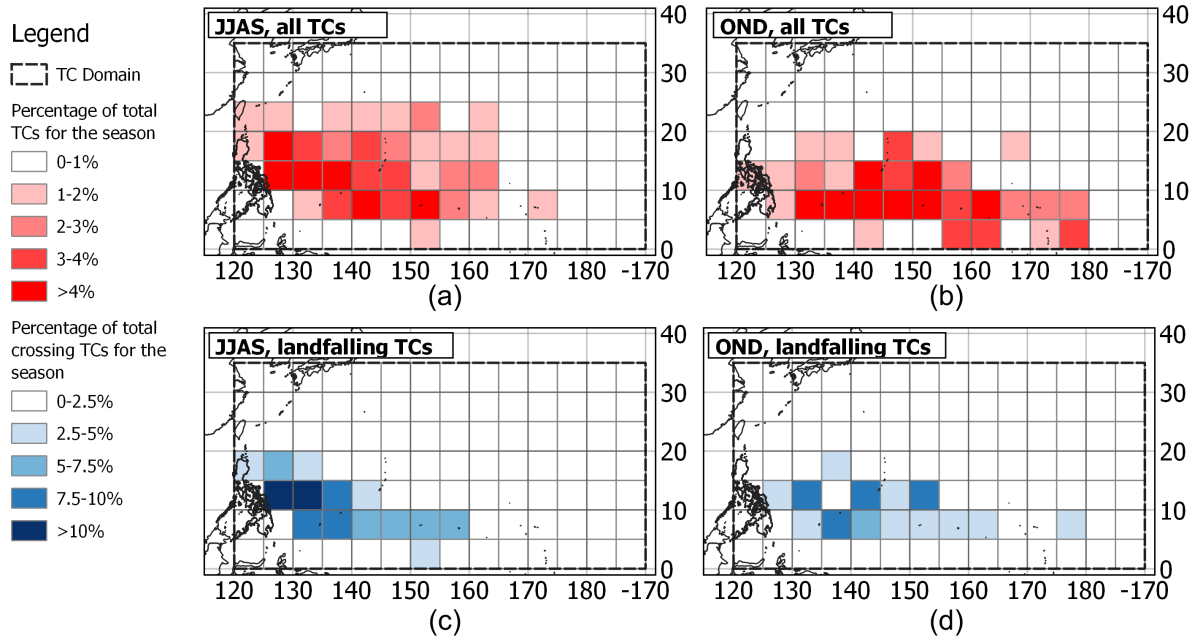

Figure 4.3: The top row shows the density of TC cyclogenesis locations in the domain for (a) TCs in JJAS and (b) TCs in OND, as a percentage of all TCs in that season between 1978 to 2015. The bottom row shows the cyclogenesis densities for (c) TCs that make landfall in Luzon in JJAS and (d) TCs that make landfall in Luzon in OND, within the same period. The percentages are calculated by dividing the number of TCs that originate in each 5° x 5° grid by the total number of TCs in the season (top row) and from the total number of TCs that make landfall (bottom row).

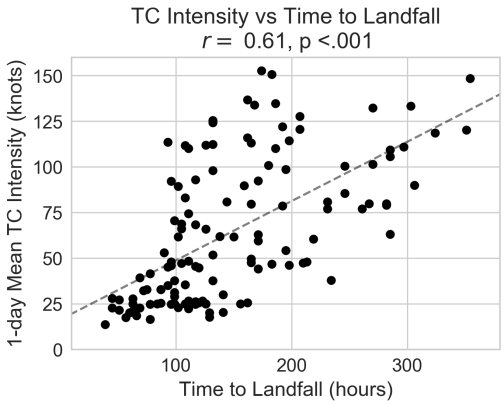

Figure 4.4: TC intensity before landfall compared to time from TC cyclogenesis until landfall in Luzon. The dashed line shows the least-squares regression slope for each relationship. The Pearson correlation coefficient (r) and P-value (p) are listed above each plot.

4.2 TC Characteristics Compared to Precipitation

4.2.1 TC Intensity and TC Movement Speed compared to Mean Precipitation and WPE

We then examine the relationship between the mean precipitation across Luzon during the 2 days centred on landfall and the pre-landfall TC characteristics for all TCs. For the purposes of this study, for all statistical analysis we consider the threshold value of $P = 0.05$. While we initially considered calculating for the maximum velocity, or v_{max}, we opted for the mean TC intensity to represent the average TC characteristics, as TCs exhibit rapid fluctuations prior to landfall. Additionally, these characteristics were compared to 2-day precipitation means to take into account TC precipitation prior to landfall and after landfall to take into account the impact of the TC before and after it crosses land.

The 1-day mean TC intensity compared to the 2-day mean precipitation is shown in Figure 4.5a while the comparison for the 1-day mean TC movement speed is shown in Figure 4.5b. There is a significant ($P < .001$), moderate positive relationship ($r = 0.37$) between mean precipitation and TC intensity. There is also a very weak negative correlation ($r = -0.14$) between mean precipitation and TC movement speed ($P = .125$). These show that TCs that are strong before landfall may produce more mean rainfall than weaker TCs, while there is not sufficient evidence to conclude that the movement speed of TCs before landfall has a linear relationship with mean precipitation after landfall.

We then proceeded to compare TC characteristics with the Weighted Mean Precipitation Exceedance (WPE), a measure of extreme precipitation that considers both the magnitude and spatial extent of extreme TC-associated precipitation. As discussed in Section 3.2.1.3, WPE is calculated by taking the difference between TC-precipitation with the local 95^{th} percentile precipitation threshold over Luzon, and then multiplying the difference by the spatial extent of precipitation. Figure 4.6 shows the distribution of WPE for all TC cases included in this study. The median WPE of all the 127 TCs is 12.84 mm/2 days, while the mean is 23.24 mm/2 days. Although the distribution is positively skewed, most TCs that make landfall in Luzon (94.49%) have a

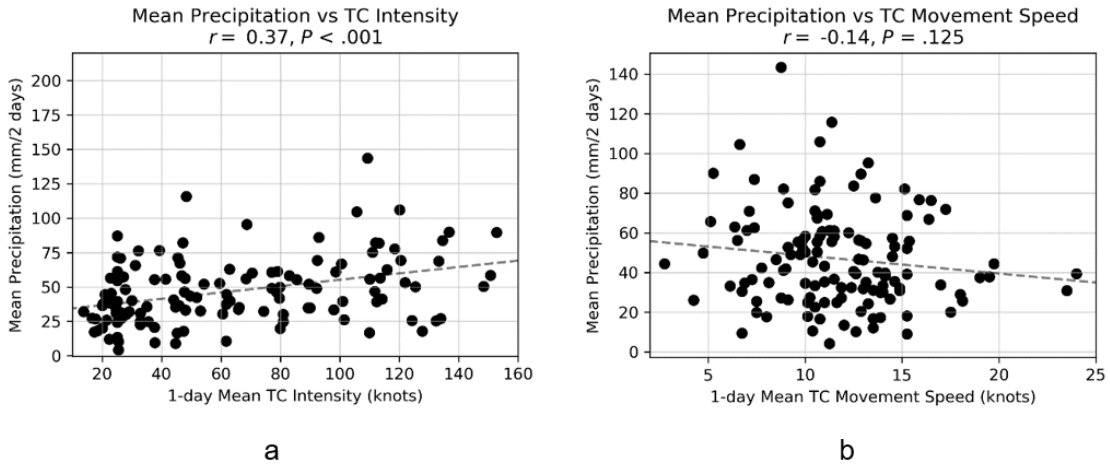

Figure 4.5: Similar to Figure 4.4 but for mean precipitation 2-days centred on landfall vs (a) 1-day mean TC intensity before landfall and (b) 1-day mean TC movement speed before landfall, for 127 TCs that made landfall in Luzon between 1978 and 2015.

non-zero WPE. Thus, many of the TCs produce extreme rainfall, as the TC-associated precipitation exceeds the 95th percentile threshold for at least one grid point in Luzon.

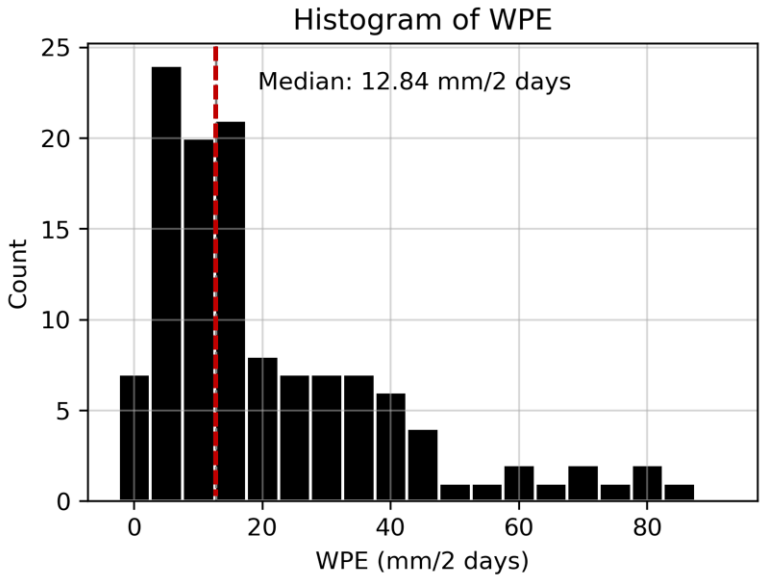

Figure 4.6: The histogram of WPE for all TC cases. The leftmost bin includes only zero WPE values, and the dashed red line shows the median WPE of 12.84 mm/2 days

Next, we compare WPE against pre-landfall TC intensity (measured by TC maximum wind speed) in Figure 4.7a and pre-landfall movement speed in Figure 4.7b. While stronger TC winds do not necessarily cause stronger precipitation, at $\alpha = 0.05$, WPE has a significant moderate positive relationship with intensity ($r = 0.32$, $P < .001$) and a non-significant weak negative correlation with movement speed ($r = -0.14$, $P = .059$). Fitting a logarithmic relationship (not shown) between WPE and movement speed also does not yield significant results ($r = -0.14$ and $P = 0.26$). This shows that stronger TCs may pose additional risks due to a combination of stronger winds and higher amounts of precipitation. However, as the relationships are not especially strong and there is clearly a substantial amount of inter-storm WPE variance that is not

explained by either intensity or movement speed, we decided to group TCs in categories to show likelihood of higher WPE. While this may not explain the variance, this allows us to compare inter-storm WPE between conveniently identifiable categories in a more probabilistic manner. These categories will be discussed in the next subsection.

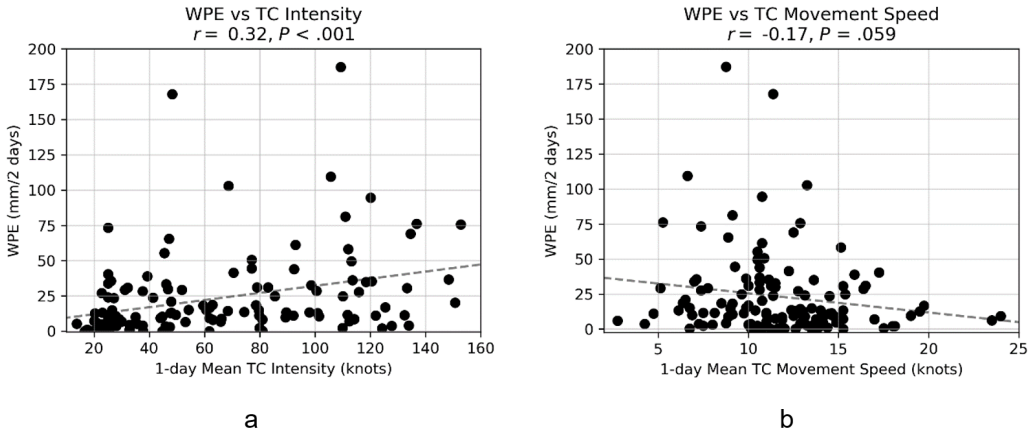

Figure 4.7: Similar to Figure 4.4 but for WPE 2 days centered on landfall vs (a) 1-day mean TC intensity before landfall and (b) 1-day mean TC movement speed before landfall.

4.2.2 TC Characteristics Categories compared to WPE

As mentioned in the previous Section, relationships between TC precipitation and movement speed or intensity were not as apparent. Thus, we grouped TCs into different easily identifiable categories based on intensity, movement speed, and season. We grouped according to TC intensity based on the Saffir-Simpson Hurricane Wind Scale (The Saffir-Simpson Team, 2021), where TCs with 1-minute averaged maximum sustained TC wind speeds above 64 knots were categorised as Typhoons (TY), and as Non-Typhoons (Non-TY) otherwise. The groups and threshold for movement speed was simply calculated from the median movement speed of the TCs in the dataset. Finally, TCs were categorised TCs according to seasons they made landfall, based on the monsoon months JJAS or OND, which we previously introduced in Section 3.2.1.1.

Table 4.1 shows the TC counts for the different categorisations. From all landfalling westward moving TCs in Luzon, 72 (or 57% of TCs) are Non-Typhoons (Non-TY) and 55 (or 43%) are Typhoons (TY). This is consistent with the results of Cinco et al. (2016) where they report that more Non-TYs than TYs make landfall. We used the median pre-landfall movement speed of TCs of 11.38 knots to categorise TCs as Slow or Fast. Finally, while there are more TCs in JJAS (71) than in OND (56), their monthly frequencies are similar at 17.75 and 18.67 TCs per month, respectively.

For all following comparisons between categories, Kruskal-Wallis tests were conducted to test the difference between the median of the populations at a significance level of $\alpha = 0.05$. Figures 4.8a and 4.8b show boxplots that compare WPE between TC movement speed and intensity categories, while Figure 4.8c compares WPE between seasons. Figure 4.9, on the other hand, shows boxplots that compare WPE for combined categories, particularly for intensity and movement speed (Figure 4.9a), season and intensity (Figure 4.9b), and

Intensity Classification		
Category	**Intensity**	**Total TCs**
Non-TY	$< 64\,knots$	72
TY	$\geq 64\,knots$	55
Movement Speed Classification		
Category	**Movement Speed**	**Total TCs**
Slow	$< 11.38\,knots$	63
Fast	$\geq 11.38\,knots$	64
Season Classification		
Category	**Total TCs**	
JJAS	71	
OND	56	

Table 4.1: Total counts of TCs for the three different categorisations. The intensity categorisation is based on a threshold of 64 knots to separate Non-TYs and TYs. TCs are also categorised according to movement speed based on the median of 11.38 knots, and finally, according to season.

season and movement speed (Figure 4.9c).

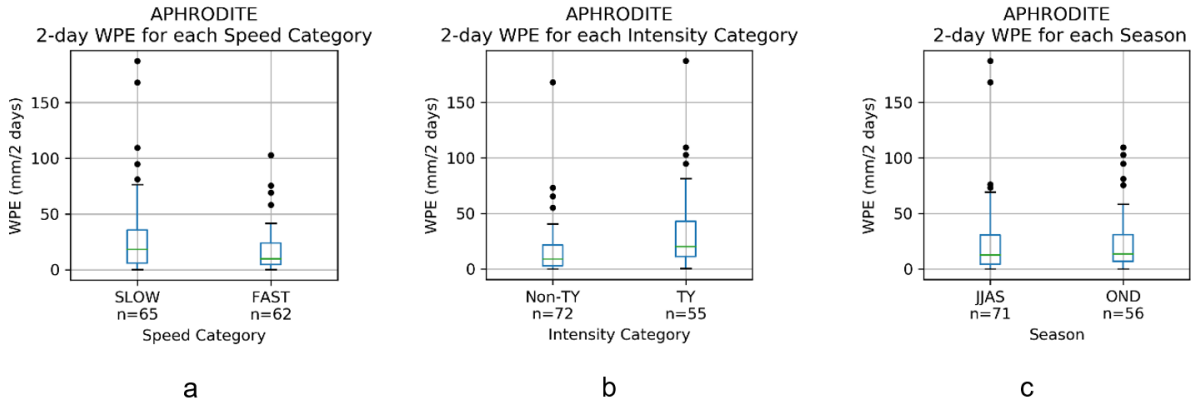

Figure 4.8: Boxplots similar to Figure 4.2 but for comparing WPE between (a) Slow and Fast TCs, (b) Non-TYs and TYs, and (c) for TCs in JJAS and OND.

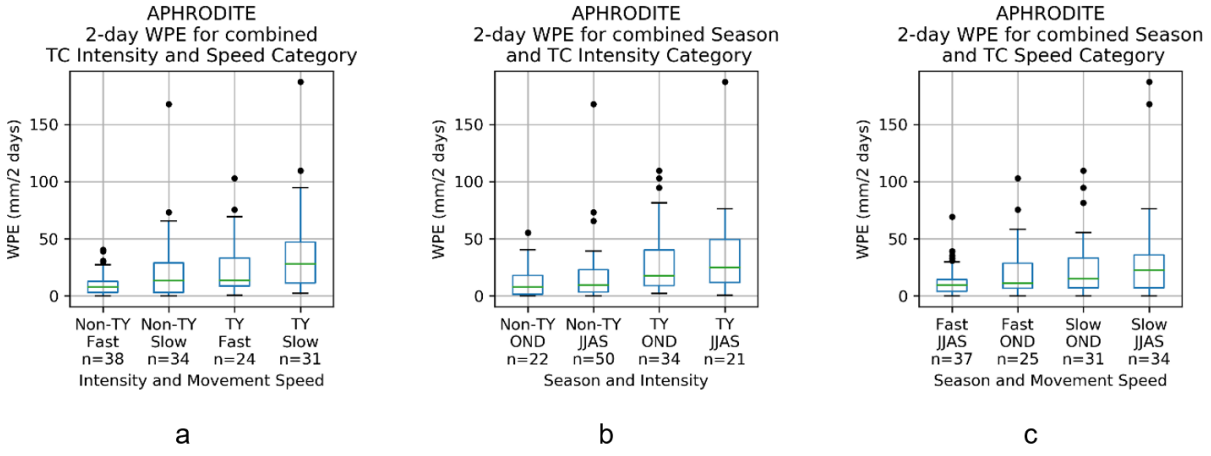

Figure 4.9: Boxplots similar to Figure 4.2 but for comparing WPE between (a) the combined intensity and movement speed categories, (b) the combined season and intensity categories, and (c) for the combined season and movement speed categories.

From Figure 4.8a, Slow TCs yield higher WPE compared to Fast TCs ($P = .017$), while 4.8b shows that TYs yield higher WPE compared to non-TYs ($P < .001$). Upon combining the intensity and movement speed categories in Figure 4.9a, no significant differences in WPE were found between Fast TYs and Slow

TYs, or between Fast Non-TYs and Slow Non-TYs. On the other hand, Figure 4.9a shows that Slow TYs yield higher WPE compared to Slow Non-TYs ($P = .01$), while Fast TYs similarly yield higher WPE compared to Fast Non-TYs ($P = .003$). Simply put, for similar movement speeds, stronger TCs cause more extreme precipitation. However, when TCs are of similar intensity categories, extreme precipitation tends to be similar between TCs of different movement speed categories. This means that TC intensity is more influential in determining extreme precipitation than TC movement speed.

Figure 4.8c shows that at $\alpha = 0.05$, no significant difference was found between the WPE of JJAS and OND TCs. When categorised by both season and intensity (Figure 4.9b), there is also no significant difference between JJAS TYs and OND TYs, or between JJAS Non-TYs and OND Non-TYs. However, JJAS TYs yield higher WPE than JJAS Non-TYs ($P = .001$) while OND TYs similarly yield higher WPE than OND Non-TYs ($P = .007$). In terms of combined season and movement speed categories, when considering similar seasons, JJAS Slow TCs have higher WPE than JJAS Fast TCs, while there is no significant difference between Fast and Slow TCs during OND (Figure 4.9c). From these results, we can see that within the same season, stronger TCs (TYs) cause higher precipitation, while movement speed only tends to cause higher WPE during the JJAS season. As such, when considering TCs in the same season, TC intensity is again more important than movement speed in determining extreme precipitation.

The above analysis suggests that for either TCs of similar movement speed or TCs within the same season, stronger TCs cause more extreme precipitation. However, from Figures 4.2a and 4.2b respectively, it was previously observed that while TC movement speeds are similar between the two seasons, OND TCs tend to be stronger than that of JJAS TCs ($P < .001$). This raises the apparent contradiction of why OND TCs, which are typically more intense than JJAS TCs (Figure 4.2b), have similar WPE to JJAS TCs (Figure 4.8c). To address this, we conduct a decision table analysis that will be discussed in the following section.

4.3 WPE Decision Table Analysis

At first glance, it seems counterintuitive that while strong TCs yield higher WPE than weak TCs, and there is a higher number of strong TCs in OND than JJAS, the WPE of OND TCs is not statistically different from that of JJAS TCs. To resolve this apparent contradiction, a decision table was formed to examine how the combination of all categories (season, intensity, and movement speed) is related to WPE. Table 4.2 shows the different categories (Season, Intensity, and Movement Speed) in the first three columns, along with the mean WPE and the total number of TCs per category in the fourth and fifth columns. We then compared the distribution of WPE for TCs in each category to the median WPE of all TCs of 5.90 mm/day (sixth column) to determine the percentage of TCs in each category that exceed the median WPE (seventh column).

Based on Table 4.2, OND has a higher fraction of TYs (60.71%) compared to JJAS (29.58%). In both seasonal categories, TYs in general have higher chances of exceeding the median WPE compared to Non-TYs.

Season	Intensity	Movement Speed	Mean WPE (mm/day)	Count	TCs that exceed median WPE of all TCs	Probability to exceed median WPE of all TCs
JJAS	Non-TY	Fast	17.87	26	6	23.08%
		Slow	19.73	24	14	58.33%
	TY	Fast	22.15	11	7	63.64%
		Slow	56.32	10	8	80.00%
OND	Non-TY	Fast	13.63	12	4	33.33%
		Slow	17.07	10	4	40.00%
	TY	Fast	30.13	13	8	61.54%
		Slow	30.49	21	13	61.90%

Table 4.2: Decision table for combined categories of season, intensity, and movement speed. The mean WPE for each category is shown in the fourth column. The fractional counts of TCs for each category that exceed the median WPE of all TCs are calculated as probabilities and are listed in the seventh column.

Between seasons, JJAS TCs tend to have higher mean WPE and are also more likely to exceed the median WPE of all TCs compared to most OND TCs in the same intensity and movement speed categories. However, there are a few exceptions: the OND TY Fast category has a higher mean WPE (30.13 mm/2 days) compared to the JJAS TY Fast category (22.15 mm/2 days), while the OND Non-TY Fast category has a higher probability to exceed the median WPE (33.33%) compared to the JJAS Non-TY Fast category (23.08%). Regardless of movement speed, there is a higher proportion of JJAS TYs that exceed the median WPE (71.43%) compared to OND TYs (61.76%). Besides the mentioned exceptions, most of these means and probabilities between categories show that while intensity and movement speed matter for anticipating higher WPE, this relationship is stronger for most JJAS TCs than for OND TCs.

We hypothesise that the higher precipitation rates overall during the JJAS season is due to the source and amount of moisture. We first show in Figure 4.10 the seasonal average monthly satellite derived Total Column Water Vapour (TCWV) over the ocean for the years 2015-2020 (Copernicus Climate Change Service, 2022). We observe higher amounts of TCWV within the vicinity of the Philippines during JJAS (Figure 4.10a). The higher amounts of moisture during JJAS is further compounded by southwesterly monsoonal flow (Bagtasa, 2017) during the said season. In contrast, lower amounts of WV are observed during the OND season, where most water vapour is constrained nearer the equator (Figure 4.10b). Besides the lower amounts of moisture, OND is characterised by the drier northeasterly flow in the WNP during the season (Guo et al., 2017; Yihui and Chan, 2005).

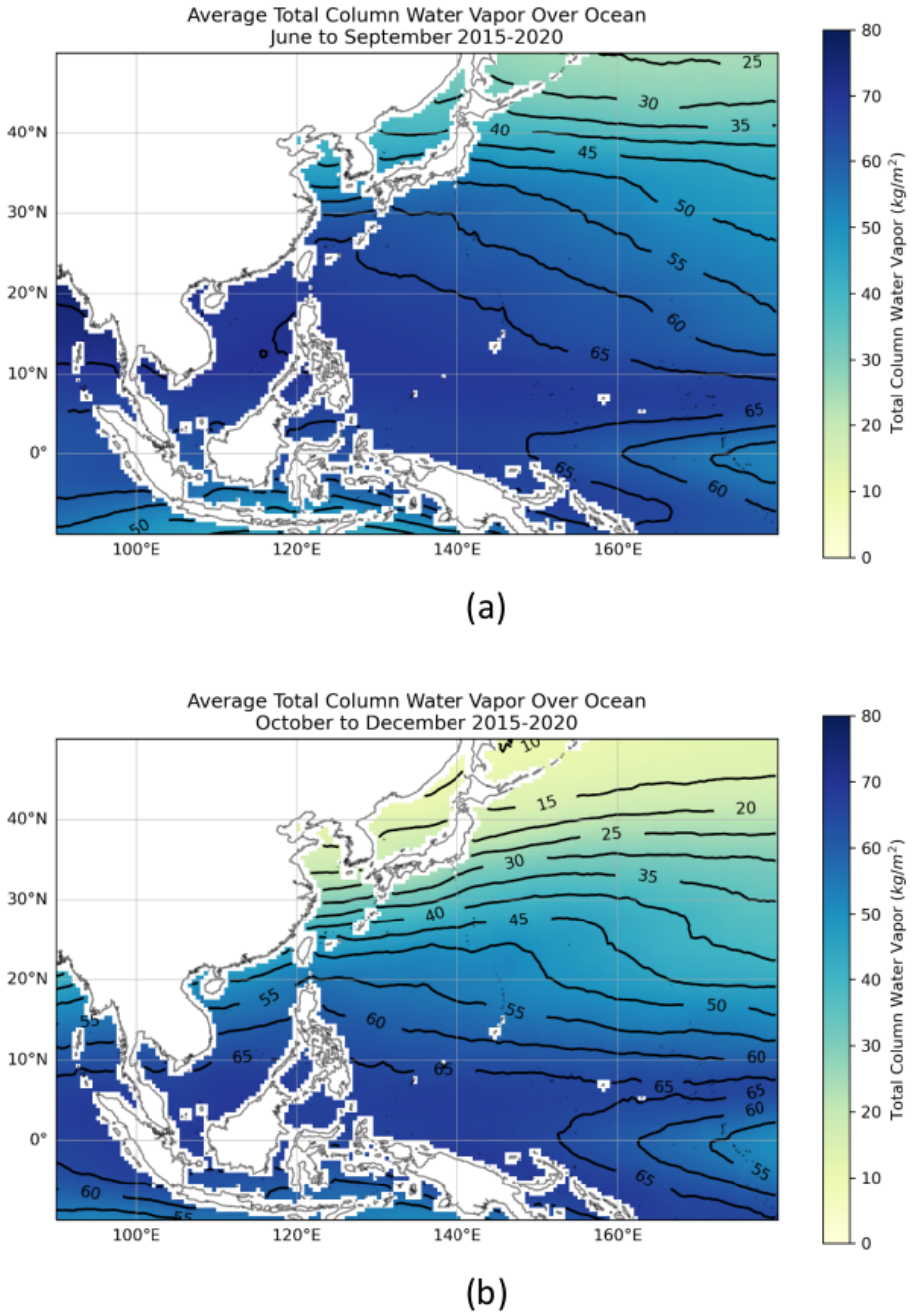

Figure 4.10: Satellite-derived average TCWV over the ocean for (a) JJAS and (b) OND. The contour lines denote 5 kg/m^2 intervals. TCWV Data is provided by Copernicus Climate Change Service (2022)

4.4 WPE Comparison and Decision Table Using TRMM

The above analyses, particularly the comparisons between categories with WPE as well as the decision table (Table 4.2, were also conducted using the $TRMM_{3hr}$ dataset. While it is true that there are fewer TCs that we can include in the analysis due to the shorter time period involved, using a higher temporal resolution dataset eliminates the need for assuming a uniform distribution of precipitation throughout the day as was done in the $APHRO_{uniform}$ dataset. Furthermore, while there are still differences between the datasets, using WPE as a metric works fairly well in terms of eliminating a systematic difference in the means between these datasets.

Figures 4.11b and 4.11c show that results remained the same for the WPE comparison between the intensity and season categories separately: TYs yield higher WPE than Non-TYs, while there is no significant difference between the WPE of JJAS and OND TCs. When comparing WPE for combined intensity and season categories, results remained similar between $TRMM_{3hr}$ and $APHRO_{uniform}$. Figure 4.12a shows that TYs continue to cause higher median WPE than Non-TYs in both the JJAS ($P = 0.03$) and OND ($P = 0.08$) seasons. Likewise, from Figure 4.12 we see that when TC intensity is similar, there is no significant difference in the WPE between the TCs in the JJAS and OND seasons.

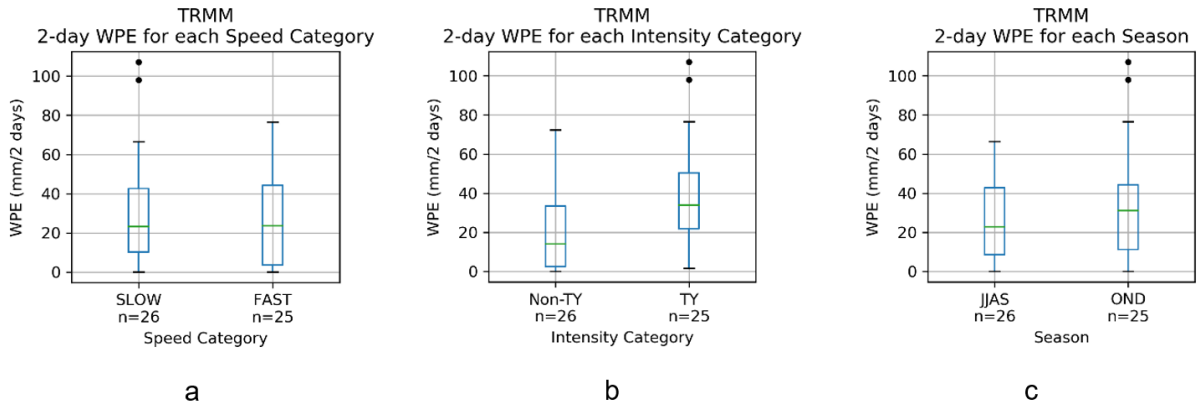

Figure 4.11: Boxplots similar to Figure 4.2 but for comparing WPE from $TRMM_{3hr}$ between (a) Slow and Fast TCs, (b) Non-TYs and TYs and, (c) for TCs in JJAS and OND.

The differences between $TRMM_{3hr}$ and $APHRO_{uniform}$ arise when considering TC movement speeds in comparing WPE between categories. In contrast to our previous results using $APHRO_{uniform}$, there is no significant difference between the WPE of Fast and Slow TCs in $TRMM_{3hr}$ (Figure 4.11a). From Figure 4.12a, while WPE continues to be higher for Slow TYs compared to Slow Non-TYs ($P < 0.001$) and there continues to be no significant difference between Fast Non-TY and Slow Non-TY, there is no significant difference between the Fast TY and Fast Non-TY categories. Slow TYs now yield higher WPE than Fast TY ($P = 0.029$) when using $TRMM_{3hr}$ in our calculations.

Comparing the decision tables between $APHRO_{uniform}$ (Table 4.2) and $TRMM_{3hr}$ (Table 4.3), JJAS TCs continue to mostly have higher probabilities to exceed the median WPE for their respective datasets. One exception is the JJAS Non-TY Slow category that has a lower probability of exceeding the median WPE

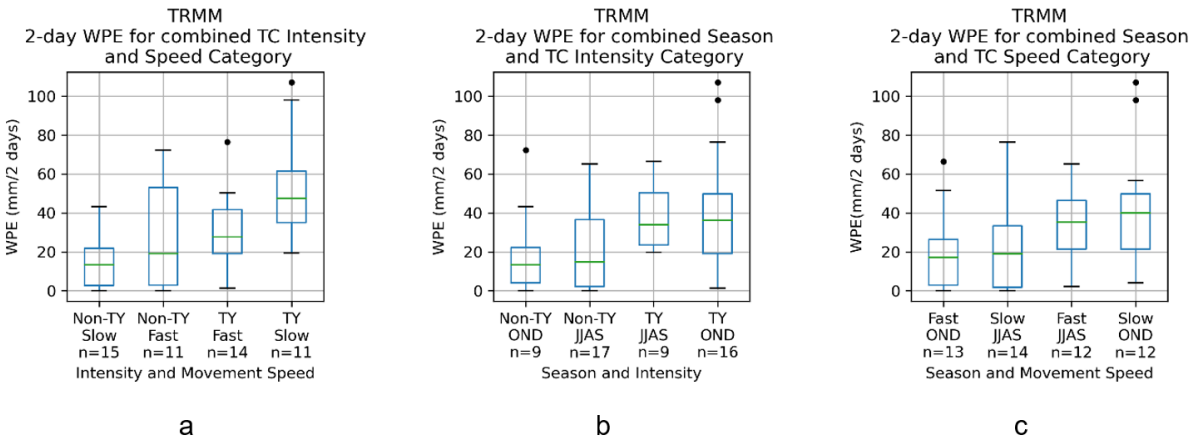

Figure 4.12: Boxplots similar to Figure 4.2 but for comparing WPE from $TRMM_{3hr}$ between (a) the combined intensity and movement speed categories, (b) the combined season and intensity categories, and (c) for the combined season and movement speed categories.

(18.18%) compared to the OND Non-TY Slow TC category (25.00%). However, it should be noted that since there are fewer TCs included in $TRMM_{3hr}$, any small difference in the number of TCs for each category that exceed the median WPE of all TCs can greatly affect their probabilities and relationships.

Season	Intensity	Movement Speed	Mean WPE (mm/day)	Count	TCs that exceed median WPE of all TCs	Probability to exceed median WPE of all TCs
JJAS	Non-TY	Fast	35.55	6	4	66.67%
		Slow	12.50	11	2	18.18%
	TY	Fast	32.42	6	4	63.64%
		Slow	48.34	3	3	100.00%
OND	Non-TY	Fast	20.79	5	1	20.00%
		Slow	20.68	4	1	25.00%
	TY	Fast	26.39	8	5	50.00%
		Slow	54.97	8	7	61.90%

Table 4.3: Decision table same as Table 4.2, but for $TRMM_{3hr}$

4.5 Chapter Discussion

All TCs included in this study originate in the WNP (Figure 2.1) before tracking west and making landfall in Luzon. At the beginning of the Southwest Monsoon season in June, the number of landfalling TCs in Luzon increases, peaking by July, and then decreases towards the end of the monsoon season in September (Figure 3.1). The number of landfalling TCs in Luzon increases again by the start of the Northeast Monsoon season in October and then tapers off by December. According to Cinco et al. (2016), more TCs cross or form within the Philippine Area of Responsibility (a region of TC monitoring used by forecasters in the Philippines) in JJAS than OND. However, the ratio of TCs that make landfall in Luzon compared to the total TCs that make landfall in the Philippines is higher in OND (37%) than in JJAS (27%). As landfalling TCs cause significant damages due to strong winds and high amounts of precipitation (Camargo and Hsiang, 2015), the higher likelihood of

TCs making landfall in Luzon in OND also means higher disaster risk during the season.

As mentioned in Section 4.1.2, one possible reason for the higher ratio of TC landfalls in Luzon compared to landfalls in the Philippines during OND is the combination of the retraction of the monsoon trough towards the east, as well as the extension of the western Pacific subtropical high towards the west. The monsoon trough is part of the Intertropical Convergence Zone that increases the chance of TC formation (Gray, 1977). Regarding TC movement direction, Bagtasa (2017) hypothesises that the western Pacific subtropical high acts as a steering ridge causing a more southerly and westward movement of TCs during the months of September to December. We hypothesise that the combination of TCs forming further east along with a more southerly and westward movement of TCs in the season may cause higher ratios of TC making landfall in Luzon during OND.

TCs in OND are typically stronger if they do make landfall (Figure 4.2b). We hypothesise that one possible factor why landfalling OND TCs are more intense is due to these TCs forming further to the east (Figure 4.3d) allowing for a TC to further intensify as it spends more time over the ocean before making landfall in Luzon (Figure 4.4). In terms of precipitation, it is seemingly counterintuitive that while stronger TCs yield higher WPE, the WPE of typically stronger OND TCs is similar to that of typically weaker JJAS TCs. However, upon comparing the likelihood of higher WPE between the seasons through a decision table, compared to OND, JJAS TCs have higher chances of exceeding the median WPE of all TCs regardless of intensity. This suggests that while intensity is important in anticipating higher WPE, this relationship is stronger for JJAS TCs than OND TCs. We hypothesise that this is due to an environment with higher moisture during JJAS and thus higher amounts of precipitation during a TC event. This is especially true if the TC interacts with the southwest monsoon, enhancing precipitation in the southwestern regions of Luzon in the process (Bagtasa, 2017; Cayanan et al., 2011).

Precipitation during TC days in JJAS is similar in spatial pattern to, but stronger than, the mean daily precipitation. Figure 4.1b shows that during days with landfalling TCs in Luzon, rainfall is mostly distributed towards the western regions of Luzon towards the western flank of the CMR and southwestern section of the Zambales Mountain Range. As previously mentioned, this is due to the moisture source in JJAS from the warmer and moister southwesterly winds during the season (Xiang et al., 2013) where additional and higher rainfall is observed towards the western region of Luzon during TC-landfall days (Bagtasa, 2020). As TCs tend to move towards the north during JJAS they bring more precipitation to the southwestern regions of Luzon, causing extreme precipitation in the process.

On the other hand, landfalling TCs in OND tend to move towards the central and southern regions of Luzon, while precipitation is distributed in regions that otherwise experience comparatively less extreme precipitation for the season. This is more apparent, particularly towards the eastern flanks of the CMR and the northern portion of the Sierra Madre Mountain Range (Figure 4.1e). This may pose problems for crops, particularly rice, that are planted in Luzon during the prior months of October-December and then grown between

the dry season of January-June (Koide et al., 2013). Abnormally high precipitation and strong winds during extreme weather conditions such as TCs hamper the growth of rice crops, thus reducing yield (Lansigan et al., 2000).

Based on our results, the season, intensity, and then finally the movement speed one day prior can help to anticipate the associated extreme precipitation of landfalling TCs. While TC movement speed is important, TC intensity along with season can be more useful to estimate the WPE of TCs. Understanding the implications when which season a TC forms and makes landfall can be helpful in estimating both the likelihood of extreme precipitation as well as its spatial distribution. TCs making landfall in JJAS have a higher likelihood of causing more extreme precipitation, while TCs making landfall in OND distribute precipitation in other regions. The decision table (Table 4.2) can be used as a reference to help anticipate the probability of extreme precipitation caused by westward-moving TCs expected to make landfall in Luzon. However, we recommend that our results be considered as a preliminary tool, to be used together with quantitative precipitation forecasts from NWP models. The application of our results to prediction also requires verification in an operational setting. Other TC characteristics, such as radius, landfall location, and movement direction may also be related to extreme precipitation which unfortunately were not explored in this study. This study also does not consider TCs that make landfall from other directions and we also did not examine the extreme precipitation of TCs that recurve instead of making landfall. As such, in future studies, we may also consider TC landfall location, direction, as well as the distance between TC and land in estimating extreme precipitation as well as taking a further look at their spatial distribution.

One limitation of this study is data availability, both for TC characteristics and precipitation. Only TCs between 1978 and 2015 were considered, as TC intensity data are very limited in the pre-satellite era (Knapp et al., 2010; Knutson et al., 2010) and the APHRODITE record ends in 2015. While APHRODITE has been used in previous precipitation studies in the Philippines, these data are approximated from the available weather stations through an interpolation method (Yatagai et al., 2012). While it is a comprehensive dataset, it is still limited by the availability and quality of weather observations in the country (see Akasaka et al. (2007) for the locations of these stations). Finally, APHRODITE only has daily accumulations. As such, it is possible that our estimates of 48-hour precipitation accumulation centred on landfall may be biased by the lack of sub-daily information.

Satellite-based precipitation products such as TRMM, CMORPH, and the Global Precipitation Measurement (GPM) mission by the National Aeronautics and Space Administration are also available and could be used for TC precipitation studies. While these products offer higher spatial and temporal resolution precipitation estimates, they are available only in more recent years (TRMM from 1998 to 2019, CMORPH from 2002 to the present, and GPM from 2000 to the present). Using these satellite products would reduce the sample size of TCs, potentially making the relationships between TC characteristics and extreme precipitation less apparent. According to Jamandre and Narisma (2013), when compared with observations from weather sta-

tions, satellite products such as TRMM and CMORPH perform well in estimating daily precipitation in eastern Luzon during rainfall events where precipitation is greater than a threshold of 100mm. However, they have also noted that measurements below this threshold tend to overestimate precipitation. This may have an impact on estimating rainfall amounts during TCs with lower amounts of precipitation. Another possible issue that may arise is the technical differences between these satellites as well as their different precipitation estimation algorithms, which may lead to discrepancies between measurements especially if we were to use measurements from different satellites along with gridded precipitation datasets through different years.

Despite the limited number of TCs during the available period of $TRMM_{3hr}$, we included analysis of the higher temporal resolution dataset in our calculations for this study to provide an additional line of evidence. While there are key differences in the results between $APHRO_{uniform}$ and $TRMM_{3hr}$ that we cannot ignore, our primary findings, particularly for TC intensity and season, remain consistent between the two datasets. TC intensity and season continue to be more important in determining extreme precipitation than movement speed. It should be noted, however, that the lower sample size of TCs in $TRMM_{3hr}$ reduces the robustness of the relationships between the different categories as well as the probabilities in our decision tables. As data becomes available and more TCs may continue to make landfall in Luzon, in future studies, we may consider a combined approach to evaluate extreme TC precipitation using estimates derived from rain gauges, satellites, and modelling as demonstrated by Kim et al. (2019).

Another limitation of this study is the time scales involved in using WPE as a measure of extreme precipitation. As WPE is limited in measuring TC precipitation for 48 hours centered on TC landfall, it is very likely that the total precipitation throughout a TCs lifetime is not included in our measurements. However, using WPE as an index of extreme rainfall ensures that we have a consistent method of comparing landfalling TCs at their point of immediate impact during the 48-hour period centered on landfall. This measure of TC precipitation severity may be useful for anticipating rapid onset hazards which may arise during TC landfalls such as urban flooding, flash flooding, and landslides. Comparing TC characteristics with the total precipitation of all TCs affecting the Philippines (both landfalling and non-landfalling) throughout their lifetimes may be considered in a future study.

4.6 Chapter Conclusion

This study was motivated by the need to quantify the relationships between TC characteristics (such as intensity, movement speed, and season) and TC precipitation. Previous TC precipitation studies in the Philippines typically focus on the interaction of TCs with the southwest monsoon and its effects on precipitation while others analyse case studies on the effect of topography on TC rainfall. To the best of our knowledge, there are no studies that compare characteristics of westward-moving TCs that make landfall in Luzon with precipitation. Relationships established in this study can be used in conjunction with NWP forecasts during TC events to augment precipitation estimates for TCs that are expected to make landfall.

Our results suggest that WPE (Weighted Precipitation Exceedance, a measure of extreme precipitation) has a stronger relationship with pre-landfall TC intensity than with pre-landfall TC movement speed or season: stronger TCs tend to cause higher amounts of precipitation that are more widespread. However, we also found that although OND TCs are typically stronger than JJAS TCs, TCs making landfall in JJAS caused stronger rains. We then raised a few hypotheses to explain the differences between TCs of the JJAS and OND seasons.

First, we hypothesised that there is a higher ratio of TCs making landfall in OND due to a combination of the shifting of the monsoon troughs from south to east along with the western Pacific subtropical high extending further towards the South China Sea. The combination of these two factors may then cause higher TC landfalls in Luzon during OND. as well as resulting in stronger OND TCs due to the longer time to develop before making landfall. Besides the cyclogenesis location and intensity of OND TCs, we have also hypothesised that JJAS TCs, for a given intensity, cause more rainfall because there is more moisture available to them. However, validating these hypotheses is not within the scope of this study. These may be explored in further studies to explain the climatology and characteristics of TCs that make landfall in Luzon.

Chapter 5

The Effect of the Cordillera Mountain Range on Tropical Cyclone Rainfall in the Northern Philippines

In Section 4, we were able to establish associations between TC characteristics and extreme precipitation in Luzon. However, we were unable to adequately explain the underlying processes that link TC winds and precipitation. We hypothesise that one of the primary drivers of TC precipitation upon landfall is the orographic effect, where impinging winds on mountain ranges lead to forced ascent of moist air, causing precipitation along the windward flanks of the mountain (Roe, 2005; Smith, 1979). As there are limited studies on the effect of orography on TCs, especially in the Philippine context, this Chapter discusses the numerical experiments we conducted to answer the thesis's second objective, which is to determine the effect of the orography of Luzon, particularly the Cordillera Mountain Range (CMR), on the characteristics and precipitation of TCs. To understand the interactions between mountains, TCs, and precipitation, we used the WRF model (introduced in Section 3.2.2.1) to simulate eight TCs for four different CMR orography experiments (Control, Flat, Reduced, and Enhanced).

We first validate the Control simulations with observations (Section 5.1), and then evaluate the effects of the CMR orography experiments on TC intensity and movement (Section 5.2), and precipitation (Section 5.3). In Section 5.4, we establish empirical relationships between precipitation and physical variables such as wind and mountain slope. We found that the combination of stronger TC winds blowing up along steeper slopes causes mechanical uplift of moist winds, causing condensation and higher amounts of precipitation along the mountain range. A manuscript based on the results presented in this Chapter was published in Racoma et al.

(2023).

5.1 Evaluation of Control Simulations Against Observations

We simulated TCs that made landfall in Luzon between 2000-2015 and caused extreme precipitation based on the WPE criteria defined in Section 3.2.1.3. Based on observations, these TCs intensified along the Pacific Ocean, tracked from East to West, made landfall along Luzon, and then crossed the CMR in a westward direction. For the different simulations, we estimate the central position of the TC using a simple algorithm of seeking the grid with the lowest Mean Sea Level Pressure (MSLP). The coordinates of the grid cell with the lowest MSLP is taken as the center of the TC, and the value is taken as the TC's intensity. Visual inspection and manual corrections were made for tracks significantly deviating from the general TC movement.

To evaluate modelled TC track accuracy, we calculate the Direct Positional Error (DPE). DPE is the geodesic distance between TC position in model simulations and the best track (Aragon and Pura, 2016; Chen et al., 2015), and is defined by the following equation

$$DPE = 2R\sin^{-1}\left(\sqrt{\left(\frac{1}{2}\sin\left(\phi_o - \phi_m\right)\right)^2 + \cos(\phi_o)\cos(\phi_m)\left(\frac{1}{2}\sin(\lambda_o - \lambda_m)\right)^2}\right) \tag{5.1}$$

where R is the radius of the Earth (6,371km), and (λ_o, ϕ_o) and (λ_m, ϕ_m) are the coordinates from observation (IBTrACS) and model (WRF).

We calculate the DPE between the TC tracks from IBTrACS and the Control simulations for matching 3-hourly TC track points from 48 hours before landfall up until 24 hours after TC landfall. The TCs we simulated in this study along with their relevant DPE are listed in Table 5.1.

TC Name	Date of Philippine Landfall	Min. Central Pressure Upon Luzon Landfall (millibars)	DPE (km)	ONI Phase
Bebinca	2 November 2000	990	128.00	Cold
Imbudo	22 July 2003	950	115.73	Neutral
Prapiroon	31 July 2006	1002	142.06	Neutral
Cimaron	29 October 2006	920	102.06	Warm
Megi	18 October 2010	885	182.56	Cold
Nesat	26 September 2011	950	66.67	Cold
Nari	11 October 2013	970	141.32	Neutral
Koppu	17 October 2015	925	68.07	Warm

Table 5.1: The eight TCs simulated in this study. Their landfall dates are listed in the second column, the intensity upon Luzon landfall in the third column, and the Direct Positional Error (DPE) of each TC in the fourth column. Calculated DPE has a standard deviation of 36.70 km, mean of 118.31 km, and median of 121.86 km. The fifth column denotes the Oceanic Niño Index (ONI) phase (taken from https://psl.noaa.gov/data/correlation/oni.data) during TC landfall.

We first plot the TC tracks derived from the Control simulations and compare them with tracks from IBTrACS (black tracks in Figure 5.1). From Table 5.1, the DPE of the TCs in the Control runs ranges from a

minimum of 66.67 km (Nesat) to a maximum of 182.56 km (Megi). The DPE for the eight TCs has a standard deviation of 36.70 km, a median of 121.86 km, and an average of 118.31 km. Based on these values, most TC tracks are reasonably modelled compared to observations. While the modelled TC tracks do not perfectly coincide with observations, the simulated TCs still moved along Luzon and across the CMR during each of the model runs.

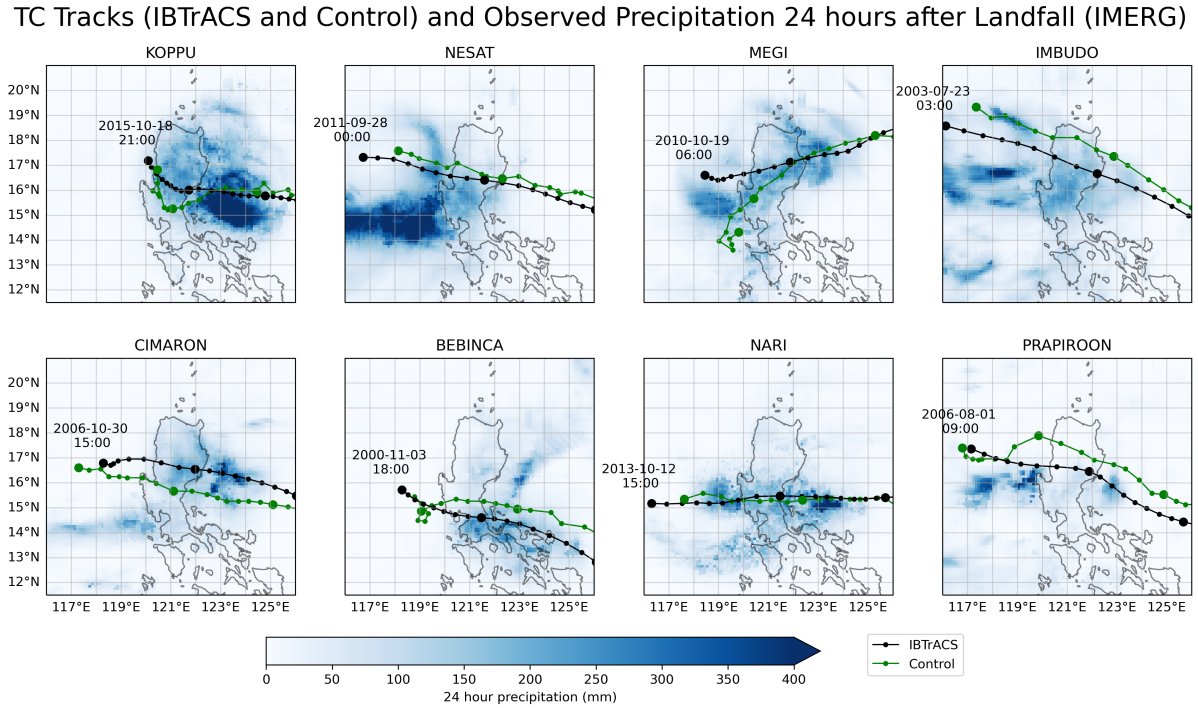

Figure 5.1: 3-hourly observed (black) and simulated (green) TC track points for Control for all eight cases. These are plotted for up to 24 hours after observed TC landfall based on IBTrACS. Larger markers denote 24-hour periods, matched between observations and simulations, while the final point in the model track corresponds to the same time and date as the labelled observed point. The blue shading denotes the 24-hour accumulated precipitation (in mm) from IMERG. Observed track data are from IBTrACS (Knapp et al., 2018), while precipitation data are from IMERG (NASA Goddard Earth Sciences Data And Information Services Center, 2019)

The modelled precipitation differs significantly from observed IMERG precipitation (Figure 5.1), with Control showing precipitation over the mountain ranges of Luzon that were not detected by IMERG (Figure 5.2). While IMERG does measure regional precipitation patterns well, it has large uncertainty in measuring precipitation over mountainous terrain (Hsu et al., 2013; Pradhan et al., 2022). Although there remains uncertainty in the results of the WRF model, a detailed evaluation of model accuracy, as well as its improvement, is not within the scope of this thesis. As we aim to understand the sensitivity of TC rainfall to the height of mountain ranges, the WRF model, which can produce the mountain-associated features in rainfall distribution, allows us to quantitatively measure precipitation over Luzon and over the CMR. Additionally, as WRF has been previously used in similar studies involving orography experiments (Huang et al., 2020; Lagmay et al., 2015; Minamide and Yoshimura, 2014; Racoma et al., 2016; Tang and Chan, 2014), we believe that the WRF model is sufficient for the aims of this study.

To understand how the CMR affects TC precipitation, we analyse the accumulated precipitation 24 hours

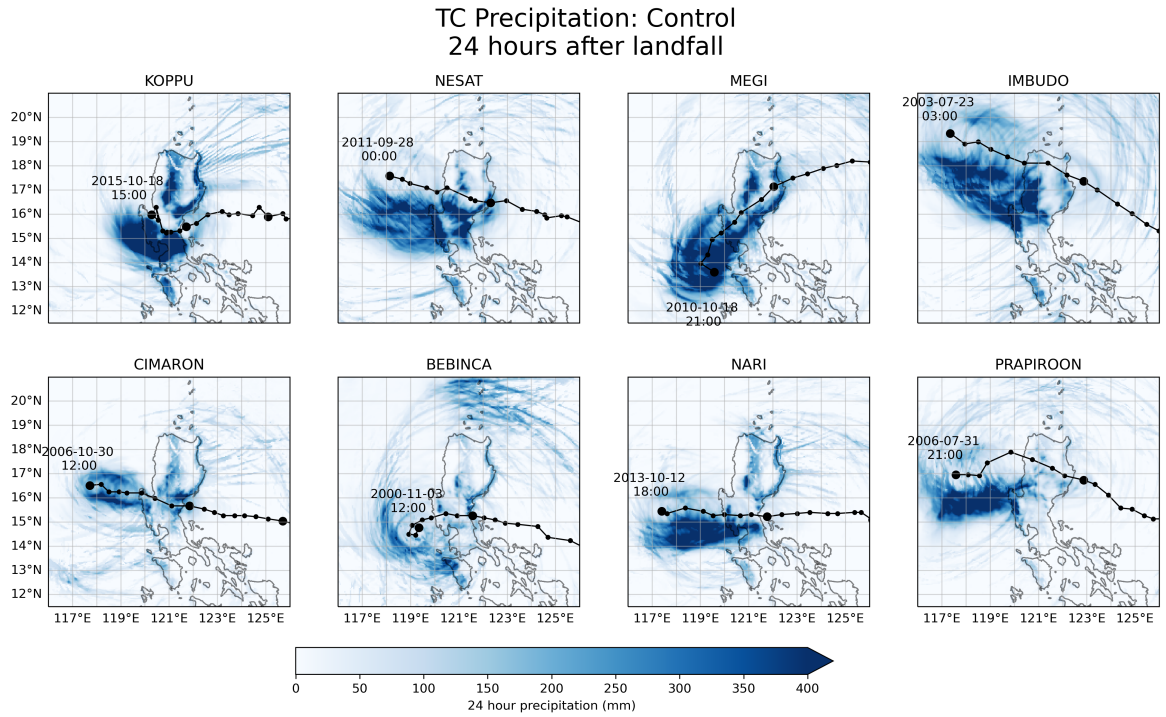

Figure 5.2: Accumulated precipitation 24 hours after simulated landfall (shading) for Control, with the simulated 3-hourly TC tracks in black lines. Tracks are plotted up to 24 hours after landfall, with each 24-hour period plotted in larger markers.

after TC landfall for Control. For most of the TC simulations, heavy precipitation was found along the eastern slopes of the CMR (Figure 5.2). However, for Imbudo and Prapiroon, there is more precipitation towards the western section of the CMR. This difference in precipitation distribution can be attributed to the different windward and leeward sides based on the TC cyclonic flow (Racoma et al., 2016). To consider the sensitivity of precipitation to TC track, from here on we classify the TCs according to two categories depending on their movement across the CMR: the North-tracking TCs (NTCs: Imbudo and Prapiroon) and South-tracking TCs (STCs: the other six TCs).

5.2 Effect of Mountain Height on TC Intensity and Track

To understand the effects of mountain height on TC characteristics, in this section we evaluate the differences of TC intensity and movement between the modified orography experiments (Flat, Reduced, and Enhanced) and the Control simulation from 48 hours before landfall up to 24 hours after landfall. Section 3.2.2.2 discusses how the height of CMR was either reduced or enhanced for these sensitivity experiments. We first calculate the mean intensity, latitude, and movement speed of the TCs for the modified orography experiments and then evaluate their difference with the Control.

While the Flat and Reduced experiments show no significant effect on TC intensity (Figures 5.3a and b), increasing the height of CMR in the Enhanced experiment significantly weakens most TCs as early as 12 hours prior to landfall (Figure 5.3c). It is expected that TCs weaken as they make landfall especially if they traverse

mountain ranges due to the changes in basic flow (Bender et al., 1987b), and advection of dry air along with vorticity stretching (Liu et al., 2016; Tang and Chan, 2014). However, no significant change in TC strength was observed in Flat and Reduced experiments, despite the flatter terrain compared to Control. For the eight TCs simulated in this study, TC intensity is sensitive to higher CMR, but not sensitive to lower CMR heights. This indicates nonlinear relationships between CMR height and TC metrics. Also, this means that the actual CMR has minimal effects on the intensity of passing TCs as its influence does not significantly differ from Flat and Reduced. We also find that changing the mountain height has little or no significant effect on other TC meridional position (Figures 5.3d, e, and f) and, movement speed (Figures 5.3g, h, and i).

Although we find no systematic changes in TC track with respect to varying CMR heights in terms of meridional position, there are observed deflections in TC tracks for certain TC cases, particularly after landfall in the Enhanced experiment. We see these track deflections in KOPPU, CIMARON, NARI, and PRAPIROON after the TCs cross Luzon and the mountain ranges (red tracks in Figure 5.4). While these track deflections are notable, we cannot currently determine the cause of these deflections as they are not systematic nor consistent in nature, particularly for the TCs in this study. As described in Lin et al. (2005) and Lin et al. (2016), it is possible that the TC tracks are deflected due to vortices induced by the orographic blocking of the Enhanced CMR on crossing TCs. However, further idealised TC studies focused on Luzon are recommended to determine whether CMR or SMMR induce similar vortices and track deflections.

5.3 Effect of Mountain Height on TC Precipitation

We next compare maps of the differences in 24-hour post-landfall accumulated precipitation between the orography experiments. It is apparent that there are dry regions along the eastern slopes of CMR in all Flat experiments (Figure 5.5) except for Imbudo, wherein increased rainfall is seen in the immediate vicinity of its track. A closer look at the 24-hour precipitation difference between Flat and Control is shown in Figure 5.6. In the Reduced experiments (Figure 5.7), the spatial distribution of the dry regions seen in the Flat experiments are still apparent but with less amount. A zoomed-in version of Figure 5.7 is shown in Figure 5.8. In contrast, the Enhanced experiments (Figures 5.9 and 5.9) show a shift to an increase in rainfall on the eastern slopes of the CMR except for the two NTCs - Imbudo and Prapiroon. The dry regions across CMR for the two NTCs is explained by two reasons, one is the reduction of the TC intensity in the Enhanced runs, as discussed above, reduced the overall rain-rate of the TCs, and two, the windward side of CMR shifted to the west of the mountain range for the two NTCs, thus, the higher mountain height served to block the rainfall induced by the TC circulation along the CMR, resulting in the drier slopes in the cases of Imbudo and Prapiroon. The results show significant changes in rainfall amounts for varying CMR heights, which confirms that TC-orography interaction plays a major role in TC rainfall production along the CMR region.

A closer inspection of the simulated TC tracks reveals that there is a northward shift in the tracks of Bebinca and Nari with respect to their respective Control runs, particularly for the Enhanced and Reduced

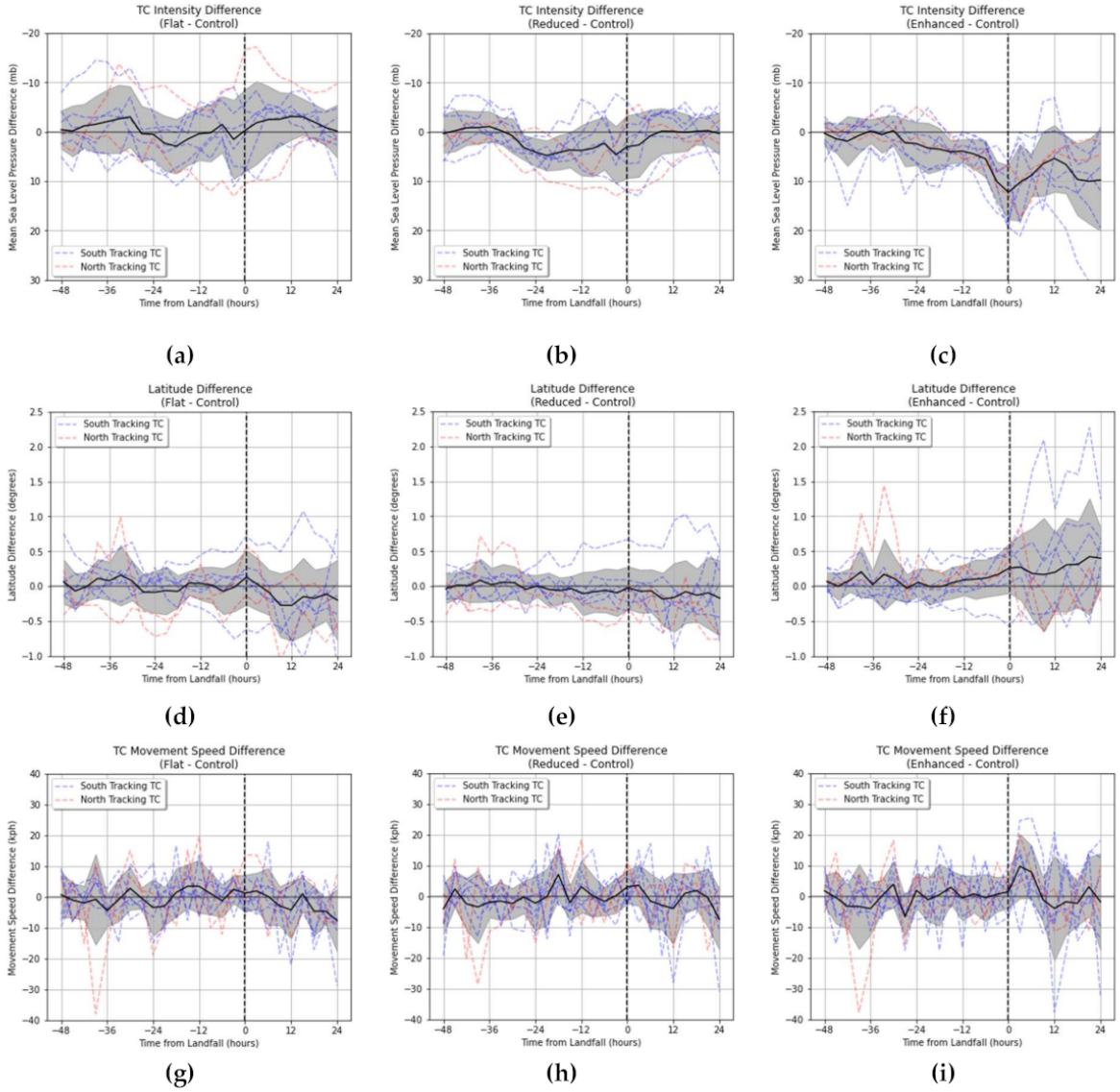

Figure 5.3: TC intensity comparison for (a) Flat - Control, (b) Reduced – Control (c) Enhanced - Control; TC location comparison for (d) Flat - Control, (e) Reduced - Control, and (f) Enhanced - Control; TC movement speed comparison for (g) Flat - Control, (h) Reduced - Control, and (i) Enhanced - Control. Take note of the inverted y-axis for (a) and (b) to highlight the decrease in the intensity of the TCs. The red dashed lines represent the NTCs, with the blue dashed lines representing STCs. The black line represents the mean of all cases, with the grey shading showing the standard error. The vertical black dashed line is the time of landfall, or $t = 0$.

(for Bebinca only) simulations. The track shifts alone will obviously contribute to the rainfall differences notwithstanding the changes in orography. We distinguished the precipitation difference from the track shifts and orographic height changes by first determining the radial TC-rainfall profile from the model output along the eastern slopes of the CMR where the differences are most prominent. We found that the TC-rainfall profile of Nari decays logarithmically the farther the distance from the TC center while the rainfall profile of Bebinca follows an almost flat profile that gradually tapers at distances around >250 to 300 km from the TC center. The difference in the rainfall profiles is due to the difference in landfall intensities where Nari made landfall as a typhoon and Bebinca only as a tropical storm (their intensities are shown in Table 5.1). We estimated the mean track shifts of 32 km and 51 km for Nari and Bebinca, respectively. We then shifted the rainfall profiles of both

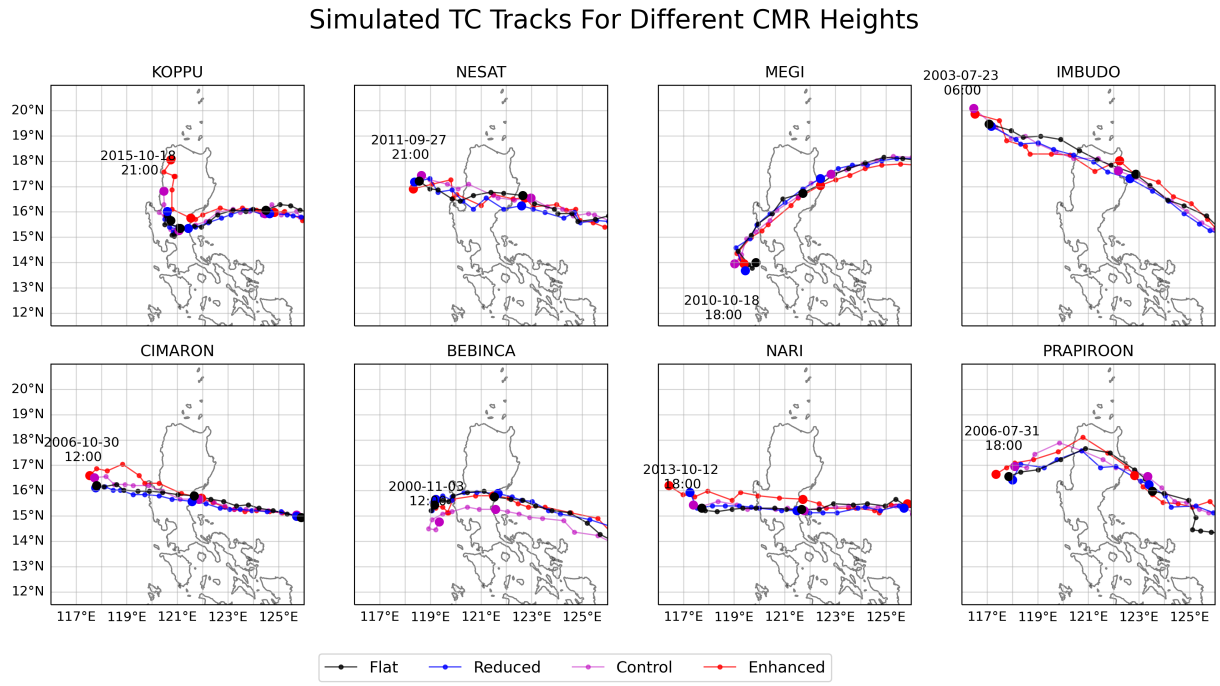

Figure 5.4: TC tracks for the different orography experiments, Flat (black), Reduced (blue), Control (magenta), and Enhanced (red). Tracks are plotted up to 24 hours after landfall, with each 24-hour period plotted in larger markers.

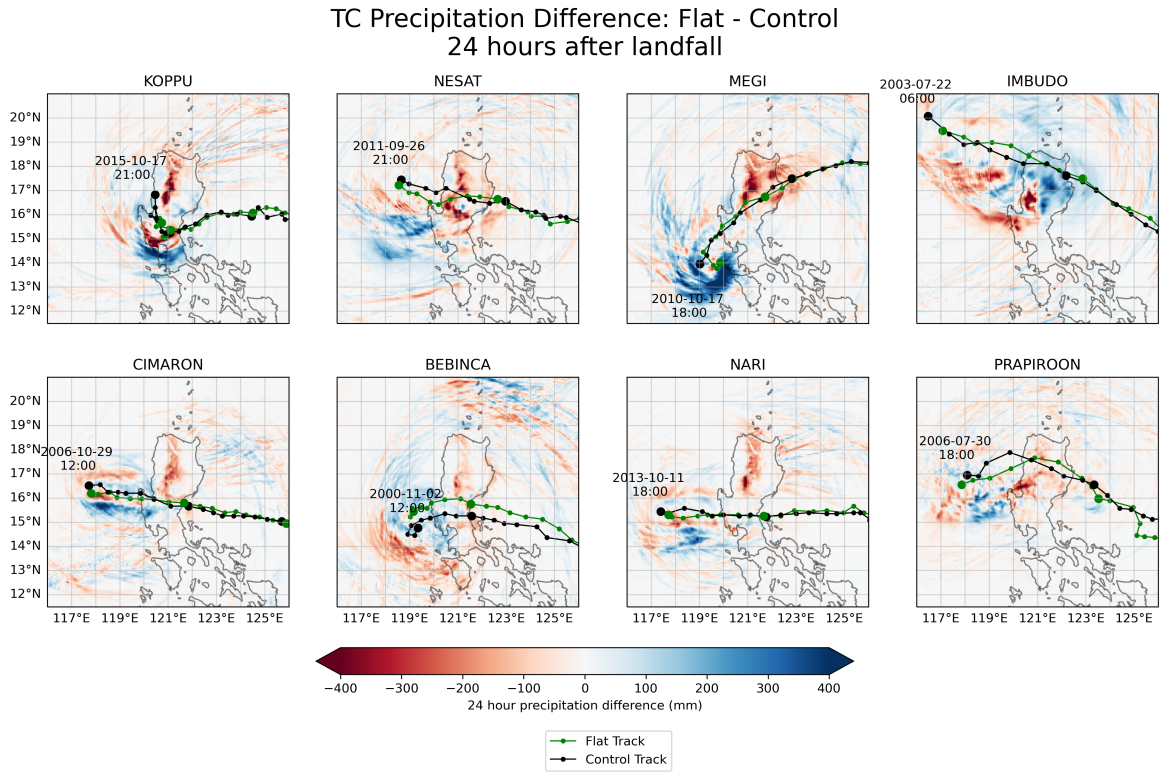

Figure 5.5: Difference in 24-hour accumulated precipitation after landfall (shading) between Flat and Control. 3-hourly TC tracks for Flat and Control are coloured in green and black, respectively. Tracks are plotted up to 24 hours after landfall, with each 24-hour period plotted in larger markers, with the final points in both model tracks corresponding to the same time and date as labelled.

TCs according to their respective track shifts to calculate the rainfall differences due to their tracks shifting in the Enhanced runs. In the Enhanced runs, we found that for Nari, 74.5% of rainfall changes is due to the orography change and 25.5% is due to its track shifting northward closer to the CMR. In the case of Bebinca,

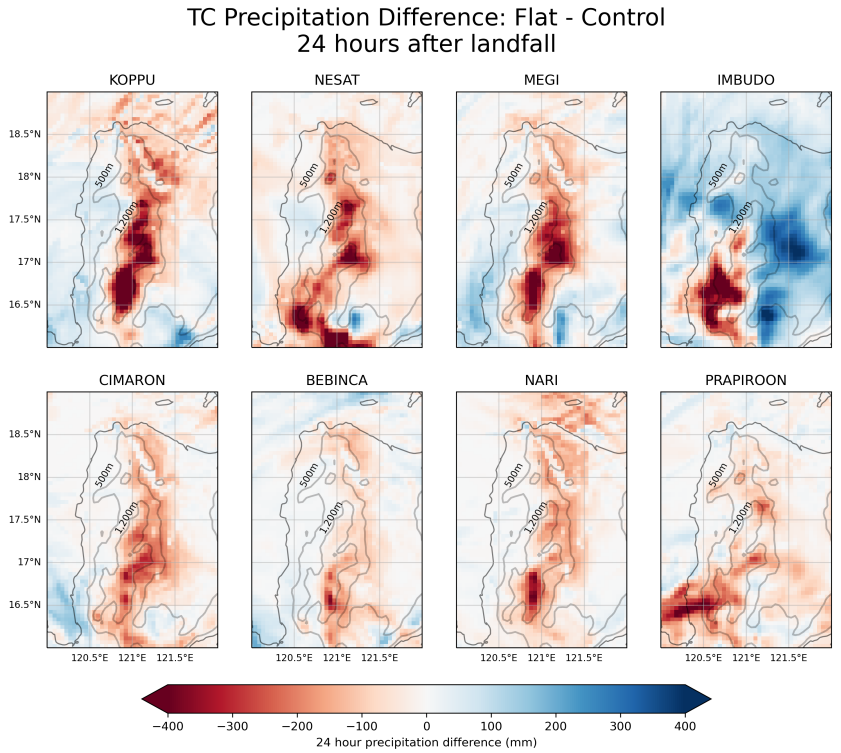

Figure 5.6: Similar to Figure 5.5 but zoomed in to highlight the difference in precipitation over CMR's terrain. Contour lines for 500m and 1,200m heights are labelled accordingly.

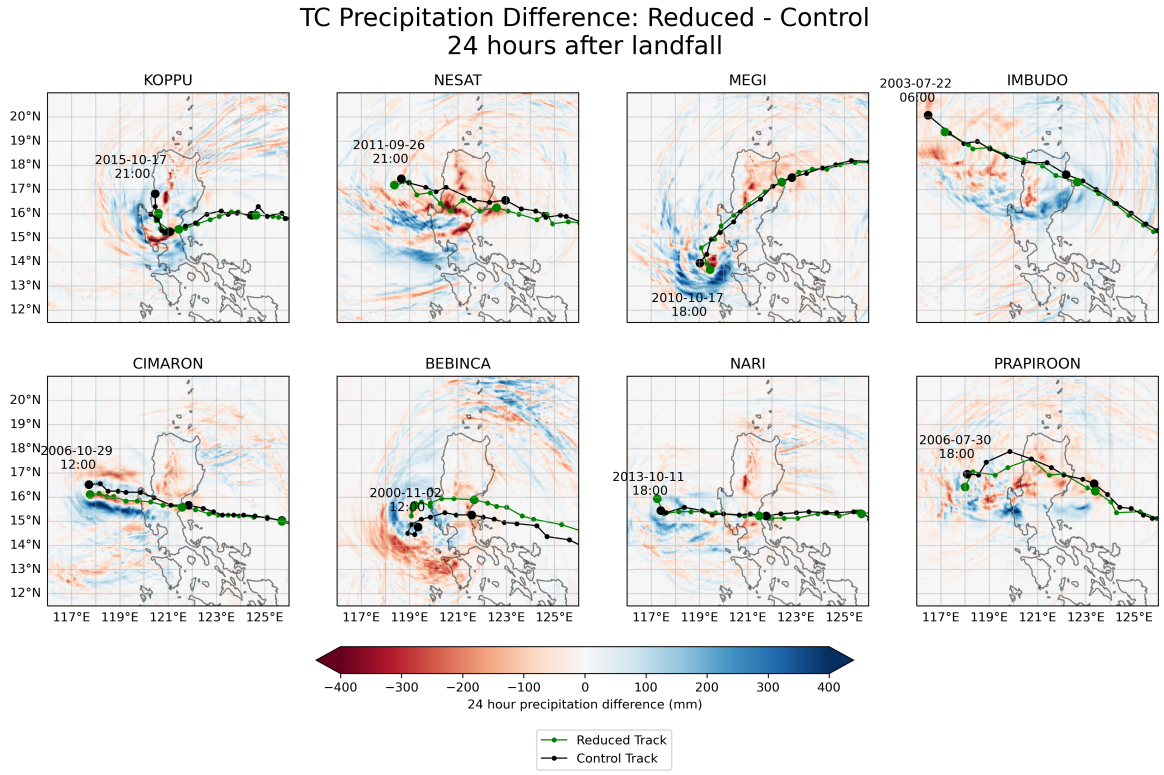

Figure 5.7: Similar to Figure 5.5, but for the difference in 24-hour accumulated precipitation after landfall between Reduced and Control.

92.6% of the rainfall difference is attributed to the orographic change and just 7.4% due to the track shift, this smaller difference is because the flat rainfall profile of the weaker Bebinca along the CMR did not change much even if its track was meridionally shifted more than Nari. In the Reduced run of Bebinca, its northward track

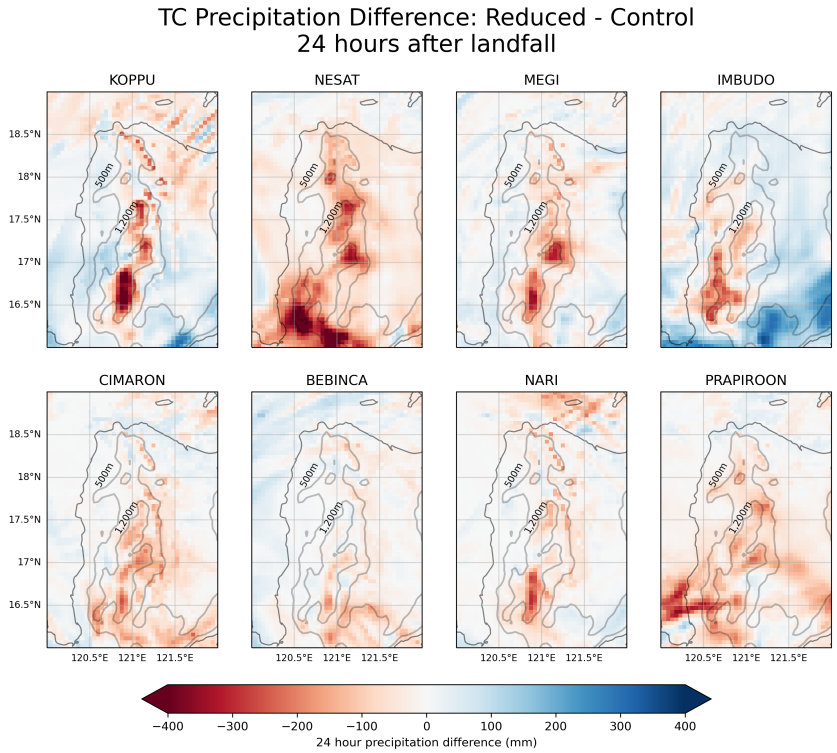

Figure 5.8: Similar to Figure 5.7 but zoomed in to highlight the difference in precipitation over CMR's terrain. Contour lines for 500m and 1,200m heights are labelled accordingly.

shift resulted in an overall increase in rainfall by 67.2% and the lower CMR height reduced rainfall by 169.5%, this explains why Bebinca had the smallest observed difference along CMR as the track shift just compensated the expected rainfall reduction due to the lower mountain height.

While differences in the amount of TC precipitation due to the change in mountain height show regional variations, it is also necessary to estimate the precipitation response as the TC moves along Luzon. For every 3-hourly model output timestep from 48 hours prior to ($t = -48$) and until 24 hours after landfall ($t = 24$), we calculate the mean overland precipitation over Luzon and over the CMR. For the mean overland precipitation over Luzon, we find that there is no significant difference for Flat, Reduced, and Enhanced when compared with Control (Figure 5.11). While there are indeed different spatial patterns in overland precipitation in the different orography experiments (as previously shown in Figures 5.7 and 5.9), the average differences remain low. It is worth noting that for the Enhanced case, Luzon precipitation for NTCs (red dashed lines in Figure 5.11c) generally show negative values compared to STCs (blue dashed lines). It is possible that rainfall from NTCs generally do not reach further inland due to the taller barrier introduced in Enhanced CMR. This can also be seen in Figure 5.10, where there is less rainfall the flat regions towards the east of CMR for the NTCs IMBUDO and PRAPIROON.

Over CMR (mountainous region enclosed in red in Figure 3.7), however, an increase in precipitation is found for increasing mountain height. Figure 5.12 shows the difference in precipitation averaged over CMR (black line). After TC landfall ($t > 0$), the lower mountain height results in a decrease in precipitation over CMR (Figure 5.12a) and the higher mountain height corresponds to an increase in precipitation (Figure 5.12b).

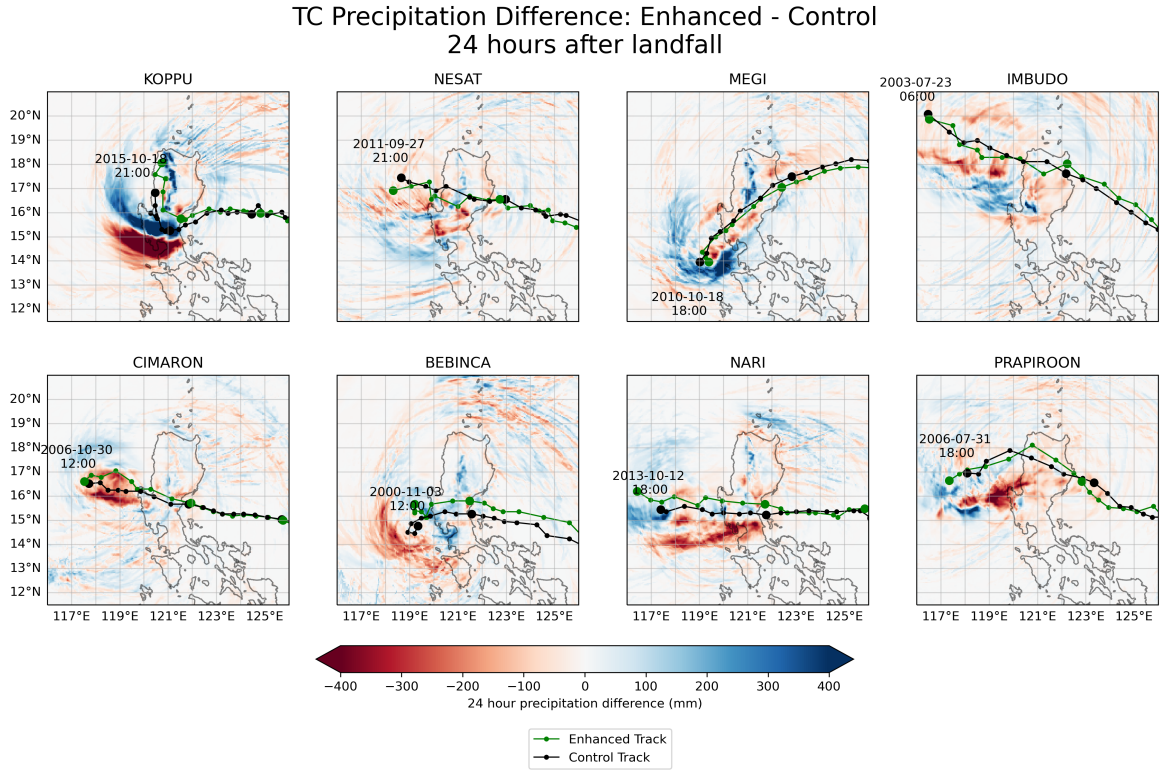

Figure 5.9: Similar to Figure 5.5, but for the difference in 24-hour accumulated precipitation after landfall between Enhanced and Control.

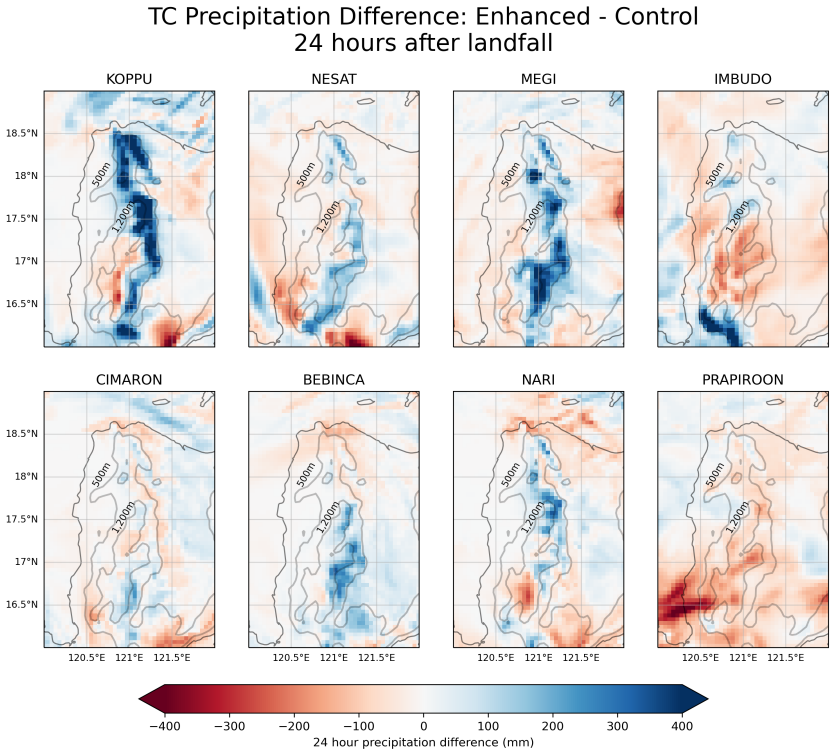

Figure 5.10: Similar to Figure 5.9 but zoomed in to highlight the difference in precipitation over CMR's terrain. Contour lines for 500m and 1,200m heights are labelled accordingly.

However, a decrease in precipitation was observed in NTCs in the Enhanced CMR (red dashed lines in Figure 5.12b).

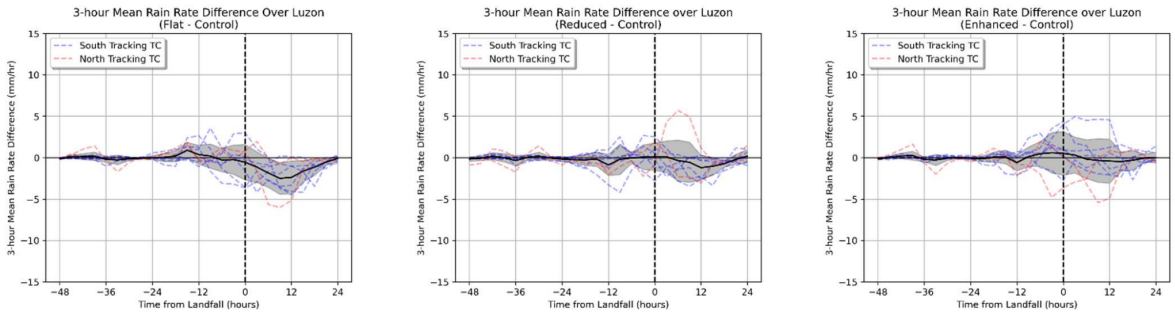

Figure 5.11: Similar to Figure 5.3, but for overall Luzon precipitation difference for (a) Flat - Control, (b) Reduced - Control, and (c) Enhanced - Control.

Based on the previous analyses, for the eight TCs in our study, NTCs and STCs respond differently to different orography changes. STCs tend to have more precipitation over CMR and Luzon when mountain heights increase. On the other hand, NTCs tend to have less precipitation when mountain heights increase. As mentioned earlier in this Subsection, we hypothesise that the lower amounts of precipitation for NTCs for taller mountain heights is due to a combination of weaker TC intensity reducing overall rain-rate, the shifting of the windward side towards the western section of CMR, and finally, the physical blocking introduced by taller mountains in Enhanced CMR. However, as we were only able to simulate two NTCs in this study, these findings for NTCs are less conclusive.

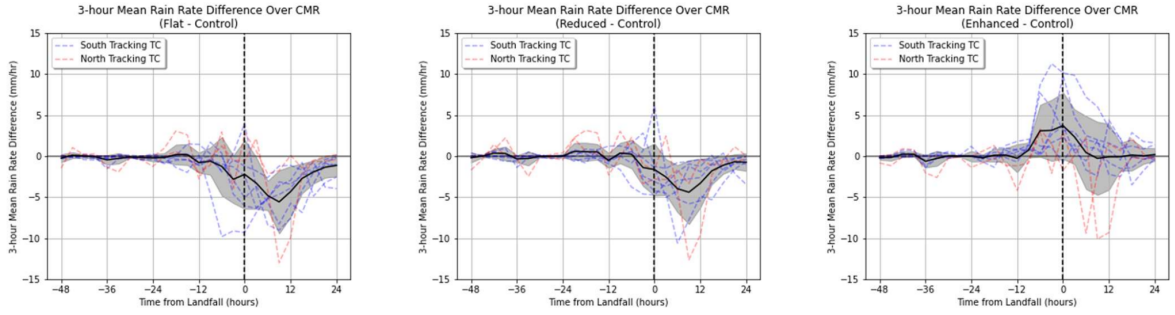

Figure 5.12: Similar to Figure 5.3, but for CMR precipitation difference for (a) Flat - Control, (b) Reduced - Control, and (c) Enhanced - Control.

5.4 Relationship between Precipitation, Wind Speed, and Mountain Slope

The TC tracks in the different model experiments (Figure 5.4), as well as the precipitation difference maps (Figures 5.5 to 5.10) in the previous section, have shown the sensitivity of precipitation on TC movement. As the tracks of the TCs change due to the different CMR heights, precipitation falls along different regions of Luzon. To further understand the direct effect of the CMR height on orographic precipitation during TC passage, in this section we focus on CMR itself. We do this by isolating the slopes of the CMR and then

investigating the empirical relationships between precipitation and individual physical variables such as the zonal easterly winds 1 km above the surface approaching from the plains (u_p), zonal easterly winds moving up the mountain slope (u_s), barrier height (h), barrier slope (h/w, where w is the average width of the barrier), and moist Froude Number (F_w). F_w is calculated according to the following equation as in Chu and Lin (2000)

$$F_w = \frac{u_p}{Nh} \tag{5.2}$$

c where u_p is the wind speed perpendicular to the barrier, h is the barrier height, and N is the moist Brunt–Väisälä frequency.

Durran and Klemp (1982) describe the different dynamical properties and implications between the Brunt–Väisälä frequency of dry and saturated air. In particular, the effective Brunt–Väisälä frequency of saturated air is lower than that of dry air. This is due to dry air and saturated air having different adiabatic lapse rates, hence, affecting air parcel buoyancy. It is then important to consider moisture by considering the saturated adiabatic lapse rate Γ_m in calculating the moist Brunt–Väisälä frequency in the following simplified equation:

$$N^2 = \frac{g}{T}\left(\frac{dT}{dZ} + \Gamma_m\right) \tag{5.3}$$

where g is the acceleration due to gravity, T is the sensible temperature. As the expression in Equation 5.3 produces reasonable accurate numerical results in estimating the moist Brunt–Väisälä frequency (Durran and Klemp, 1982), we continued to use this estimation for this study.

According to Chu and Lin (2000), precipitation is constrained within the plains and upslope regions of the mountain for low to moderate F_w with precipitation falling near the peaks and the downslope regions (lee side) for higher F_w. Additionally, Sinclair (1994) mentions that precipitation is assumed to be enhanced when air is forced over a barrier - this enhancement of precipitation is proportional to the low-level flow and the barrier slope.

We focus on three regions (Northern, Central, and Southern) of average width $w = 27.75$km towards the east of CMR (Figure 5.13). These are further divided into mountain slopes (a, b, and c) and plains regions (d, e, and f) inside the solid and dashed boxes in Figure 5.13, respectively.

Three-hourly data from 24 hours before landfall until 24 hours after are used in calculating these variables. For all TCs, each variable is compared against the mean rain rate along the mountain slope (a, b, and c in Figure 5.13) for all four orography experiments (Control, Flat, Reduced, and Enhanced). This is to establish empirical relationships between winds, mountain height, and mountain precipitation.

We first compare the mean precipitation rate in the eastern slope of the mountain range with the average mountain height (h) and incoming zonal easterly wind speeds along the slope (u_s), excluding eastward downslope winds coming from the western side of the CMR. During the TC landfall period, there is a weak positive relationship between precipitation and perpendicular upslope wind speed u_s (Figure 5.14a). Similarly, the pre-

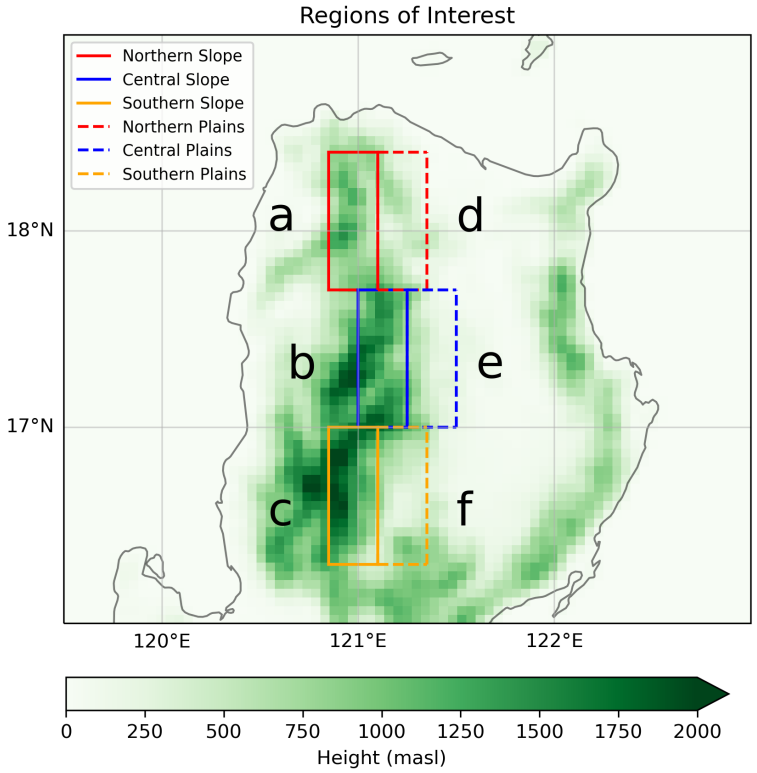

Figure 5.13: The Northern (red), Central (blue), and Southern (yellow) regions towards the east of CMR. The solid boxes (a, b, and c) enclose the eastern slope of the mountain, while the dashed boxes (d, e, and f) show the plains regions towards the east of the mountains.

cipitation rate tends to be greater with taller mountains (Figure 5.14b). These results show that considered on their own, neither the wind speed nor the mountain height is a good indicator of rainfall along the mountain slope.

As the relationship between precipitation and wind speeds is somewhat weak and there is large variability between precipitation rates for the same mountain heights, we next turn to F_w, which is the ratio of wind speeds from the plains u_p and mountain height h (all divided by stability N). Figure 5.14c shows a weak relationship between the precipitation rate and F_w, with Figure 5.15 showing that there is no significant linear relationship between the precipitation rates and the reciprocal of F_w. These show that both F_w and $1/F_w$ are not appropriate descriptors of mountain rainfall. We do notice that the highest values of rainfall are found with low values of F_w, hinting at a negative relationship as found in the low flow regime (Regime I, $F_w < 0.33$) where convective cells are generated over the upslope of the mountain for stratified low bulk flow (Chu and Lin, 2000). However, the analysis of different flow regimes is not within the scope of this study.

We find that the precipitation rate along the mountain is well correlated with the product of the upslope zonal easterly wind and mountain slope ($u_s \times h/w$). Figure 5.14d shows that $u_s \times h/w$ is strongly and positively correlated with the precipitation rate. When the mountain becomes steeper and TC upslope winds become stronger, TC precipitation increases. This is presumably due to the combined effect of stronger winds and steeper slopes, which both favour the mechanical uplift of moist winds, which then causes more condensation and higher amounts of precipitation. This is consistent with the concept of Sinclair (1994) that a strong

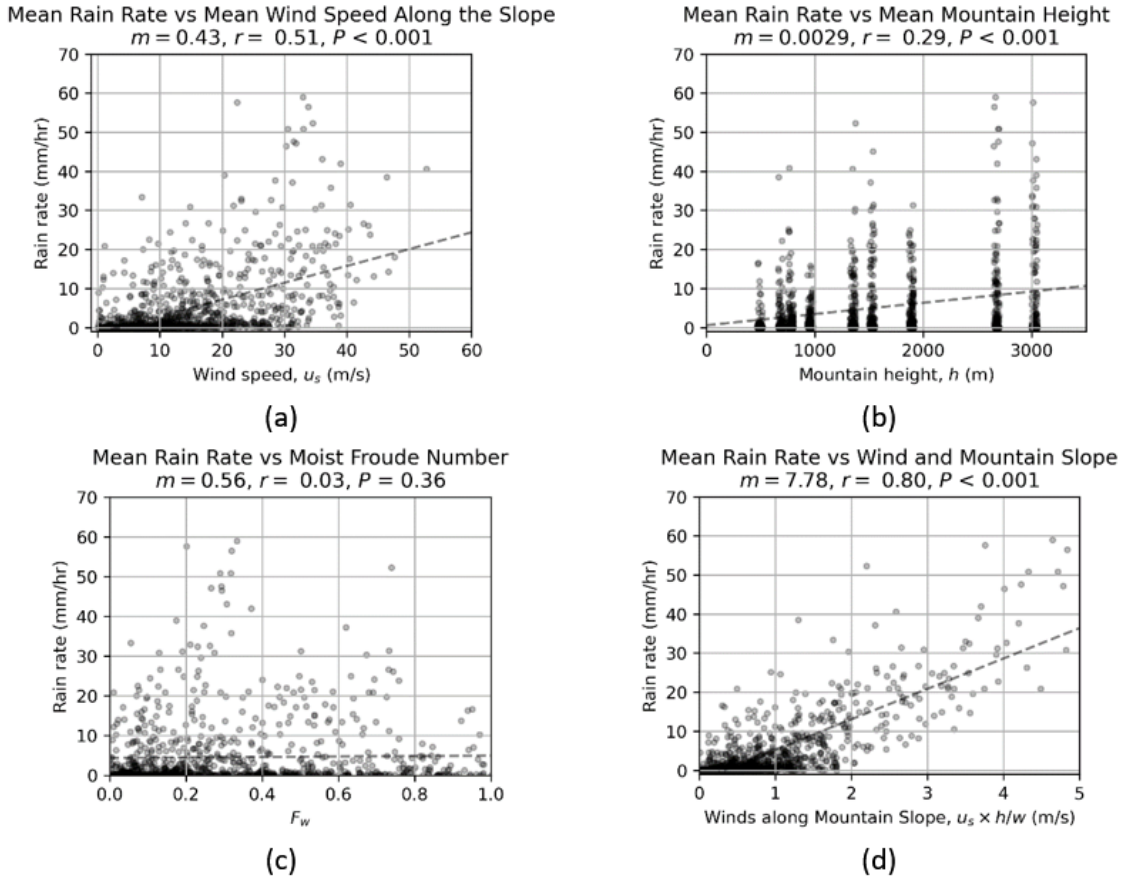

Figure 5.14: Mean rain rate over the slopes of CMR as compared to (a) upslope wind speed u_s, (b) mountain height h, (c) F_w, and (d) the product of wind u_s and mountain slope. Each data point represents 3-hourly periods at different times around TC landfall: from 24 hours before landfall, the time of landfall, and up to 24 hours after landfall. The comparisons that include wind speeds (a and d) do not include winds coming from the west. The dashed lines show the least-squares regression slope for each relationship. The Pearson correlation coefficient (r) and P-value (P) are included above each plot.

vertical motion results in the enhancement of precipitation. We also see from Figure 5.16 that mountain height does not affect horizontal wind speed. Considering all these factors, it is important to take into account both horizontal winds as well as mountain height or slope when estimating rainfall along the mountain. Finally, upon including Precipitable Water (PW) in the relationship between mountain rainfall and winds along the mountain slope (5.17, we see similar relationships with Figure 5.14c. This shows that while sufficiently high PW is an important requirement for precipitation, the horizontal wind speed and mountain slope is enough to estimate possible rainfall along the mountain range, presumably because the PW is high and varies relatively less than the other factors in these TC cases.

To highlight the relationship between winds, slope, and precipitation, we take snapshots of the vertical-zonal cross-section averaged across the latitude range of the Central region (blue enclosed region in Figure 5.13). For Koppu, a TC that showed dramatic differences in orographic impacts between the different experiments, as the product of westward wind and slope at each longitude increases, precipitation similarly increases along the mountain slopes (Figure 5.18). Due to the absence of the CMR in the Flat experiment, minimal precipitation was observed along this section of Luzon (Figure 5.18a). As the terrain heights increase in the

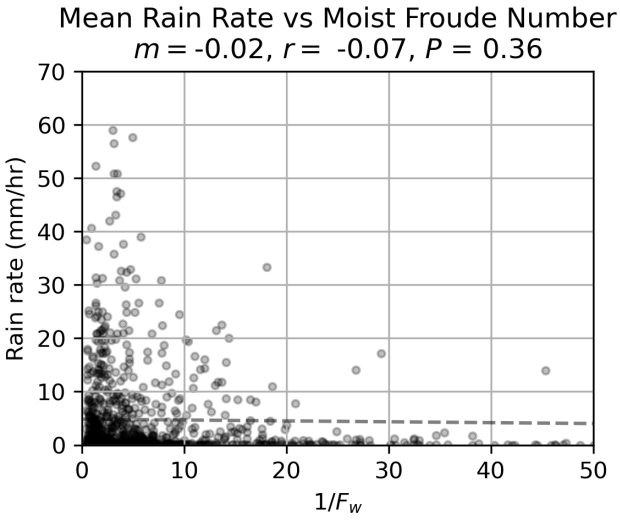

Figure 5.15: Similar to Figure 5.14, but for $1/F_w$.

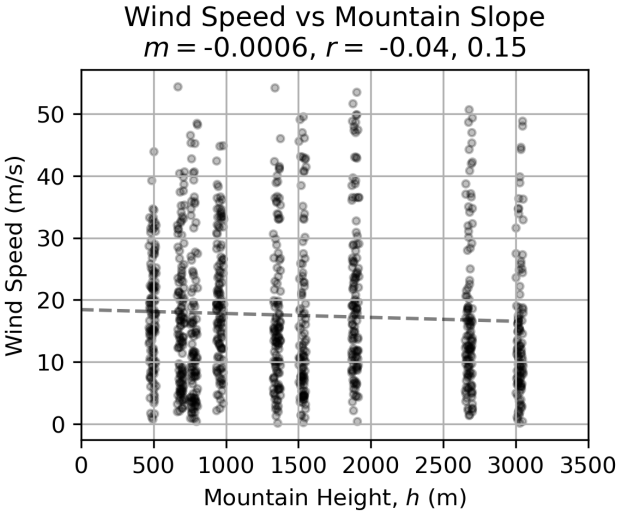

Figure 5.16: Similar to Figure 5.14, but for u_s vs h.

Reduced experiment (Figure 5.18b), precipitation is observed along the general region of the CMR (120.4°E to 121.6°E). Steeper mountain slopes in Control (Figure 5.18c) and Enhanced (Figure 5.18d) show stronger vertical uplift along the slopes, as well as higher amounts of precipitation. As the TC winds flow above the mountaintop (between 121.0°E and 121.1°E), the average TC winds start to descend, and we observe smaller amounts of precipitation towards the leeward side of the mountain. These demonstrate the increase of precipitation for stronger upslope winds flowing along steeper slopes. While low amounts of precipitation were observed in the absence of the CMR, as the mountain slope increases from Reduced, to Control, and finally to Enhanced, the product of the horizontal wind speed and the increasing mountain slope is directly correlated with the precipitation along the windward mountain slope.

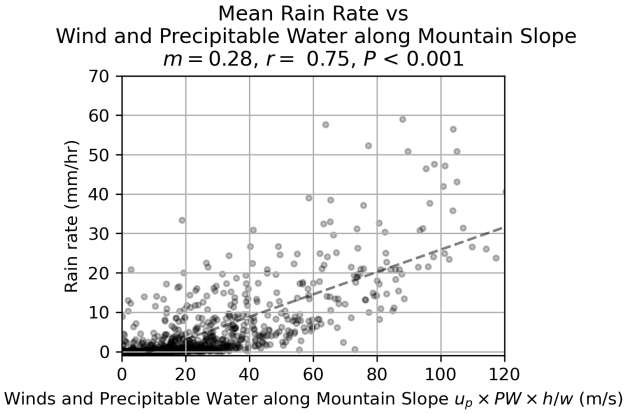

Figure 5.17: Similar to Figure 5.14, but for the product of wind u_s, mountain slope, and Precipitable Water.

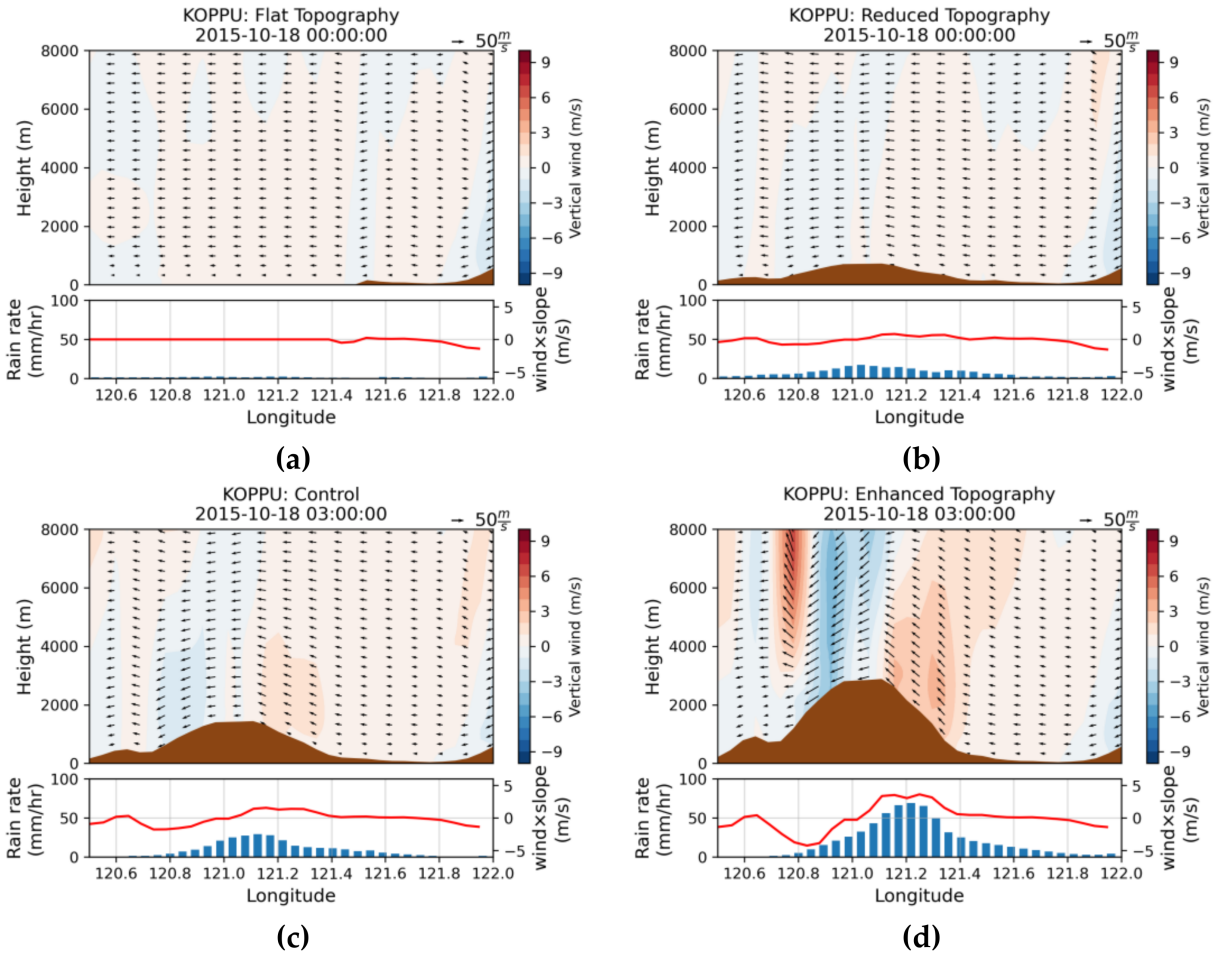

Figure 5.18: Zonal-vertical cross section (averaged across the latitude range of the "Central" region shown in Figure 5.13) of vertical wind (red-blue shading) and mountain height (filled brown curve) during TC Koppu landfall (upper part of each panel) and the average precipitation along the cross-section (lower part of each panel) for (a) Flat, (b) Reduced, (c) Control, and (d) Enhanced. In the lower panels, red lines are for the product of the wind speed and slope, and blue bars show average precipitation. The arrows are wind vectors calculated from horizontal and vertical winds normalised to a scale of 50 m/s as shown in the upper right of each panel. Longer arrows in the figure denote stronger winds.

5.5 Chapter Discussion and Conclusions

This study was motivated by the need to understand the effects of local orography on TCs making landfall in Luzon. While there have been studies on the effects of orography on precipitation (Kirshbaum et al., 2018;

Sinclair, 1994; Smith, 1979; Roe, 2005; Rostom and Lin, 2021), the effects of Luzon's orography on TC characteristics and TC precipitation are not well understood. As such, we examine the effect of the Cordillera Mountain Range, or CMR, the largest mountain range in Luzon, on the precipitation and characteristics of TCs making landfall in the region.

We simulated eight TCs for four different CMR heights (Flat, Reduced, Control, and Enhanced) using the WRF model and evaluated the sensitivity of TC precipitation to the CMR height. From our results, CMR by itself already has a profound effect on TC precipitation, as shown in the accumulated precipitation in the Control experiment (Figure 5.2). To further understand the sensitivity of TC characteristics to mountain ranges, we then modified the orography of the CMR by either decreasing or increasing its height. While changing the mountain height is not possible in real-world scenarios, this allows for further understanding of the interactions between TCs and mountain ranges.

We found that during TC landfall, precipitation along the mountain range slopes increases for increasing CMR height on average, while there are no significant changes for TC movement speeds and TC position for different terrain profiles. TCs tend to weaken for steeper CMR in the Enhanced experiment compared to the Control. In contrast, the weakening of TCs between Flat or Reduced and Control was not apparent. These results suggest a nonlinear relationship between CMR heights and the characteristics of the eight TCs simulated in this study. Moreover, the results also suggest that the actual CMR has minimal effect on TC intensity as it does not differ from the Flat and Reduced experiments. However, we still recommend that more simulations be performed for additional terrain heights and additional TCs to further evaluate the effects of terrain heights on TC intensity.

We also highlight the sensitivity of TC precipitation to TC track — precipitation along the slopes of CMR increases for South-tracking TCs (STCs), while there is less consistency for North-tracking TCs (NTCs). It is possible that this is due to the direction of swirling winds moving towards the western region of CMR, causing precipitation to fall over the South China Sea instead of land and the CMR itself serving to block the eastward moisture flow. For almost all TC cases in this study, orographically-induced TC rainfall varied with modification of orography. In the case of Nari and Bebinca, their tracks also shifted northward, particularly in the Enhanced experiment. While we do not see a systematic pattern between the TC track shifts and orographic changes, TC track shifts can also have non-negligible contribution in precipitation differences in the CMR, especially for more intense TCs.

From Section 4, we found that stronger TCs making landfall in Luzon have higher chances of causing extreme precipitation. As shown in the results of our study, mechanical uplift caused by stronger winds blowing up steeper slopes result in higher amounts of precipitation along the CMR (Figures 5.14d and Figure 5.18). While our results show that TC precipitation is increased towards the eastern regions of CMR, particularly for STCs, the taller mountain ranges in the Enhanced experiment also weaken TCs (compared to Control) as they make landfall. The effects of the mountain range experiments on TC rainfall vary with TC cases, highlighting

the complexity of the mountain, wind, and rainfall relationship. While taller mountain ranges may indeed weaken TCs as they make landfall, a combination of steeper slopes and still-strong upslope winds may cause higher amounts of precipitation along the mountain slopes

While modelling gives us clear representations of the physical processes involved, model errors may affect our results. Similarly, only CMR height was varied in this study, while keeping its land use categories and the heights of the other mountain ranges of Luzon constant. The other mountain ranges may have profound impacts on TCs as well that are yet to be understood and will be considered for future studies. The interactions of orography with other large scale meteorological phenomena (such as monsoons or non-landfalling TCs) may also be considered for future works.

Knowing the effects of the mountain ranges of Luzon on TCs can be helpful for the Philippines, and for other countries in the Northwest Pacific. Man-chi and Chun-Wing (2015) previously mentioned that TCs crossing Luzon from east to west are more likely to affect Hong Kong and Vietnam, and understanding the effects of the mountain ranges of Luzon on TC intensity may be helpful in anticipating possible hazards in those regions. For the Philippines, understanding how TCs interact with mountain ranges may help in identifying local enhancement of precipitation due to stronger moist upslope winds across mountain ranges. However, as taller mountain ranges themselves may indeed weaken TCs intensity (and hence, winds), there are further nuances to consider in terms of anticipating the amount of precipitation incoming TCs may bring.

Chapter 6

Conclusions and Future Work

6.1 Key Findings

This thesis presents an attempt to deepen our understanding of Tropical Cyclones (TC), particularly those that affect the northern Philippine province of Luzon. In order to better understand what affects a TC's precipitation, our goal was to first establish which TC characteristics are connected to extreme precipitation and then evaluate how Luzon's orography could influence TC characteristics and precipitation.

In the first part of our thesis (Chapter 4), we evaluated the historical record of westward-moving TCs that made landfall in Luzon between 1978 and 2015. We first created a TC dataset with similar paths upon landfall where TCs originate from the Western North Pacific (WNP), traverse Luzon from an East to West direction, and then finally exit towards the South China Sea. The similar westward moving TC tracks reduces the possible uncertainties that discontinuous or dissimilar tracks may introduce in the dataset. We then developed the Weighted Mean Precipitation Exceedance (WPE), a measure of extreme precipitation that combines both magnitude and spatial extent, that allowed us to statistically compare the extreme precipitation of different TCs for different categories based on their characteristics. We found that Typhoons (TY), or TCs that are strong prior to landfall (intensity $>$ 64 knots), tend to yield higher WPE than weaker TCs (Non-Typhoons, or Non-TYs), while Slow TCs (movement speed $<$ 11.38 knots) yield higher WPE than Fast TCs. Upon considering TCs of similar intensity, we found that there is no significant difference in WPE between categories regardless of TC movement speed. However, for TCs of similar movement speed, Slow or Fast TYs tend to have higher WPE than Non-TYs of the same movement speed categories. On a similar note, while there is no significant difference in WPE between the seasons June to September and October to December (JJAS and OND, respectively), TYs yield higher WPE compared to Non-TYs within the same season categories. These results suggest that

WPE has a stronger relationship with pre-landfall TC intensity than TC movement speed or season.

However, when evaluating the difference in TC intensity between JJAS and OND, we found that OND TCs tend to be stronger than JJAS TCs — TCs that make landfall during OND are stronger than JJAS TCs due to OND TCs forming further to the southeast, allowing for further TC intensification. This raises the apparent contradiction of the typically stronger OND TCs having similar WPE with JJAS TCs. By evaluating the probabilities of different combined categories to exceed a WPE threshold by establishing a decision table (Table 4.2), we found that, compared to OND TC subcategories most JJAS TC subcategories have higher probabilities of exceeding the median WPE of all TCs. We also found that while intensity and movement speed matter for anticipating higher WPE, this relationship between WPE and TC intensity is stronger for most JJAS TCs than for OND TCs.

While identifying which TC characteristics are associated with extreme precipitation is useful in determining the possible impacts of an incoming TC, this does not necessarily explain how these characteristics affect precipitation. In the second part of this thesis (Chapter 5) we conducted Numerical Weather Prediction (NWP) model experiments to understand how TC winds interact with mountain ranges. Using the Weather Research and Forecast (WRF) model, we simulated the sensitivity of eight TCs to different heights of the Cordillera Mountain Range (CMR): Reduced ($0.5\times$ CMR height), Control, and Enhanced ($2.0\times$ CMR height). The TCs that we modelled were selected based on their WPE and their track: these TCs have high WPE and made landfall in Luzon while moving along CMR.

We found that as the height of CMR is increased from Control to Enhanced, TCs weaken as early as 12 hours prior to landfall. In contrast, the weakening of TCs between Reduced and Control was not apparent, and it is possible that TC intensity is less sensitive to mountain ranges at or below the height of the actual CMR. We also found that TC movement was not significantly affected by the modification of orography. Due to Luzon's limited east-west extent (approximately 300km) and the fact that most TCs spend little time over land, it is possible that the TC translation speed and position are not considerably affected by Luzon. Instead, TC track is likely more determined by the steering flow in which TCs are usually embedded.

In terms of rainfall, as a TC crosses Luzon, CMR in itself has a profound effect on TC precipitation as seen in the accumulated precipitation maps of the Control experiments. Furthermore, as the height of CMR increases — from Reduced to Control, and from Control to Enhanced — precipitation increases along the slopes of the mountain range. The increase in precipitation over CMR occurs after landfall for most TCs in Reduced, and as early as 12 hours prior to landfall for Enhanced. Additionally, TC rainbands slightly vary with the modification of orography for most cases in this study. However, as previously mentioned, no consistent or significant patterns in storm tracks (hence precipitation distribution) were found due to orography changes.

We split our sample of 8 simulated TCs into two northward (NTC) and six southward (STC) tracking TCs according to their tracks over Luzon. Comparing the Control and Enhanced experiments, while average precipitation increased for STCs during TC landfall, there was a decrease in precipitation for the two NTCs. The

track of NTCs combined with the increase in mountain height may have led to the reduction of TC wind strength downwind of the CMR, and the inner regions of Luzon. This shows that for the eight TCs we simulated for this study, the CMR precipitation of NTCs and STCs respond differently in the different orography experiments. However, as we only simulated a limited number of TCs for this study, it is recommended that more TCs, especially NTCs, be included in future studies.

Finally, by isolating the central region of CMR, we established empirical relationships between precipitation and individual physical variables such as the zonal winds 1km above the surface approaching from the plains (u_p), zonal winds moving up the mountain slope (u_s), barrier height (h), barrier slope (h/w), and moist Froude Number (F_w). We found that there are weak relationships between precipitation and wind speed, barrier height, or Froude Number. This shows that considered on their own, the wind speed, the mountain height, or Froude Number are poor predictors of rainfall along the mountain slope. However, we found that the product of the zonal wind and mountain slope ($u_s \times h/w$) is well correlated with the precipitation rates along the mountain. Mechanical uplift caused by stronger winds blowing up steeper slopes results in higher amounts of precipitation along the mountain range, This is further supported by the average cross-sections of rainfall, winds, and mountain heights during TC Koppu's landfall for Reduced, Control, and Enhanced. As we traverse the cross-section from West to East along the longitude, we observed higher amounts of precipitation for steeper slopes with stronger winds, where we also found stronger vertical winds.

6.2 Implications and Scientific Advances

In this thesis, we presented factors that, either directly or indirectly, contribute to severe precipitation in the Philippines during TC landfall. Using localised precipitation thresholds, we presented a novel approach of determining extreme precipitation that considers both spatial extent and magnitude. As we were able to quantitatively compare the precipitation of different TCs using a single variable, WPE, we were able to develop a decision table that can be used as a guide to anticipate the possible impacts of TCs that are anticipated to make landfall in Luzon. By determining the season, the intensity, and the movement speed of an approaching TC, we can quickly establish whether it has a greater likelihood of causing extreme precipitation.

We also found that mountains have profound effects on landfalling TCs. By conducting multiple NWP experiments for different orography configurations, we found that both intensity and precipitation are highly sensitive to mountain height. While changing the orography is not possible in real-world scenarios, this allows for further understanding of the interactions between TCs and mountain ranges.

Our results in this two-part study may aid in forecasts in the Philippines, particularly for disaster risk reduction and mitigation efforts. As mentioned in our findings, TCs bring precipitation to otherwise climatologically drier regions of Luzon, mostly along the slopes of the CMR. It is essential to mention that CMR borders two major river basins in the Philippines — the Cagayan River basin, and the Pampanga River basin

— both of which are heavily populated downstream (Macalalad et al., 2021). TC precipitation along the slopes of the CMR may accumulate and generate high amounts of runoff, causing flash floods along the plains of the aforementioned river basins. Understanding how CMR influences precipitation, where this precipitation may fall, as well as how the mountain range may affect TC intensity, can be crucial in future forecasting and preparation efforts in the communities within the vicinity of mountain ranges in the Philippines. Additionally, the decision table introduced in Section 4.3 can be used as a tool to provide quick insights during forecasting.

6.3 Limitations and Future Works

One limitation of this study is the historical data we used. While we were able to use accessible and open data such as IBTrACS, APHRODITE, TRMM, and IMERG, these are limited spatially, temporally, and in terms of data included and data availability. For example, TC intensity data are severely limited in the pre-satellite era, with the IBTrACS database having limited TC intensity records before 1978. Additionally, the gridded precipitation data from APHRODITE versions V1101 and V1101EX are only available between 1951 and 2015 due to the different methodologies involved between APHRODITE versions. APHRODITE, while comprehensive, is also limited by the interpolation method, and the availability and quality of weather stations in the Philippines. In terms of temporal resolution, APHRODITE lacks sub-daily precipitation information which may lead to biases in precipitation estimation. While satellite-based precipitation products such as TRMM and IMERG offer gridded precipitation data in higher temporal and spatial resolutions, these are only available in more recent years, with TRMM available from 1998 to 2019 and IMERG from 2000 to the present. Using these products would severely reduce the sample size of TCs we can analyse, potentially making the relationships between TC characteristics and extreme precipitation less apparent. Nevertheless, initial evaluations of using either APHRODITE or TRMM in our WPE analysis yield similar results in most of the comparisons between TC categories. Finally, while IMERG does measure regional precipitation patterns well, its performance in measuring precipitation over mountainous terrain still needs improvement (Hsu et al., 2021; Pradhan et al., 2022).

Despite the availability of other models, we opted to continue working with WRF due to familiarity with the model. This allowed for consistent and automated workflows from download, to pre-processing, to model running, and finally, post-processing. Other high-resolution NWP models, such as the Unified Model developed by the United Kingdom Met Office, may be considered in future experiments.

In our modelling experiments, we mainly evaluated the TC-land interactions and their effects on intensity and rainfall. While slope and winds were key variables to estimate possible rainfall along the mountain ranges for the selected TCs in this study, there are many different factors that may affect TC formation, strength, and precipitation. These factors include but are not limited to, environmental relative humidity, wind shear, prevailing winds, other existing weather systems and land use. Analysing the effects of these factors on TCs may be considered in future studies.

As we primarily focused on the analysis of historical observations, as well as the direct interactions of TCs and land, we have yet to take into account how climate change may affect TC-associated precipitation in the future. According to the Sixth Assessment Report of the Intergovernmental Panel on Climate Change (IPCC) the intensity and frequency of climate extremes, which includes the intensification of extreme precipitation associated with TCs, may increase in the future due to human-induced greenhouse gas emissions (Seneviratne et al., 2021). While we now have a deeper understanding of the physical mechanisms associated with extreme TC-related precipitation in Luzon, we have yet to evaluate the impact of these TCs, especially in the context of a changing climate.

Finally, while understanding the impact of TCs (its intensity, winds, precipitation, and movement) in the context of disaster risk reduction and mitigation is of key importance, we have not yet conducted impact-based analysis based on the results of this study. Additional insights based on the orography, morphology, and hydrological response of CMR may be considered to augment existing hazard maps in the region. This may be done in future studies where NWP forecasts focused on mountainous regions be considered and included in impact-based hazard maps.

Bibliography

Abon, C. C., C. P. C. David, and N. E. B. Pellejera, 2011: Reconstructing the Tropical Storm Ketsana flood event in Marikina River, Philippines. *Hydrology and Earth System Sciences*, **15 (4)**, 1283–1289, doi: 10.5194/hess-15-1283-2011, URL http://www.hydrol-earth-syst-sci.net/15/1283/2011/.

Akasaka, I., W. Morishima, and T. Mikami, 2007: Seasonal march and its spatial difference of rainfall in the Philippines. *International Journal of Climatology*, **27 (6)**, 715–725, doi: 10.1002/joc.1428, URL http://doi.wiley.com/10.1002/joc.1428.

Aragon, L. G. B., and A. G. Pura, 2016: Analysis of the displacement error of the WRF-ARW model in predicting tropical cyclone tracks over the Philippines: Analysis of the displacement error of the WRF-ARW model in TC tracks. *Meteorological Applications*, **23 (3)**, 401–408, doi: 10.1002/met.1564, URL https://onlinelibrary.wiley.com/doi/10.1002/met.1564.

Arlene Laing, J.-L. E., 2011: Ch. 8.7.1: Tropical Cyclones: The "β-Effect" and Environmental "β" effect. *Introduction to Tropical Meteorology*, Boulder, Colorado, United States of America, URL https://ftp.comet.ucar.edu/memory-stick/tropical/textbook_2nd_edition/navmenu.php_tab_9_page_7.1.0.htm, MIT OpenCourseWare.

Bagtasa, G., 2017: Contribution of Tropical Cyclones to Rainfall in the Philippines. *Journal of Climate*, **30 (10)**, 3621–3633, doi: 10.1175/JCLI-D-16-0150.1, URL http://journals.ametsoc.org/doi/10.1175/JCLI-D-16-0150.1.

Bagtasa, G., 2019: Enhancement of summer monsoon rainfall by tropical cyclones in northwestern philippines. *Journal of the Meteorological Society of Japan. Ser. II*, **97 (5)**, 967–976, doi: 10.2151/jmsj.2019-052.

Bagtasa, G., 2020: Influence of Madden–Julian Oscillation on the Intraseasonal Variability of Summer and Winter Monsoon Rainfall in the Philippines. *Journal of Climate*, **33 (22)**, 9581–

9594, doi: 10.1175/JCLI-D-20-0305.1, URL https://journals.ametsoc.org/jcli/article/33/22/9581/354290/Influence-of-MaddenJulian-Oscillation-on-the.

Bakkensen, L. A., and R. O. Mendelsohn, 2019: Global Tropical Cyclone Damages and Fatalities Under Climate Change: An Updated Assessment. *Hurricane Risk*, J. M. Collins, and K. Walsh, Eds., Springer International Publishing, Cham, 179–197, doi: 10.1007/978-3-030-02402-4_9, URL https://doi.org/10.1007/978-3-030-02402-4_9.

Basconcillo, J., and I.-J. Moon, 2021: Recent increase in the occurrences of Christmas typhoons in the Western North Pacific. *Scientific Reports*, **11 (1)**, 7416, doi: 10.1038/s41598-021-86814-x, URL http://www.nature.com/articles/s41598-021-86814-x.

Bender, M. A., R. E. Tuleya, and Y. Kurihara, 1987a: A numerical study of the effect of island terrain on tropical cyclones. *Monthly Weather Review*, **115 (1)**, 130 – 155, doi: https://doi.org/10.1175/1520-0493(1987)115⟨0130:ANSOTE⟩2.0.CO;2, URL https://journals.ametsoc.org/view/journals/mwre/115/1/1520-0493_1987_115_0130_ansote_2_0_co_2.xml.

Bender, M. A., R. E. Tuleya, and Y. Kurihara, 1987b: A Numerical Study of the Effect of Island Terrain on Tropical Cyclones. *Monthly Weather Review*, **115 (1)**, 130–155, doi: 10.1175/1520-0493(1987)115⟨0130:ANSOTE⟩2.0.CO;2, URL http://journals.ametsoc.org/doi/10.1175/1520-0493(1987)115⟨0130:ANSOTE⟩2.0.CO;2.

Bowman, K. P., and M. D. Fowler, 2015: The Diurnal Cycle of Precipitation in Tropical Cyclones. *Journal of Climate*, **28 (13)**, 5325–5334, doi: 10.1175/JCLI-D-14-00804.1, URL https://journals.ametsoc.org/jcli/article/28/13/5325/106239/The-Diurnal-Cycle-of-Precipitation-in-Tropical.

Camargo, S. J., and S. M. Hsiang, 2015: Tropical Cyclones: From the Influence of Climate to Their Socioeconomic Impacts. *Geophysical Monograph Series*, M. Chavez, M. Ghil, and J. Urrutia-Fucugauchi, Eds., John Wiley & Sons, Inc, Hoboken, NJ, 303–342, doi: 10.1002/9781119157052.ch18, URL http://doi.wiley.com/10.1002/9781119157052.ch18.

Camargo, S. J., and A. H. Sobel, 2005: Western North Pacific Tropical Cyclone Intensity and ENSO. *Journal of Climate*, **18 (15)**, 2996–3006, doi: 10.1175/JCLI3457.1, URL https://journals.ametsoc.org/jcli/article/18/15/2996/30662/Western-North-Pacific-Tropical-Cyclone-Intensity.

Cayanan, E., T.-C. Chen, J. Argete, M.-C. Yen, and P. Nilo, 2011: The Effect of Tropical Cyclones on Southwest Monsoon Rainfall in the Philippines. *Journal of the Meteorological Society of Japan*, **89A**, 123–139, doi: 10.2151/jmsj.2011-A08, URL http://joi.jlc.jst.go.jp/JST.JSTAGE/jmsj/2011-A08?from=CrossRef.

Chan, J. C., 2005a: The Physics Of Tropical Cyclone Motion. *Annual Review of Fluid Mechanics*, **37 (1)**, 99–128, doi: 10.1146/annurev.fluid.37.061903.175702, URL https://www.annualreviews.org/doi/10.1146/annurev.fluid.37.061903.175702.

Chan, J. C. L., 2005b: Interannual and interdecadal variations of tropical cyclone activity over the western North Pacific. *Meteorology and Atmospheric Physics*, **89 (1-4)**, 143–152, doi: 10.1007/s00703-005-0126-y, URL http://link.springer.com/10.1007/s00703-005-0126-y.

Chan, J. C. L., and C. Li, 2004: The East Asia Winter Monsoon. *World Scientific Series on Asia-Pacific Weather and Climate*, **02**, WORLD SCIENTIFIC, 54–106, doi: 10.1142/9789812701411_0002, URL http://www.worldscientific.com/doi/abs/10.1142/9789812701411_0002.

Chavas, D. R., K. A. Reed, and J. A. Knaff, 2017: Physical understanding of the tropical cyclone wind-pressure relationship. *Nature Communications*, **8 (1)**, 1360, doi: 10.1038/s41467-017-01546-9, URL https://www.nature.com/articles/s41467-017-01546-9.

Chen, G., H. Yu, and Q. Cao, 2015: Evaluation of Tropical Cyclone Forecasts from Operational Global Models Over the Western North Pacific in 2013. *Tropical Cyclone Research and Review*, **4 (1)**, 18–26, doi: 10.6057/2015TCRR01.03, URL https://www.sciencedirect.com/science/article/pii/S2225603218301218.

Chen, R., W. Zhang, and X. Wang, 2020: Machine learning in tropical cyclone forecast modeling: A review. *Atmosphere*, **11 (7)**, doi: 10.3390/atmos11070676, URL https://www.mdpi.com/2073-4433/11/7/676.

Chen, Y., and X. Yu, 2016: Enhancement of wind stress evaluation method under storm conditions. *Climate Dynamics*, **47 (12)**, 3833–3843, doi: 10.1007/s00382-016-3044-4, URL http://link.springer.com/10.1007/s00382-016-3044-4.

Cheung, K., and Coauthors, 2018: Recent Advances in Research and Forecasting of Tropical Cyclone Rainfall. *Tropical Cyclone Research and Review*, **7 (2)**, 106–126, doi: 10.6057/2018TCRR02.03.

Cheung, K. K. W., L.-R. Huang, and C.-S. Lee, 2008: Characteristics of rainfall during tropical cyclone periods in Taiwan. *Natural Hazards and Earth System Sciences*, **8 (6)**, 1463–1474, doi: 10.5194/nhess-8-1463-2008, URL https://www.nat-hazards-earth-syst-sci.net/8/1463/2008/.

Chia, H. H., and C. F. Ropelewski, 2002: The Interannual Variability in the Genesis Location of Tropical Cyclones in the Northwest Pacific. *Journal of Climate*, **15**, 11.

Chu, C.-M., and Y.-L. Lin, 2000: Effects of Orography on the Generation and Propagation of Mesoscale Convective Systems in a Two-Dimensional Conditionally Unstable Flow. *Journal of the Atmospheric Sciences*, **57 (23)**, 3817–3837, doi: 10.1175/1520-0469(2001)057⟨3817:EOOOTG⟩2.0.CO;2, URL http://journals.ametsoc.org/doi/abs/10.1175/1520-0469%282001%29057%3C3817%3AEOOOTG%3E2.0.CO%3B2.

Cinco, T. A., and Coauthors, 2016: Observed trends and impacts of tropical cyclones in the Philippines. *International Journal of Climatology*, **36 (14)**, 4638–4650, doi: 10.1002/joc.4659, URL http://doi.wiley.com/10.1002/joc.4659.

Copernicus Climate Change Service, 2022: Monthly and 6-hourly total column water vapour over ocean from 1988 to 2020 derived from satellite observations. ECMWF, URL https://cds.climate.copernicus.eu/doi/10.24381/cds.92db7fef, doi: 10.24381/CDS.92DB7FEF.

Corporal-Lodangco, I. L., and L. M. Leslie, 2016: Cluster Analysis of Philippine Tropical Cyclone Climatology: Applications to Forecasting. *Journal of Climatology & Weather Forecasting*, **04 (01)**, 1–17, doi: 10.4172/2332-2594.1000152, URL http://www.esciencecentral.org/journals/cluster-analysis-of-philippine-tropical-cyclone-climatology-applicationsto-forecasting-2332-2594-1000152.php?aid=68033.

Corporal-Lodangco, I. L., L. M. Leslie, and P. J. Lamb, 2016: Impacts of ENSO on Philippine Tropical Cyclone Activity. *Journal of Climate*, **29 (5)**, 1877–1897, doi: 10.1175/JCLI-D-14-00723.1, URL http://journals.ametsoc.org/doi/10.1175/JCLI-D-14-00723.1.

Craig, G. C., and S. L. Gray, 1996: CISK or WISHE as the Mechanism for Tropical Cyclone Intensification. *Journal of the Atmospheric Sciences*, **53 (23)**, 3528–3540, doi: 10.1175/1520-0469(1996)053⟨3528:COWATM⟩2.0.CO;2, URL http://journals.ametsoc.org/doi/10.1175/1520-0469(1996)053⟨3528:COWATM⟩2.0.CO;2.

Cruz, F., G. Narisma, M. Villafuerte, K. Cheng Chua, and L. Olaguera, 2013: A climatological analysis of the southwest monsoon rainfall in the Philippines. *Atmospheric Research*, **122**, 609–616, doi: 10.1016/j.atmosres.2012.06.010, URL https://linkinghub.elsevier.com/retrieve/pii/S0169809512001858.

Cruz, F. T., and G. T. Narisma, 2016: WRF simulation of the heavy rainfall over Metropolitan Manila, Philippines during tropical cyclone Ketsana: a sensitivity study. *Meteorology and Atmospheric Physics*, **128 (4)**, 415–428, doi: 10.1007/s00703-015-0425-x, URL http://link.springer.com/10.1007/s00703-015-0425-x.

David, C. P. C., B. A. B. Racoma, J. Gonzales, and M. V. Clutario, 2013: A Manifestation of Climate Change? A Look at Typhoon Yolanda in Relation to the Historical Tropical Cyclone Archive. *Science Diliman*, 8.

Delfino, R. J., G. Bagtasa, K. Hodges, and P. L. Vidale, 2022: Sensitivity of simulating Typhoon Haiyan (2013) using WRF: the role of cumulus convection, surface flux parameterizations, spectral nudging, and initial and boundary conditions. *Natural Hazards and Earth System Sciences*, **22 (10)**, 3285–3307, doi: 10.5194/nhess-22-3285-2022, URL https://nhess.copernicus.org/articles/22/3285/2022/.

Delfino, R. J., P. L. Vidale, G. Bagtasa, and K. Hodges, 2023: Response of damaging Philippines tropical cyclones to a warming climate using the pseudo global warming approach. *Climate Dynamics*, **61 (7-8)**, 3499–3523, doi: 10.1007/s00382-023-06742-6, URL https://link.springer.com/10.1007/s00382-023-06742-6.

Diffenbaugh, N. S., J. S. Pal, R. J. Trapp, and F. Giorgi, 2005: Fine-scale processes regulate the response of extreme events to global climate change. *Proceedings of the National Academy of Sciences*, **102 (44)**, 15 774–15 778, doi: 10.1073/pnas.0506042102, URL http://www.pnas.org/cgi/doi/10.1073/pnas.0506042102.

Durran, D. R., and J. B. Klemp, 1982: On the Effects of Moisture on the Brunt-Väisälä Frequency. *Journal of the Atmospheric Sciences*, **39 (10)**, 2152–2158, doi: 10.1175/1520-0469(1982)039⟨2152:OTEOMO⟩2.0.CO;2, URL http://journals.ametsoc.org/doi/10.1175/1520-0469(1982)039⟨2152:OTEOMO⟩2.0.CO;2.

Emanuel, K., 2003: Tropical Cyclones. *Annual Review of Earth and Planetary Sciences*, **31 (1)**, 75–104, doi: 10.1146/annurev.earth.31.100901.141259, URL https://www.annualreviews.org/doi/10.1146/annurev.earth.31.100901.141259.

Emanuel, K., 2005: Increasing destructiveness of tropical cyclones over the past 30 years. *Nature*, **436 (7051)**, 686–688, doi: 10.1038/nature03906, URL https://www.nature.com/articles/nature03906.

Emanuel, K., 2017: Assessing the present and future probability of Hurricane Harvey's rainfall. *Proceedings of the National Academy of Sciences*, **114 (48)**, 12 681–12 684, doi: 10.1073/pnas.1716222114, URL http://www.pnas.org/lookup/doi/10.1073/pnas.1716222114.

Emanuel, K. A., 1986: An Air-Sea Interaction Theory for Tropical Cyclones. Part I: Steady-State Maintenance. *Journal of the Atmospheric Sciences*, **43 (6)**, 585–605, doi: 10.1175/1520-0469(1986)043⟨0585:AASITF⟩2.0.CO;2, URL http://journals.ametsoc.org/doi/10.1175/1520-0469(1986)043⟨0585:AASITF⟩2.0.CO;2.

Emerald Group Publishing Limited, 2001: Weather. *Disaster Prevention and Management: An International Journal*, **10 (4)**, doi: 10.1108/dpm.2001.07310dac.003, URL https://www.emerald.com/insight/content/doi/10.1108/dpm.2001.07310dac.003/full/html.

Fei, R., J. Xu, Y. Wang, and C. Yang, 2020: Factors Affecting the Weakening Rate of Tropical Cyclones over the Western North Pacific. *Monthly Weather Review*, **148 (9)**, 3693–3712, doi: 10.1175/MWR-D-19-0356.1, URL http://journals.ametsoc.org/doi/10.1175/MWR-D-19-0356.1.

Feng, X., N. P. Klingaman, and K. I. Hodges, 2021: Poleward migration of western North Pacific tropical cyclones related to changes in cyclone seasonality. *Nature Communications*, **12 (1)**, 6210, doi: 10.1038/s41467-021-26369-7, URL https://www.nature.com/articles/s41467-021-26369-7.

Fu, D., P. Chang, C. M. Patricola, R. Saravanan, X. Liu, and H. E. Beck, 2021: Central American mountains inhibit eastern North Pacific seasonal tropical cyclone activity. *Nature Communications*, **12 (1)**, 4422, doi: 10.1038/s41467-021-24657-w, URL https://www.nature.com/articles/s41467-021-24657-w.

Fujiwhara, S., 1923: On the growth and decay of vortical systems: ON THE GROWTH AND DECAY OF VORTICAL SYSTEMS. *Quarterly Journal of the Royal Meteorological Society*, **49 (206)**, 75–104, doi: 10.1002/qj.49704920602, URL http://doi.wiley.com/10.1002/qj.49704920602.

Ge, X., T. Li, and M. Peng, 2013: Effects of Vertical Shears and Midlevel Dry Air on Tropical Cyclone Developments*. *Journal of the Atmospheric Sciences*, **70 (12)**, 3859–3875, doi: 10.1175/JAS-D-13-066.1, URL https://journals.ametsoc.org/doi/10.1175/JAS-D-13-066.1.

Gray, W. M., 1968: Global view of the origin of tropical disturbances and storms. *Monthly Weather Review*, **96 (10)**, 669 – 700, doi: https://doi.org/10.1175/1520-0493(1968)096⟨0669:GVOTOO⟩2.0.CO;2, URL https://journals.ametsoc.org/view/journals/mwre/96/10/1520-0493_1968_096_0669_gvotoo_2_0_co_2.xml.

Gray, W. M., 1977: Tropical Cyclone Genesis in the Western North Pacific. *Journal of the Meteorological Society of Japan. Ser. II*, **55 (5)**, 465–482, doi: 10.2151/jmsj1965.55.5_465, URL https://www.jstage.jst.go.jp/article/jmsj1965/55/5/55_5_465/_article.

Gray, W. M., 1998: The formation of tropical cyclones. *Meteorology and Atmospheric Physics*, **67 (1-4)**, 37–69, doi: 10.1007/BF01277501, URL http://link.springer.com/10.1007/BF01277501.

GSFC, P. P. S. P. A. N., 2018: GPM IMERG Final Precipitation L3 Half Hourly 0.1 degree x 0.1 degree V05. NASA Goddard Earth Sciences Data and Information Services Center, URL https://disc.gsfc.nasa.gov/datacollection/GPM_3IMERGHH_06.html, type: dataset, doi: 10.5067/GPM/IMERG/3B-HH/05.

Guo, L., N. P. Klingaman, P. L. Vidale, A. G. Turner, M.-E. Demory, and A. Cobb, 2017: Contribution of Tropical Cyclones to Atmospheric Moisture Transport and Rainfall over East Asia. *Journal of Climate*, **30 (10)**, 3853–3865, doi: 10.1175/JCLI-D-16-0308.1, URL http://journals.ametsoc.org/doi/10.1175/JCLI-D-16-0308.1.

Hersbach, H., and Coauthors, 2020: The ERA5 global reanalysis. *Quarterly Journal of the Royal Meteorological Society*, **146 (730)**, 1999–2049, doi: 10.1002/qj.3803, URL https://onlinelibrary.wiley.com/doi/abs/10.1002/qj.3803.

Holland, G. J., 1983: Tropical cyclone motion: Environmental interaction plus a beta effect. *Journal of Atmospheric Sciences*, **40 (2)**, 328 – 342, doi: https://doi.org/10.1175/1520-0469(1983)040⟨0328:TCMEIP⟩2.0.CO;2, URL https://journals.ametsoc.org/view/journals/atsc/40/2/1520-0469_1983_040_0328_tcmeip_2_0_co_2.xml.

Hou, A. Y., and Coauthors, 2014: The Global Precipitation Measurement Mission. *Bulletin of the American Meteorological Society*, **95 (5)**, 701–722, doi: 10.1175/BAMS-D-13-00164.1, URL http://journals.ametsoc.org/doi/10.1175/BAMS-D-13-00164.1.

Hsu, J., W.-R. Huang, and P.-Y. Liu, 2021: Performance assessment of GPM-based near-real-time satellite products in depicting diurnal precipitation variation over Taiwan. *Journal of Hydrology: Regional Studies*, **38**, 100 957, doi: 10.1016/j.ejrh.2021.100957, URL https://linkinghub.elsevier.com/retrieve/pii/S2214581821001865.

Hsu, L.-H., H.-C. Kuo, and R. G. Fovell, 2013: On the Geographic Asymmetry of Typhoon Translation Speed across the Mountainous Island of Taiwan. *Journal of the Atmospheric Sciences*, **70 (4)**, 1006–1022, doi: 10.1175/JAS-D-12-0173.1, URL http://journals.ametsoc.org/doi/abs/10.1175/JAS-D-12-0173.1.

Huang, C.-Y., C.-A. Chen, S.-H. Chen, and D. S. Nolan, 2016: On the Upstream Track Deflection of Tropical Cyclones Past a Mountain Range: Idealized Experiments. *Journal of the Atmospheric Sciences*, **73 (8)**, 3157–3180, doi: 10.1175/JAS-D-15-0218.1, URL https://journals.ametsoc.org/doi/10.1175/JAS-D-15-0218.1.

Huang, C.-Y., C.-W. Chou, S.-H. Chen, and J.-H. Xie, 2020: Topographic Rainfall of Tropical Cyclones past a Mountain Range as Categorized by Idealized Simulations. *Weather and Forecasting*, **35 (1)**, 25–49, doi: 10.1175/WAF-D-19-0120.1, URL https://journals.ametsoc.org/view/journals/wefo/35/1/waf-d-19-0120.1.xml.

Huffman, G. J., and Coauthors, 2007: The TRMM Multisatellite Precipitation Analysis (TMPA): Quasi-Global, Multiyear, Combined-Sensor Precipitation Estimates at Fine Scales. *Journal of Hydrometeorology*, **8 (1)**, 38–55, doi: 10.1175/JHM560.1, URL http://journals.ametsoc.org/doi/10.1175/JHM560.1.

Ito, K., C.-C. Wu, K. T. F. Chan, R. Toumi, and C. Davis, 2020: Recent Progress in the Fundamental Understanding of Tropical Cyclone Motion. *Journal of the Meteorological Society of Japan. Ser. II*, **98 (1)**, 5–17, doi: 10.2151/jmsj.2020-001, URL https://www.jstage.jst.go.jp/article/jmsj/98/1/98_2020-001/_article.

Jamandre, C., and G. Narisma, 2013: Spatio-temporal validation of satellite-based rainfall estimates in the Philippines. *Atmospheric Research*, **122**, 599–608, doi: 10.1016/j.atmosres.2012.06.024, URL http://linkinghub.elsevier.com/retrieve/pii/S0169809512002220.

Jansen, M., and R. Ferrari, 2009: Impact of the latitudinal distribution of tropical cyclones on ocean heat transport. *Geophysical Research Letters*, **36 (6)**, 2008GL036 796, doi: 10.1029/2008GL036796, URL https://agupubs.onlinelibrary.wiley.com/doi/10.1029/2008GL036796.

Jorgensen, D. P., E. J. Zipser, and M. A. LeMone, 1985: Vertical Motions in Intense Hurricanes. *Journal of the Atmospheric Sciences*, **42 (8)**, 839–856, doi: 10.1175/1520-0469(1985)042⟨0839:VMIIH⟩2.0.CO;2, URL http://journals.ametsoc.org/doi/10.1175/1520-0469(1985)042⟨0839:VMIIH⟩2.0.CO;2.

Kim, I.-W., J. Oh, S. Woo, and R. H. Kripalani, 2019: Evaluation of precipitation extremes over the Asian domain: observation and modelling studies. *Climate Dynamics*, **52 (3-4)**, 1317–1342, doi: 10.1007/s00382-018-4193-4, URL http://link.springer.com/10.1007/s00382-018-4193-4.

Kirshbaum, D., B. Adler, N. Kalthoff, C. Barthlott, and S. Serafin, 2018: Moist Orographic Convection: Physical Mechanisms and Links to Surface-Exchange Processes. *Atmosphere*, **9 (3)**, 80, doi: 10.3390/atmos9030080, URL http://www.mdpi.com/2073-4433/9/3/80.

Knapp, K. R., H. J. Diamond, J. P. Kossin, M. C. Kruk, and C. J. Schreck, 2018: International Best Track Archive for Climate Stewardship (IBTrACS) Project, Version 4. NOAA National Centers for Environmental Information, URL https://data.nodc.noaa.gov/cgi-bin/iso?id=gov.noaa.ncdc:C01552, type: dataset, doi: 10.25921/82TY-9E16.

Knapp, K. R., M. C. Kruk, D. H. Levinson, H. J. Diamond, and C. J. Neumann, 2010: The International Best Track Archive for Climate Stewardship (IBTrACS): Unifying Tropical Cyclone Data. *Bulletin of the American Meteorological Society*, **91 (3)**, 363–376, doi: 10.1175/2009BAMS2755.1, URL http://journals.ametsoc.org/doi/10.1175/2009BAMS2755.1.

Knutson, T., and Coauthors, 2019: Tropical Cyclones and Climate Change Assessment: Part I: Detection and Attribution. *Bulletin of the American Meteorological Society*, **100 (10)**, 1987–2007, doi: 10.1175/BAMS-D-18-0189.1, URL https://journals.ametsoc.org/view/journals/bams/100/10/bams-d-18-0189.1.xml.

Knutson, T., and Coauthors, 2020: Tropical Cyclones and Climate Change Assessment: Part II: Projected Response to Anthropogenic Warming. *Bulletin of the American Meteorological Society*, **101 (3)**, E303–E322, doi: 10.1175/BAMS-D-18-0194.1, URL https://journals.ametsoc.org/view/journals/bams/101/3/bams-d-18-0194.1.xml.

Knutson, T. R., and Coauthors, 2010: Tropical cyclones and climate change. *Nature Geoscience*, **3 (3)**, 157–163, doi: 10.1038/ngeo779, URL http://www.nature.com/articles/ngeo779.

Koide, N., A. W. Robertson, A. V. M. Ines, J.-H. Qian, D. G. DeWitt, and A. Lucero, 2013: Prediction of Rice Production in the Philippines Using Seasonal Climate Forecasts. *Journal of Applied Meteorology and Climatology*, **52 (3)**, 552–569, doi: 10.1175/JAMC-D-11-0254.1, URL https://journals.ametsoc.org/jamc/article/52/3/552/18950/Prediction-of-Rice-Production-in-the-Philippines.

Kossin, J. P., 2018: A global slowdown of tropical-cyclone translation speed. *Nature*, **558 (7708)**, 104–107, doi: 10.1038/s41586-018-0158-3, URL http://www.nature.com/articles/s41586-018-0158-3.

Kossin, J. P., T. L. Olander, and K. R. Knapp, 2013: Trend Analysis with a New Global Record of Tropical Cyclone Intensity. *Journal of Climate*, **26 (24)**, 9960–9976, doi: 10.1175/JCLI-D-13-00262.1, URL http://journals.ametsoc.org/doi/10.1175/JCLI-D-13-00262.1.

Kruskal, W. H., and W. A. Wallis, 1952: Use of ranks in one-criterion variance analysis. *Journal of the American Statistical Association*, **47 (260)**, 583–621, URL http://www.jstor.org/stable/2280779.

Kubota, H., and B. Wang, 2009: How Much Do Tropical Cyclones Affect Seasonal and Interannual Rainfall Variability over the Western North Pacific? *Journal of Climate*, **22 (20)**, 5495–5510, doi: 10.1175/2009JCLI2646.1, URL http://journals.ametsoc.org/doi/10.1175/2009JCLI2646.1.

Kunze, S., 2021: Unraveling the Effects of Tropical Cyclones on Economic Sectors Worldwide: Direct and Indirect Impacts. *Environmental and Resource Economics*, **78 (4)**, 545–569, doi: 10.1007/s10640-021-00541-5, URL https://link.springer.com/10.1007/s10640-021-00541-5.

Lagmay, A. M. F., G. Bagtasa, I. A. Crisologo, B. A. B. Racoma, and C. P. C. David, 2015: Volcanoes magnify

Metro Manila's southwest monsoon rains and lethal floods. *Frontiers in Earth Science*, **2**, 1–9, doi: 10.3389/feart.2014.00036, URL http://journal.frontiersin.org/article/10.3389/feart.2014.00036/abstract.

Lagmay, M., and B. A. Racoma, 2019: Lessons from tropical storms Urduja and Vinta disasters in the Philippines. *Disaster Prevention and Management: An International Journal*, **28 (2)**, 154–170, doi: 10.1108/DPM-03-2018-0077, URL https://www.emeraldinsight.com/doi/10.1108/DPM-03-2018-0077.

Lai, Y., and Coauthors, 2020: Greater flood risks in response to slowdown of tropical cyclones over the coast of China. *Proceedings of the National Academy of Sciences*, **117 (26)**, 14 751–14 755, doi: 10.1073/pnas.1918987117, URL http://www.pnas.org/lookup/doi/10.1073/pnas.1918987117.

Lansigan, F., W. de los Santos, and J. Coladilla, 2000: Agronomic impacts of climate variability on rice production in the Philippines. *Agriculture, Ecosystems & Environment*, **82 (1-3)**, 129–137, doi: 10.1016/S0167-8809(00)00222-X, URL https://linkinghub.elsevier.com/retrieve/pii/S016788090000222X.

Lanzante, J. R., 2019: Uncertainties in tropical-cyclone translation speed. *Nature*, **570 (7759)**, E6–E15, doi: 10.1038/s41586-019-1223-2, URL https://www.nature.com/articles/s41586-019-1223-2, number: 7759 Publisher: Nature Publishing Group.

Leppert, K. D., and D. J. Cecil, 2016: Tropical Cyclone Diurnal Cycle as Observed by TRMM. *Monthly Weather Review*, **144 (8)**, 2793–2808, doi: 10.1175/MWR-D-15-0358.1, URL https://journals.ametsoc.org/mwr/article/144/8/2793/72124/Tropical-Cyclone-Diurnal-Cycle-as-Observed-by-TRMM.

Li, Q., Y. Wang, and Y. Duan, 2015: Impacts of Evaporation of Rainwater on Tropical Cyclone Structure and Intensity—A Revisit. *Journal of the Atmospheric Sciences*, **72 (4)**, 1323–1345, doi: 10.1175/JAS-D-14-0224.1, URL https://journals.ametsoc.org/doi/10.1175/JAS-D-14-0224.1.

Liebmann, B., H. H. Hendon, and J. D. Glick, 1994: The relationship between tropical cyclones of the western pacific and indian oceans and the madden-julian oscillation. *Journal of the Meteorological Society of Japan. Ser. II*, **72 (3)**, 401–412, doi: 10.2151/jmsj1965.72.3_401.

Lin, I., and Coauthors, 2020: ENSO and Tropical Cyclones. *Geophysical Monograph Series*, M. J. McPhaden, A. Santoso, and W. Cai, Eds., 1st ed., Wiley, 377–408, doi: 10.1002/9781119548164.ch17, URL https://onlinelibrary.wiley.com/doi/10.1002/9781119548164.ch17.

Lin, Y.-L., S.-H. Chen, and L. Liu, 2016: Orographic Influence on Basic Flow and Cyclone Circulation and Their Impacts on Track Deflection of an Idealized Tropical Cyclone. *Journal of the Atmospheric Sciences*, **73 (10)**, 3951–3974, doi: 10.1175/JAS-D-15-0252.1, URL http://journals.ametsoc.org/doi/10.1175/JAS-D-15-0252.1.

Lin, Y.-L., S.-Y. Chen, C. M. Hill, and C.-Y. Huang, 2005: Control Parameters for the Influence of a Mesoscale Mountain Range on Cyclone Track Continuity and Deflection. *Journal of the Atmospheric Sci-*

ences, **62 (6)**, 1849–1866, doi: 10.1175/JAS3439.1, URL https://journals.ametsoc.org/jas/article/62/6/1849/25813/Control-Parameters-for-the-Influence-of-a.

Lin, Y.-L., D. B. Ensley, S. Chiao, and C.-Y. Huang, 2002: Orographic Influences on Rainfall and Track Deflection Associated with the Passage of a Tropical Cyclone. *Monthly Weather Review*, **130 (12)**, 2929–2950, doi: 10.1175/1520-0493(2002)130⟨2929:OIORAT⟩2.0.CO;2, URL http://journals.ametsoc.org/doi/10.1175/1520-0493(2002)130⟨2929:OIORAT⟩2.0.CO;2.

Lin, Y.-L., J. Han, D. W. Hamilton, and C.-Y. Huang, 1999: Orographic Influence on a Drifting Cyclone. *Journal of the Atmospheric Sciences*, **56**, 29.

Liu, L., Y.-L. Lin, and S.-H. Chen, 2016: Effects of Landfall Location and Approach Angle of an Idealized Tropical Cyclone over a Long Mountain Range. *Frontiers in Earth Science*, **4**, 1–14, doi: 10.3389/feart.2016.00014, URL http://journal.frontiersin.org/Article/10.3389/feart.2016.00014/abstract.

Lyon, B., and S. J. Camargo, 2009: The seasonally-varying influence of ENSO on rainfall and tropical cyclone activity in the Philippines. *Climate Dynamics*, **32 (1)**, 125–141, doi: 10.1007/s00382-008-0380-z, URL http://link.springer.com/10.1007/s00382-008-0380-z.

Macalalad, R. V., R. A. Badilla, O. C. Cabrera, and G. Bagtasa, 2021: Hydrological Response of the Pampanga River Basin in the Philippines to Intense Tropical Cyclone Rainfall. *Journal of Hydrometeorology*, **22 (4)**, 781–794, doi: 10.1175/JHM-D-20-0184.1, URL https://journals.ametsoc.org/view/journals/hydr/22/4/JHM-D-20-0184.1.xml.

Man-chi, W., and C. Chun-Wing, 2015: An Observational Study of the Changes in the Intensity and Motion of Tropical Cyclones Crossing Luzon. *Tropical Cyclone Research and Review*, **4 (3)**, 15, doi: https://doi.org/10.6057/2015TCRRh3.01.

McTaggart-Cowan, R., E. L. Davies, J. G. Fairman, T. J. Galarneau, and D. M. Schultz, 2015: Revisiting the 26.5°C Sea Surface Temperature Threshold for Tropical Cyclone Development. *Bulletin of the American Meteorological Society*, **96 (11)**, 1929–1943, doi: 10.1175/BAMS-D-13-00254.1, URL https://journals.ametsoc.org/doi/10.1175/BAMS-D-13-00254.1.

Mendelsohn, R., K. Emanuel, S. Chonabayashi, and L. Bakkensen, 2012: The impact of climate change on global tropical cyclone damage. *Nature Climate Change*, **2 (3)**, 205–209, doi: 10.1038/nclimate1357, URL https://www.nature.com/articles/nclimate1357.

Minamide, M., and K. Yoshimura, 2014: Orographic Effect on the Precipitation with Typhoon Washi in the Mindanao Island of the Philippines. *SOLA*, **10**, 67–71, doi: 10.2151/sola.2014-014, URL https://www.jstage.jst.go.jp/article/sola/10/0/10_2014-014/_article.

Moon, I.-J., S.-H. Kim, and J. C. L. Chan, 2019: Climate change and tropical cyclone trend. *Nature*, **570 (7759)**, E3–E5, doi: 10.1038/s41586-019-1222-3, URL http://www.nature.com/articles/s41586-019-1222-3.

NASA Goddard Earth Sciences Data And Information Services Center, 2019: GPM IMERG Late Precipitation L3 1 day 0.1 degree x 0.1 degree V06. NASA Goddard Earth Sciences Data and Information Services Center, URL https://disc.gsfc.nasa.gov/datacollection/GPM_3IMERGDL_06.html, type: dataset, doi: 10.5067/GPM/IMERGDL/DAY/06.

NASA JPL, 2020: NASADEM Merged DEM Global 1 arc second V001. NASA EOSDIS Land Processes DAAC, URL https://lpdaac.usgs.gov/products/nasadem_hgtv001, type: dataset, doi: 10.5067/MEASURES/NASADEM/NASADEM_HGT.001.

National Oceanic and Atmospheric Administration, 2023: Tropical cyclone structure. URL https://www.noaa.gov/jetstream/tropical/tropical-cyclone-introduction/tropical-cyclone-structure.

National Oceanic and Atmospheric Administration, N., 2021: Worldwide Tropical Cyclone Centers. URL https://www.nhc.noaa.gov/aboutrsmc.shtml.

Nesbitt, S. W., and E. J. Zipser, 2003: The Diurnal Cycle of Rainfall and Convective Intensity according to Three Years of TRMM Measurements. *Journal of Climate*, **16**, 20.

Nolan, D., and M. McGauley, 2012: Tropical cyclogenesis in wind shear: Climatological relationships and physical processes. *Cyclones: Formation, Triggers and Control*, 1–36.

Olaguera, L. M. P., F. A. T. Cruz, J. M. B. Dado, and J. R. T. Villarin, 2022: Complexities of Extreme Rainfall in the Philippines. *Extreme Natural Events*, A. Unnikrishnan, F. Tangang, and R. J. Durrheim, Eds., Springer Nature Singapore, Singapore, 129–146, doi: 10.1007/978-981-19-2511-5_5, URL https://link.springer.com/10.1007/978-981-19-2511-5_5.

O'Neill, M. E., D. Perez-Betancourt, and A. A. Wing, 2017: Accessible Environments for Diurnal-Period Waves in Simulated Tropical Cyclones. *Journal of the Atmospheric Sciences*, **74 (8)**, 2489–2502, doi: 10.1175/JAS-D-16-0294.1, URL https://journals.ametsoc.org/jas/article/74/8/2489/342627/Accessible-Environments-for-DiurnalPeriod-Waves-in.

Palmén, E., 1948: On the formation and structure of tropical cyclones. *Geophysica*, **3**, 26–38.

Patricola, C. M., S. J. Camargo, P. J. Klotzbach, R. Saravanan, and P. Chang, 2018: The Influence of ENSO Flavors on Western North Pacific Tropical Cyclone Activity. *Journal of Climate*, **31 (14)**, 5395–5416, doi: 10.1175/JCLI-D-17-0678.1, URL https://journals.ametsoc.org/doi/10.1175/JCLI-D-17-0678.1.

Peatman, S. C., N. P. Klingaman, and K. I. Hodges, 2019: Tropical Cyclone–Related Precipitation over the Northwest Tropical Pacific in Met Office Global Operational Forecasts. *Weather and Forecasting*, **34 (4)**,

923–941, doi: 10.1175/WAF-D-19-0017.1, URL http://journals.ametsoc.org/doi/10.1175/WAF-D-19-0017.1.

Persson, A., 1998: How do we understand the coriolis force? *Bulletin of the American Meteorological Society*, **79 (7)**, 1373 – 1386, doi: https://doi.org/10.1175/1520-0477(1998)079⟨1373:HDWUTC⟩2.0.CO;2, URL https://journals.ametsoc.org/view/journals/bams/79/7/1520-0477_1998_079_1373_hdwutc_2_0_co_2.xml.

Pezzulli, S., D. B. Stephenson, and A. Hannachi, 2005: The Variability of Seasonality. *Journal of Climate*, **18 (1)**, 71–88, doi: 10.1175/JCLI-3256.1, URL http://journals.ametsoc.org/doi/10.1175/JCLI-3256.1.

Pradhan, R. K., and Coauthors, 2022: Review of GPM IMERG performance: A global perspective. *Remote Sensing of Environment*, **268**, 112 754, doi: 10.1016/j.rse.2021.112754, URL https://linkinghub.elsevier.com/retrieve/pii/S0034425721004740.

Precipitation Processing System (PPS) At NASA GSFC, 2018: TRMM (TMPA) Rainfall Estimate L3 3 hour 0.25 degree x 0.25 degree V7. NASA Goddard Earth Sciences Data and Information Services Center, URL https://disc.gsfc.nasa.gov/datacollection/TRMM_3B42_7.html, type: dataset, doi: 10.5067/TRMM/TMPA/3H/7.

Racoma, B. A. B., C. P. C. David, I. A. Crisologo, and G. Bagtasa, 2016: The Change in Rainfall from Tropical Cyclones Due to Orographic Effect of the Sierra Madre Mountain Range in Luzon, Philippines. *Philippine Journal of Science*, **145 (4)**, 14.

Racoma, B. A. B., C. E. Holloway, R. K. H. Schiemann, X. Feng, and G. Bagtasa, 2023: The Effect of the Cordillera Mountain Range on Tropical Cyclone Rainfall in the Northern Philippines. *Atmosphere*, **14 (4)**, 643, doi: 10.3390/atmos14040643, URL https://www.mdpi.com/2073-4433/14/4/643.

Racoma, B. A. B., N. P. Klingaman, C. E. Holloway, R. K. H. Schiemann, and G. Bagtasa, 2021: Tropical cyclone characteristics associated with extreme precipitation in the northern Philippines. *International Journal of Climatology*, **42 (6)**, 3290–3307, doi: 10.1002/joc.7416, URL https://onlinelibrary.wiley.com/doi/abs/10.1002/joc.7416.

Ren, D., M. Lynch, L. M. Leslie, and J. Lemarshall, 2014: Sensitivity of Tropical Cyclone Tracks and Intensity to Ocean Surface Temperature: Four Cases in Four Different Basins. *Tellus A: Dynamic Meteorology and Oceanography*, **66 (1)**, 24 212, doi: 10.3402/tellusa.v66.24212, URL https://a.tellusjournals.se/article/10.3402/tellusa.v66.24212/.

Rios Gaona, M. F., and G. Villarini, 2018: Characterization of the diurnal cycle of maximum rainfall in tropical cyclones. *Journal of Hydrology*, **564**, 997–1007, doi: 10.1016/j.jhydrol.2018.07.062, URL https://linkinghub.elsevier.com/retrieve/pii/S0022169418305778.

Rodolfo, K. S., A. M. F. Lagmay, R. C. Eco, T. M. L. Herrero, J. E. Mendoza, L. G. Minimo, and J. T. Santiago, 2016: The December 2012 Mayo River debris flow triggered by Super Typhoon Bopha in Mindanao, Philippines: lessons learned and questions raised. *Natural Hazards and Earth System Sciences*, **16 (12)**, 2683–2695, doi: 10.5194/nhess-16-2683-2016, URL https://www.nat-hazards-earth-syst-sci.net/16/2683/2016/.

Roe, G. H., 2005: Orographic Precipitation. *Annual Review of Earth and Planetary Sciences*, **33 (1)**, 645–671, doi: 10.1146/annurev.earth.33.092203.122541, URL http://www.annualreviews.org/doi/10.1146/annurev.earth.33.092203.122541.

Rogers, R., F. Marks, and T. Marchok, 2005: Tropical Cyclone Rainfall. *Encyclopedia of Hydrological Sciences*, M. G. Anderson, and J. J. McDonnell, Eds., 1st ed., Wiley, doi: 10.1002/0470848944.hsa030, URL https://onlinelibrary.wiley.com/doi/10.1002/0470848944.hsa030.

Rostom, R., and Y.-L. Lin, 2021: Common Ingredients and Orographic Rain Index (ORI) for Heavy Precipitation Associated with Tropical Cyclones Passing Over the Appalachian Mountains. *Earth Science Research*, **10 (1)**, 32, doi: 10.5539/esr.v10n1p32, URL http://www.ccsenet.org/journal/index.php/esr/article/view/0/44792.

Roy, C., and R. Kovordányi, 2012: Tropical cyclone track forecasting techniques — A review. *Atmospheric Research*, **104-105**, 40–69, doi: 10.1016/j.atmosres.2011.09.012, URL https://linkinghub.elsevier.com/retrieve/pii/S0169809511002973.

Royal Meteorological Society, 2020: What is El Niño Southern Oscillation (ENSO)? URL https://www.rmets.org/metmatters/what-el-nino-southern-oscillation-enso.

Scoccimarro, E., and Coauthors, 2011: Effects of Tropical Cyclones on Ocean Heat Transport in a High-Resolution Coupled General Circulation Model. *Journal of Climate*, **24 (16)**, 4368–4384, doi: 10.1175/2011JCLI4104.1, URL http://journals.ametsoc.org/doi/10.1175/2011JCLI4104.1.

Seneviratne, S., and Coauthors, 2021: *2021: Weather and Climate Extreme Events in a Changing Climate*, book section 11, 1513–1765. Cambridge University Press, URL https://www.ipcc.ch/report/ar6/wg1/downloads/report/IPCC_AR6_WGI_Chapter11.pdf.

Shrestha, B. B., and Coauthors, 2014: Fundamental Analysis for Flood Risk Management in the Selected River Basins of Southeast Asia. *Journal of Disaster Research*, **9 (5)**, 858–869, doi: 10.20965/jdr.2014.p0858, URL https://www.fujipress.jp/jdr/dr/dsstr000900050858.

Simpson, R., 1946: On the movement of tropical cyclones. *Eos, Transactions American Geophysical Union*, **27 (5)**, 641–655, doi: https://doi.org/10.1029/TR027i005p00641, URL https://agupubs.onlinelibrary.wiley.com/doi/abs/10.1029/TR027i005p00641, https://agupubs.onlinelibrary.wiley.com/doi/pdf/10.1029/TR027i005p00641.

Sinclair, M. R., 1994: A Diagnostic Model for Estimating Orographic Precipitation. *Journal of Applied Meteorology and Climatology*, **33 (10)**, 1163–1175, doi: 10.1175/1520-0450(1994)033⟨1163:ADMFEO⟩2.0.CO; 2, URL https://journals.ametsoc.org/view/journals/apme/33/10/1520-0450_1994_033_1163_admfeo_2_0_co_2.xml, publisher: American Meteorological Society Section: Journal of Applied Meteorology and Climatology.

Skamarock, W., J. Klemp, J. Dudhia, D. Gill, D. Barker, W. Wang, X.-Y. Huang, and M. Duda, 2008: A Description of the Advanced Research WRF Version 3. Tech. rep., UCAR/NCAR, 1002 KB pp. doi: 10.5065/D68S4MVH, URL http://opensky.ucar.edu/islandora/object/technotes:500, artwork Size: 1002 KB Medium: application/pdf.

Smith, R. B., 1979: The Influence of Mountains on the Atmosphere. *Advances in Geophysics*, **21**, Elsevier, 87–230, doi: 10.1016/S0065-2687(08)60262-9, URL https://linkinghub.elsevier.com/retrieve/pii/S0065268708602629.

Smith, R. K., and M. T. Montgomery, 2015: Toward Clarity on Understanding Tropical Cyclone Intensification. *Journal of the Atmospheric Sciences*, **72 (8)**, 3020–3031, doi: 10.1175/JAS-D-15-0017.1, URL https://journals.ametsoc.org/doi/10.1175/JAS-D-15-0017.1.

Sobel, A. H., and E. D. Maloney, 2000: Effect of ENSO and the MJO on western North Pacific tropical cyclones. *Geophysical Research Letters*, **27 (12)**, 1739–1742, doi: 10.1029/1999GL011043, URL http://doi.wiley.com/10.1029/1999GL011043.

Sobel, A. H., A. A. Wing, S. J. Camargo, C. M. Patricola, G. A. Vecchi, C. Lee, and M. K. Tippett, 2021: Tropical Cyclone Frequency. *Earth's Future*, **9 (12)**, e2021EF002 275, doi: 10.1029/2021EF002275, URL https://agupubs.onlinelibrary.wiley.com/doi/10.1029/2021EF002275.

Stan, C., 2018: The role of SST variability in the simulation of the MJO. *Climate Dynamics*, **51 (7-8)**, 2943–2964, doi: 10.1007/s00382-017-4058-2, URL http://link.springer.com/10.1007/s00382-017-4058-2.

Tang, B. H., and Coauthors, 2020: Recent advances in research on tropical cyclogenesis. *Tropical Cyclone Research and Review*, **9 (2)**, 87–105, doi: 10.1016/j.tcrr.2020.04.004, URL https://linkinghub.elsevier.com/retrieve/pii/S2225603220300187.

Tang, C. K., and J. C. L. Chan, 2014: Idealized simulations of the effect of Taiwan and Philippines topographies on tropical cyclone tracks: Effect of topography on tropical cyclone tracks. *Quarterly Journal of the Royal Meteorological Society*, **140 (682)**, 1578–1589, doi: 10.1002/qj.2240, URL http://doi.wiley.com/10.1002/qj.2240.

The Saffir-Simpson Team, 2021: The Saffir-Simpson Hurricane Wind Scale. National Hurricane Center, URL https://www.nhc.noaa.gov/pdf/sshws.pdf.

Tory, K. J., and W. M. Frank, 2010: Tropical Cyclone Formation. *World Scientific Series on Asia-Pacific Weather and Climate*, **4**, World Scientific, 55–91, doi: 10.1142/9789814293488_0002, URL http://www.worldscientific.com/doi/abs/10.1142/9789814293488_0002.

Touma, D., S. Stevenson, S. J. Camargo, D. E. Horton, and N. S. Diffenbaugh, 2019: Variations in the Intensity and Spatial Extent of Tropical Cyclone Precipitation. *Geophysical Research Letters*, **46 (23)**, 13 992–14 002, doi: 10.1029/2019GL083452, URL https://agupubs.onlinelibrary.wiley.com/doi/10.1029/2019GL083452.

Truchelut, R. E., P. J. Klotzbach, E. M. Staehling, K. M. Wood, D. J. Halperin, C. J. Schreck, and E. S. Blake, 2022: Earlier onset of North Atlantic hurricane season with warming oceans. *Nature Communications*, **13 (1)**, 4646, doi: 10.1038/s41467-022-31821-3, URL https://www.nature.com/articles/s41467-022-31821-3.

Tu, S., J. C. L. Chan, J. Xu, Q. Zhong, W. Zhou, and Y. Zhang, 2022: Increase in tropical cyclone rain rate with translation speed. *Nature Communications*, **13 (1)**, 7325, doi: 10.1038/s41467-022-35113-8, URL https://www.nature.com/articles/s41467-022-35113-8.

Tuleya, R. E., and Y. Kurihara, 1978: A numerical simulation of the landfall of tropical cyclones. *Journal of Atmospheric Sciences*, **35 (2)**, 242 – 257, doi: 10.1175/1520-0469(1978)035⟨0242:ANSOTL⟩2.0.CO;2, URL https://journals.ametsoc.org/view/journals/atsc/35/2/1520-0469_1978_035_0242_ansotl_2_0_co_2.xml.

Walsh, K. J., and Coauthors, 2016: Tropical cyclones and climate change. *WIREs Climate Change*, **7 (1)**, 65–89, doi: 10.1002/wcc.371, URL https://wires.onlinelibrary.wiley.com/doi/10.1002/wcc.371.

Waple, A. M., and Coauthors, 2001: Climate Assessment for 2001. *Bulletin of the American Meteorological Society*, **82 (6)**, 1304–1304, doi: 10.1175/1520-0477(2001)082⟨1304:CAF⟩2.3.CO;2, URL http://journals.ametsoc.org/doi/10.1175/1520-0477(2001)082⟨1304:CAF⟩2.3.CO;2.

Webb, P., 2020: Winds and the Coriolis Effect. Roger Williams University, URL https://geo.libretexts.org/@go/page/4511, [Online; accessed 2023-11-21].

Wikimedia Commons, 2022: File:global tropical cyclone tracks-edit2.jpg — wikimedia commons, the free media repository. Wikimedia Commons, the free media repository., URL https://commons.wikimedia.org/w/index.php?title=File:Global_tropical_cyclone_tracks-edit2.jpg, [Online; accessed 14-October-2022].

World Bank, 2022: Agricultural land (% of land area) - Philippines. Food and Agriculture Organization. Subset used: Philippines. The World Bank Group, URL https://data.worldbank.org/indicator/AG.LND.AGRI.ZS?locations=PH.

World Meteorological Organization, 2020: Tropical Cyclones. World Meteorological Organization, URL https://public.wmo.int/en/our-mandate/focus-areas/natural-hazards-and-disaster-risk-reduction/tropical-cyclones.

Wu, L., and X. Chen, 2016: Revisiting the steering principal of tropical cyclone motion in a numerical experiment. *Atmospheric Chemistry and Physics*, **16 (23)**, 14 925–14 936, doi: 10.5194/acp-16-14925-2016, URL https://acp.copernicus.org/articles/16/14925/2016/.

Wu, Q., Z. Ruan, D. Chen, and T. Lian, 2015: Diurnal variations of tropical cyclone precipitation in the inner and outer rainbands: Diurnal Variations of TC Precipitation. *Journal of Geophysical Research: Atmospheres*, **120 (1)**, 1–11, doi: 10.1002/2014JD022190, URL http://doi.wiley.com/10.1002/2014JD022190.

Wunsch, C., 2002: What Is the Thermohaline Circulation? *Science*, **298 (5596)**, 1179–1181, doi: 10.1126/science.1079329, URL https://www.science.org/doi/10.1126/science.1079329, publisher: American Association for the Advancement of Science.

Wylie, P. E., 1953: The Coriolis Effect. *The Journal of the Royal Aeronautical Society*, **57 (514)**, 655–658, doi: 10.1017/S0368393100126744, URL https://www.cambridge.org/core/product/identifier/S0368393100126744/type/journal_article.

Xiang, B., B. Wang, W. Yu, and S. Xu, 2013: How can anomalous western North Pacific Subtropical High intensify in late summer? *Geophysical Research Letters*, **40 (10)**, 2349–2354, doi: 10.1002/grl.50431, URL https://onlinelibrary.wiley.com/doi/10.1002/grl.50431.

Yamaguchi, M., J. C. L. Chan, I.-J. Moon, K. Yoshida, and R. Mizuta, 2020: Global warming changes tropical cyclone translation speed. *Nature Communications*, **11 (1)**, 47, doi: 10.1038/s41467-019-13902-y, URL http://www.nature.com/articles/s41467-019-13902-y.

Yatagai, A., K. Kamiguchi, O. Arakawa, A. Hamada, N. Yasutomi, and A. Kitoh, 2012: APHRODITE: Constructing a Long-Term Daily Gridded Precipitation Dataset for Asia Based on a Dense Network of Rain Gauges. *Bulletin of the American Meteorological Society*, **93 (9)**, 1401–1415, doi: 10.1175/BAMS-D-11-00122.1, URL http://journals.ametsoc.org/doi/abs/10.1175/BAMS-D-11-00122.1.

Yihui, D., and J. C. L. Chan, 2005: The East Asian summer monsoon: an overview. *Meteorology and Atmospheric Physics*, **89 (1-4)**, 117–142, doi: 10.1007/s00703-005-0125-z, URL http://link.springer.com/10.1007/s00703-005-0125-z.

Yu, C.-K., and L.-W. Cheng, 2013: Distribution and Mechanisms of Orographic Precipitation Associated with Typhoon Morakot (2009). *Journal of the Atmospheric Sciences*, **70 (9)**, 2894–2915, doi: 10.1175/JAS-D-12-0340.1, URL http://journals.ametsoc.org/doi/abs/10.1175/JAS-D-12-0340.1.

Zhan, R., Y. Wang, and M. Ying, 2012: Seasonal forecasts of tropical cyclone activity over the western north pacific: A review. *Tropical Cyclone Research and Review*, **1 (3)**, 307–324, doi: https://doi.org/10.6057/2012TCRR03.07, URL https://www.sciencedirect.com/science/article/pii/S2225603218300419.

Zhou, T., and Coauthors, 2009: Why the western pacific subtropical high has extended westward since the late 1970s. *Journal of Climate*, **22 (8)**, 2199 – 2215, doi: https://doi.org/10.1175/2008JCLI2527.1, URL https://journals.ametsoc.org/view/journals/clim/22/8/2008jcli2527.1.xml.